NEURONS THAT CONTROL SOCIAL STATES IN *DROSOPHILA MELANOGASTER*

Thesis by

Yonil Jung

In Partial Fulfillment of the Requirements for

the degree of

Doctor of Philosophy

CALIFORNIA INSTITUTE OF TECHNOLOGY

Pasadena, California

2020

(Defended January 16, 2020)

Yonil Jung
ORCID: 0000-0002-1673-4450

ACKNOWLEDGEMENTS

First and foremost, I would like to thank my thesis advisor, David J Anderson, for all of his support and encouragement. He truly showed me what a good scientist is supposed to be, and how to think like a real scientist. I first met him in his class and noticed how much he loves science, which made me rotate in his lab, and eventually decide to join the lab. Since then, he has been the best mentor not only for scientific matters but also for the other aspects of the life as a scientist.

Besides David, I would like to thank all my committee members, Dr. Markus Meister, Dr. Paul Sternberg, and Dr. Viviana Gradinaru, for their invaluable advice. I also want to thank my undergraduate advisor, Dr. Taekjib Ha, for his support and encouragement to pursue science.

I am also thankful for all the current and previous lab members. Thank Hidehiko Inagaki for his enormous help during the early years of my PhD program. He has been the best mentor, the best collaborator, and the best friend. Special thanks to Allan M. Wong for widening my perspective of the scientific field and teaching me multi-photon imaging. Thanks to Kiichi Watanabe, Ke Ding, and Vivian Chiu for their scientific discussion and help, and being good friends. All the former members of the fly subgroup people in the lab were helpful and generous to share ideas and advise me: Eric Hoopfer, Kenta Asahina, Rod Lim, Shuo Cao, Joe Ouadah, Brian Duistermars, and Barret Pfeiffer. Discussions with the mice subgroup were also helpful and fun. Thanks to Dongwook Kim for being a patient listener and good life-advisor, and Tomomi Karigo for being a diving buddy. Thanks to Zeynep Turan, Ann Kennedy, Lingyun Li, George Mountoufaris, Stefanos Stagkourakis, Amit Vinograd, Brady Weissbourd, Mengyu Liu, and Bin Yang. I also would like to thank Gina Mancuso and Celine Chiu for their administrative help.

I am grateful to the many friends that I met during my PhD program. Thanks to all my on-campus friends for their support and all the good memories: Hyungi Yoon, Kyuhyun Lee, and Taeyong Lee. I also thank all my off-campus friends, especially my diving mentor, Javier Lopez.

Lastly, I would like to than my family members for their continuous support throughout my PhD journey. My dad and mom, including in-laws, always encouraged me to be a good scientist with love. Thanks to my brother and brother-in-law for taking care of all the family works. I am blessed to be with my wife, Jungmin Kim, and to have my gorgeous daughter, Alice Chorok Jung, during my PhD years.

ABSTRACT

Animal behaviors are influences not only by the immediate stimuli they are receiving but also by internal states. Internal states such as fear, hunger, and arousal can change subjective “feeling”, and result in complex behavioral outcome even if animals receive the same stimuli. In most cases, these state-dependent behavioral changes persist long after the sensory input that caused internal state change is removed, and affect future behavior, reflexing previous experience. This feature of state-control allows animals to adapt their behavior to be more suitable for their internal demands.

The influence of the internal state on animal behavior has been emphasized for decades. There are multiple studies and attempts to identify persistent neuronal mechanisms which are the important feature of the internal state. However, how persistency makes the behavioral state interact with behavioral process to induce input/output relationship has been largely unknown. In addition, it is not clear what the behavioral functions of the persistence are, and what the circuit implementation of persistent activity is. Are there neurons that are persistently activated by external stimulus? Here we approached these questions by investigating social state of fruit flies, *Drosophila melanogaster*.

Fruit flies exhibit complex social behaviors that are appropriate for given social cues. For example, male flies show courtship behavior toward female flies, and show aggressive behavior such as wing threat and fighting when they encounter opponent male files. Previous studies have been focused on what sensory cues induce these behaviors: detection of female specific pheromones, 7,11-HD, causes male files to court, and male specific pheromone, cVA, induces inter-male aggression. In this study, we have focused more on how these cues might affect internal state changes rather than immediate behavioral response.

Studying persistent social state change has been challenging due to the difficulty of precise, time-resolved presentation of the social cues. For instance, courtship behaviors

require constant presence of female object toward which male flies show oriented behavior. The male-male aggressive behaviors such as lunging and tussling require constant interaction between two animals, and removal of opponent male fly is technically impossible. Therefore, we first developed an optogenetic tool in fly systems to study persistent feature of the social state change to mimic transient presentation of the social cue. In Chapter II, we describe an optogenetic tool that allows the manipulation of neural activity in a freely moving fly. We used Red activatable Channelrhodopsin (ReachR), which enabled us to manipulate activation of neurons in freely behaving adult flies in millisecond precision without interfering normal visual function. Using such an activation tool, we show that activation of female sensing neurons, P1 neurons, induces persistent courtship behaviors in male flies that last several minutes after the stimulation of P1 neurons.

Although we show that persistent internal state change can be induced by transient stimulation of the sensory cues in Chapter II, the circuit implementation of such a persistency is not clear. In Chapter III, we show that activation of P1 neurons triggers persistent activity in its downstream neurons, pCd neurons, that is necessary for the persistent social behavior induced by transient social behaviors. Interestingly, manipulation of the pCd neurons do not affect immediate behavioral response that are shown during the presentation of social cues (P1 stimulation), implying that there are parallel and dissociable pathways for the immediate response and enduring response derived from persistent internal state change, although these responses are caused by common cue. Although the neural mechanism to encode persistent activity is still unclear, this finding shows how internal state and command pathway interact with each other to affect behavioral outcome.

Altogether, these findings described in this dissertation offer new insights for future researchers to understand behavioral state control.

PUBLISHED CONTENT AND CONTRIBUTIONS

Inagaki HK, Jung Y, Hoopfer ED, Wong AM, Mishra N, Lin JY, Tsien RY, Anderson DJ. "Optogenetic control of Drosophila using a red-shifted channelrhodopsin reveals experience-dependent influences on courtship". *Nat Methods*. 2014 Mar;11(3):325-32. doi: 10.1038/nmeth.2765.

Y.J participated in the conception of the project, prepared the data, and figures for the manuscript.

Jung Y, Kennedy A, Chiu H, Mohammad F, Claridge-Chang A, Anderson DJ. "Neurons that Function within an Integrator to Promote a Persistent Behavioral State in Drosophila". *Neuron*. 2019 Nov 5;. doi: 10.1016/j.neuron.2019.10.028.

Y.J participated in the conception of the project, prepared the data, and participated in the writing of the manuscript.

TABLE OF CONTENTS

LIST OF ILLUSTRATIONS AND/OR TABLES

Chapter II

Chapter III

Chapter IV

Page

Chapter 1

INTRODUCTION

1.1 Persistent internal states influencing social behaviors in fruit flies.

Animals that encounter another organism decide how to response to it based on the identity of the opponents. However, encounters between two organisms, for example two conspecific males, do not always result in same behavioral outcome such as fighting. This is because decisions are often influenced by internal states (Anderson and Adolphs, 2014; Kennedy et al., 2014; Spunt et al., 2017). Internal states are triggered by specific stimuli and change many aspects of animal behavior, and share characteristic properties such as persistence, valence, and scalability (Anderson and Adolphs, 2014). This state is encoded in a particular brain region or distributed across multiple brain regions that influences observable behavioral outcome, cognitive changes, and physiological somatic responses (Anderson and Adolphs, 2014). Yet there is ongoing debate about the relationship between internal state and these responses. Are states a consequence or cause of the response? Is there a central state that causes multiple parallel responses, or is a different component of the state responsible for each response? Is there a particular brain region that encodes each state? These questions are intriguing yet elusive, and so are most directly addressable in genetically tractable model organisms such as *Drosophila*.

Internal states such as hunger or arousal, and motivation enable animals to adjust their behavioral response to metabolic, emotional, attentional or other demands (Chiappe et al., 2010; Maimon et al., 2010). For example, in *Drosophila* as well as in other species, starvation changes the consummatory response to tastants, typically by enhancing the acceptance of energy resources, with an associated increased tolerance for bitter-tasting contaminants (Inagaki et al., 2014b). Studies in C. elegans have identified neuropeptides, biogenic amines, and the underlying circuitry that controls opposing, persistent behavioral states such as roaming (Flavell et al., 2013). Neuromodulators, such as biogenic amines and acetylcholine,

as well as neuropeptides, play a major role in encoding or mediating internal states (Harris-Warrick and Marder, 1991; Pfaff et al., 2008), by altering the input-output properties of specific neural circuits (Birmingham and Tauck, 2003). Reproductive social behaviors such as mating and fighting are crucial for survival, and progression through the different phases of an aggressive or sexual behaviors is typically mediated by internal state of motivation, arousal, or drive (Berridge, 2004). Studies in mice have identified MPO (Simerly, 2002; Yang and Shah, 2014) and VMHvl (Lee et al., 2014) as the brain areas that control male sexual behavior. The classical view of internal state relevant to mating and fighting emphasizes the role of neuromodulators (Miczek et al., 2007; Pfaff et al., 2005), but the neural circuit level mechanisms that encode such internal states are largely unknown.

The circuitry that controls courtship behavior is one of the most intensively studied neural systems in the male fly (Dickson, 2008; Yamamoto et al., 2014), making it an ideal system to study neural circuit mechanisms encoding internal states. Fruit flies have small populations of genetically identifiable neurons, P1 neurons, that control social behaviors (Yu et al., 2010). Interestingly, activation of P1 interneurons in single male flies triggers persistent wing extensions that outlast P1 stimulation (Inagaki et al., 2014a). Transient activation of P1 neurons in pairs of male flies evoke persistent aggression (Hoopfer et al., 2015). These results indicate that P1 neurons regulate two different types of social behaviors that are the result of persistent internal state change. Although the previous study did not directly address the natural stimuli that trigger P1 mediated internal state, optogenetic activation of P1 neurons might mimic the effect of pre-exposure of male flies to female flies since P1 neurons respond to female pheromone (Clowney et al., 2015; Ruta et al., 2010), indicating that past experience can influence social behavior in fruit flies. Another such example is social isolation. This past environmental conditioning is known to increase both courtship and aggression in flies (Liu et al., 2011; Wang et al., 2011). Interestingly, social isolation increased excitability of P1 neurons, suggesting that the effect of social isolation could be mediated by the internal state being triggered by P1 neurons (Inagaki et al., 2014a). Therefore, P1 neurons would be a good entry point to investigate the circuit level mechanism of the relationship between internal state and animal behavior.

How the brain keeps the internal state change persistent even after the initial stimulus has been terminated is not clear, but there are a number of proposed mechanisms to explain persistent neuronal activity. Several studies have shown that intrinsic cellular mechanisms can produce persistent firing that is driven by stable voltage patterns, intracellular signaling dynamics, and neuromodulators (Alaburda et al., 2002; Russo and Hounsgaard, 1999). In *Drosophila*, a small cluster of neurons that contain the neuropeptide *Drosophila tachykinin* appear to control an internal state that may correspond to aggressive arousal, supporting that neuromodulators are important regulators of internal states and behavior (Asahina et al., 2014). On the other hand, recurrent synaptic feedback has long been a popular hypothesized mechanism of persistent activity even though there is little concrete evidence that recurrent synaptic feedback dominates persistent activity in an intact nervous system (Brody et al., 2003; Wang, 2001).

1.2 Optogenetics and functional imaging to map brain function.

The ability to identify neurons that control persistent behavioral states requires transient activation of such neurons in behaving animals. Optogenetics tools allow us to control neuronal activity with millisecond time resolution (Boyden, 2011; Deisseroth, 2010; Fenno et al., 2011), but use of Channelrhodopsin in Drosophila has been limited by the inability of blue light to penetrate the flies' cuticle (Inagaki et al., 2014a). This limitation has been overcome by the development of red-shifted opsins such as ReaChR and Chrimson (Inagaki et al., 2014a; Klapoetke et al., 2014). Using these optogenetic tools, we have found that transient activation of P1 interneurons evoke persistent courtship and aggression (Hoopfer et al., 2015). Since activation of P1 neurons does not trigger persistent P1 activity (Inagaki et al., 2014a), we looked for the downstream neurons that are persistently activated by transient P1 activation.

To identify neurons that are either upstream or downstream of the target neurons, it is necessary to combine optogenetics with functional imaging to measure neuronal activity in putative downstream neurons. Genetically encoded calcium indicators (e.g., GCaMP) change fluorescent intensity upon binding of calcium ions, and are widely used to measure

neuronal activity (Nakai et al., 2001). Recently developed GCaMP6 (Chen et al., 2013) and GCaMP7 (Dana et al., 2019) have superior signal to noise ratio and have excellent dF/F, making them the ideal reagent to identify functional connections between neurons. However, combining GCaMP imaging with optogenetic tools presents a generic challenge since both tools require excitation with visible light. Fortunately, red-shifted opsins previously mentioned can be excited with a wavelength that has minimal spectral-overlap with GCaMP excitation light (Inagaki et al., 2014a; Klapoetke et al., 2014). By applying appropriate optical setups such as band-pass filters and light angles, neuronal activity can be measured by GCaMP imaging without too much artificial increase derived from optogenetic activation light.

Searching for P1 downstream neurons in a large brain area using optogenetic activation and GCaMP imaging, however, presents technical challenge. Conventional point-scanning light microscopes have relatively slow imaging speed, making it hard to capture neuronal activity changes in large volumes of tissue. Recent advances in optical imaging techniques, however, allow one to acquire images from multiple optical sections with a frame rate that is fast enough to catch neuronal activity changes. There are multiple methods that have been developed by different laboratories such as light sheet microscope and its derivatives, light field microscope, and Bessel beam imaging. By adapting these fast scanning modules, P1 downstream neurons in whole fly brain are identified by optogenetic activation and GCaMP functional imaging.

Activation of neurons using optogenetic has another advantage that could not be achieved by other genetically encoded actuators such as TrpA1 (Hamada et al., 2008): thermogenetic activation. Since visible light can be focused in a diffraction-limited spot using optical tools, one can activate single cells selectively under microscope even if a large population of neurons express Channelrhodopsin (Rickgauer et al., 2014). This feature allows us to manipulate a single neuron or single cluster of neurons even when there is no genetic handle to specifically target the neuron. There are a number of techniques described to optically target single neuron using optogenetics such as spiral scanning (Rickgauer and Tank, 2009),

DMD (digital micromirror device), or SLM (spatial light modulator) (Han et al., 2019; Nikolenko et al., 2008; Pegard et al., 2017; Yang and Yuste, 2018). These techniques in conjunction with other optical tools describe above can be used to simultaneously manipulate cell activity with single cell resolution with large-scale recording of neuronal activity.

All these advanced optical techniques allowed us to investigate neuronal functions and provided useful insight that would not have been possible to make otherwise. However, each technique has its own limitations that remain to be improved. Most optogenetic tools are activated by broad spectrum of visible light, and are difficult to manipulate two different populations of neurons with different effectors (Klapoetke et al., 2014). Development of new opsins with narrowed spectrum will solve this problem. For the large-scale functional imaging, even though image acquisition speed has been improved by advance optical technique as mentioned above, extracting neuronal activities from individual cells is still challenging because increasing scanning speed in general decreases the signal to noise ratio. Use of optogenetics with focused activation beam is limited to head-fixed animals, which makes it difficult to perform during complex social behaviors that usually accompanied by high locomotor activity.

1.3 References

Alaburda, A., Perrier, J.F., and Hounsgaard, J. (2002). Mechanisms causing plateau potentials in spinal motoneurones. Adv Exp Med Biol *508*, 219-226.

Anderson, D.J., and Adolphs, R. (2014). A framework for studying emotions across species. Cell *157*, 187-200.

Asahina, K., Watanabe, K., Duistermars, B.J., Hoopfer, E., Gonzalez, C.R., Eyjolfsdottir, E.A., Perona, P., and Anderson, D.J. (2014). Tachykinin-expressing neurons control male-specific aggressive arousal in Drosophila. Cell *156*, 221-235.

Brody, C.D., Romo, R., and Kepecs, A. (2003). Basic mechanisms for graded persistent activity: discrete attractors, continuous attractors, and dynamic representations. Curr Opin Neurobiol *13*, 204-211.

Chen, T.W., Wardill, T.J., Sun, Y., Pulver, S.R., Renninger, S.L., Baohan, A., Schreiter, E.R., Kerr, R.A., Orger, M.B., Jayaraman, V.*, et al.* (2013). Ultrasensitive fluorescent proteins for imaging neuronal activity. Nature *499*, 295-300.

Clowney, E.J., Iguchi, S., Bussell, J.J., Scheer, E., and Ruta, V. (2015). Multimodal Chemosensory Circuits Controlling Male Courtship in Drosophila. Neuron *87*, 1036-1049.

Dana, H., Sun, Y., Mohar, B., Hulse, B.K., Kerlin, A.M., Hasseman, J.P., Tsegaye, G., Tsang, A., Wong, A., Patel, R.*, et al.* (2019). High-performance calcium sensors for imaging activity in neuronal populations and microcompartments. Nat Methods *16*, 649-657.

Dickson, B.J. (2008). Wired for sex: the neurobiology of Drosophila mating decisions. Science *322*, 904-909.

Hamada, F.N., Rosenzweig, M., Kang, K., Pulver, S.R., Ghezzi, A., Jegla, T.J., and Garrity, P.A. (2008). An internal thermal sensor controlling temperature preference in Drosophila. Nature *454*, 217-220.

Hoopfer, E.D., Jung, Y., Inagaki, H.K., Rubin, G.M., and Anderson, D.J. (2015). P1 interneurons promote a persistent internal state that enhances inter-male aggression in Drosophila. Elife *4*.

Inagaki, H.K., Jung, Y., Hoopfer, E.D., Wong, A.M., Mishra, N., Lin, J.Y., Tsien, R.Y., and Anderson, D.J. (2014a). Optogenetic control of Drosophila using a red-shifted channelrhodopsin reveals experience-dependent influences on courtship. Nat Methods *11*, 325-332.

Klapoetke, N.C., Murata, Y., Kim, S.S., Pulver, S.R., Birdsey-Benson, A., Cho, Y.K., Morimoto, T.K., Chuong, A.S., Carpenter, E.J., Tian, Z.*, et al.* (2014). Independent optical excitation of distinct neural populations. Nat Methods *11*, 338-346.

Liu, W., Liang, X., Gong, J., Yang, Z., Zhang, Y.H., Zhang, J.X., and Rao, Y. (2011). Social regulation of aggression by pheromonal activation of Or65a olfactory neurons in Drosophila. Nat Neurosci *14*, 896-902.

Miczek, K.A., de Almeida, R.M., Kravitz, E.A., Rissman, E.F., de Boer, S.F., and Raine, A. (2007). Neurobiology of escalated aggression and violence. J Neurosci *27*, 11803-11806.

Nakai, J., Ohkura, M., and Imoto, K. (2001). A high signal-to-noise Ca(2+) probe composed of a single green fluorescent protein. Nat Biotechnol *19*, 137-141.

Pegard, N.C., Mardinly, A.R., Oldenburg, I.A., Sridharan, S., Waller, L., and Adesnik, H. (2017). Three-dimensional scanless holographic optogenetics with temporal focusing (3D-SHOT). Nat Commun *8*, 1228.

Pfaff, D., Westberg, L., and Kow, L.M. (2005). Generalized arousal of mammalian central nervous system. J Comp Neurol *493*, 86-91.

Rickgauer, J.P., Deisseroth, K., and Tank, D.W. (2014). Simultaneous cellular-resolution optical perturbation and imaging of place cell firing fields. Nat Neurosci *17*, 1816-1824.

Rickgauer, J.P., and Tank, D.W. (2009). Two-photon excitation of channelrhodopsin-2 at saturation. Proc Natl Acad Sci U S A *106*, 15025-15030.

Russo, R.E., and Hounsgaard, J. (1999). Dynamics of intrinsic electrophysiological properties in spinal cord neurones. Prog Biophys Mol Biol *72*, 329-365.

Ruta, V., Datta, S.R., Vasconcelos, M.L., Freeland, J., Looger, L.L., and Axel, R. (2010). A dimorphic pheromone circuit in Drosophila from sensory input to descending output. Nature *468*, 686-690.

Wang, L., Han, X., Mehren, J., Hiroi, M., Billeter, J.C., Miyamoto, T., Amrein, H., Levine, J.D., and Anderson, D.J. (2011). Hierarchical chemosensory regulation of male-male social interactions in Drosophila. Nat Neurosci *14*, 757-762.

Wang, X.J. (2001). Synaptic reverberation underlying mnemonic persistent activity. Trends Neurosci *24*, 455-463.

Yamamoto, D., Sato, K., and Koganezawa, M. (2014). Neuroethology of male courtship in Drosophila: from the gene to behavior. J Comp Physiol A Neuroethol Sens Neural Behav Physiol *200*, 251-264.

Yu, J.Y., Kanai, M.I., Demir, E., Jefferis, G.S., and Dickson, B.J. (2010). Cellular organization of the neural circuit that drives Drosophila courtship behavior. Curr Biol *20*, 1602-1614.

Berridge, K.C. (2004). Motivation concepts in behavioral neuroscience. Physiol Behav *81*, 179-209.

Birmingham, J.T., and Tauck, D.L. (2003). Neuromodulation in invertebrate sensory systems: from biophysics to behavior. J Exp Biol *206*, 3541-3546.

Boyden, E.S. (2011). A history of optogenetics: the development of tools for controlling brain circuits with light. F1000 Biol Rep *3*, 11.

Chiappe, M.E., Seelig, J.D., Reiser, M.B., and Jayaraman, V. (2010). Walking modulates speed sensitivity in Drosophila motion vision. Curr Biol *20*, 1470-1475.

Deisseroth, K. (2010). Controlling the brain with light. Sci Am *303*, 48-55.

Fenno, L., Yizhar, O., and Deisseroth, K. (2011). The development and application of optogenetics. Annu Rev Neurosci *34*, 389-412.

Flavell, S.W., Pokala, N., Macosko, E.Z., Albrecht, D.R., Larsch, J., and Bargmann, C.I. (2013). Serotonin and the neuropeptide PDF initiate and extend opposing behavioral states in C. elegans. Cell *154*, 1023-1035.

Han, S., Yang, W., and Yuste, R. (2019). Two-Color Volumetric Imaging of Neuronal Activity of Cortical Columns. Cell Rep *27*, 2229-2240 e2224.

Harris-Warrick, R.M., and Marder, E. (1991). Modulation of neural networks for behavior. Annu Rev Neurosci *14*, 39-57.

Inagaki, H.K., Panse, K.M., and Anderson, D.J. (2014b). Independent, reciprocal neuromodulatory control of sweet and bitter taste sensitivity during starvation in Drosophila. Neuron *84*, 806-820.

Kennedy, A., Asahina, K., Hoopfer, E., Inagaki, H., Jung, Y., Lee, H., Remedios, R., and Anderson, D.J. (2014). Internal States and Behavioral Decision-Making: Toward an Integration of Emotion and Cognition. Cold Spring Harb Symp Quant Biol *79*, 199-210.

Lee, H., Kim, D.W., Remedios, R., Anthony, T.E., Chang, A., Madisen, L., Zeng, H., and Anderson, D.J. (2014). Scalable control of mounting and attack by Esr1+ neurons in the ventromedial hypothalamus. Nature *509*, 627-632.

Maimon, G., Straw, A.D., and Dickinson, M.H. (2010). Active flight increases the gain of visual motion processing in Drosophila. Nat Neurosci *13*, 393-399.

Nikolenko, V., Watson, B.O., Araya, R., Woodruff, A., Peterka, D.S., and Yuste, R. (2008). SLM Microscopy: Scanless Two-Photon Imaging and Photostimulation with Spatial Light Modulators. Front Neural Circuits *2*, 5.

Pfaff, D.W., Kieffer, B.L., and Swanson, L.W. (2008). Mechanisms for the regulation of state changes in the central nervous system: an introduction. Ann N Y Acad Sci *1129*, 1-7.

Simerly, R.B. (2002). Wired for reproduction: organization and development of sexually dimorphic circuits in the mammalian forebrain. Annu Rev Neurosci *25*, 507-536.

Spunt, R.P., Ellsworth, E., and Adolphs, R. (2017). The neural basis of understanding the expression of the emotions in man and animals. Soc Cogn Affect Neurosci *12*, 95-105.

Yang, C.F., and Shah, N.M. (2014). Representing sex in the brain, one module at a time. Neuron *82*, 261-278.

Yang, W., and Yuste, R. (2018). Holographic imaging and photostimulation of neural activity. Curr Opin Neurobiol *50*, 211-221.

C h a p t e r 2

Optogenetic control of Drosophila using a red-shifted channelrhodopsin reveals experience-dependent influences on courtship

Inagaki HK, Jung Y, Hoopfer ED, Wong AM, Mishra N, Lin JY, Tsien RY, Anderson DJ. "Optogenetic control of Drosophila using a red-shifted channelrhodopsin reveals experience-dependent influences on courtship". *Nat Methods*. 2014 Mar;11(3):325-32. doi: 10.1038/nmeth.2765.

2.1 Summary

Optogenetics allows the manipulation of neural activity in freely moving animals with millisecond precision, but its application in *Drosophila melanogaster* has been limited. Here we show that a recently described red activatable channelrhodopsin (ReaChR) permits control of complex behavior in freely moving adult flies, at wavelengths that are not thought to interfere with normal visual function. This tool affords the opportunity to control neural activity over a broad dynamic range of stimulation intensities. Using time-resolved activation, we show that the neural control of male courtship song can be separated into (i) probabilistic, persistent and (ii) deterministic, command-like components. The former, but not the latter, neurons are subject to functional modulation by social experience, which supports the idea that they constitute a locus of state-dependent influence. This separation is not evident using thermogenetic tools, a result underscoring the importance of temporally precise control of neuronal activation in the functional dissection of neural circuits in *Drosophila*.

2.2 Introduction

D. melanogaster is one of the most powerful model organisms available for the genetic dissection of neural circuit function (Luo et al., 2008; Venken et al., 2011). Likewise, the use of light-sensitive microbial opsins, such as channelrhodopsin, has revolutionized the functional dissection of neural circuits in behaving animals (Fenno et al., 2011; Yizhar et al.,

2011a). Unfortunately, with the exception of larval neurons and peripheral sensory neurons in adults (de Vries and Clandinin, 2013; Gordon and Scott, 2009; Inagaki et al., 2012; Pulver et al., 2009; Schroll et al., 2006; Suh et al., 2007; Venken et al., 2011; Zhang et al., 2007; Zimmermann et al., 2009), this powerful technology and model organism have been largely incompatible in the case of adult flies (but see (de Vries and Clandinin, 2013; Zimmermann et al., 2009)). Therefore, *Drosophila* researchers have, to a large extent, been unable to exploit the rapidly expanding optogenetic toolkit for neural circuit manipulation. Although P2X2, an ionotropic purinergic receptor, has been used as an optogenetic tool in adult *Drosophila*, this technique requires injection of caged ATP into the brains of individual anesthetized flies (Lima and Miesenbock, 2005). This relatively invasive technology is suboptimal for many applications, especially large-scale, high-throughput screening.

In the absence of facile optogenetic manipulation, dTRPA1, a thermosensitive cation channel, has been the preferred method for neuronal activation in freely behaving adult flies (Hamada et al., 2008; Venken et al., 2011). Because this method depends on changes in temperature to control neuronal activity, however, it lacks precision in both the temporal and intensity domains and suffers from potentially confounding influence of temperature changes on behavior.

Here we demonstrate that expression of ReaChR in adult central nervous system (CNS) neurons enables rapid and temporally precise control of behavior in freely moving adult *Drosophila*. Using this optogenetic method, we have separated the control of wing extension, a male-specific courtship behavior, into either probabilistic, state-dependent or deterministic, command-like components. Moreover, by combining ReaChR activation with functional calcium imaging, we have also identified a neural correlate of the influence of social experience on male courtship behavior.

2.3 Result

Optogenetic vs. thermogenetic control of gustatory neurons

We reasoned that previously described channelrhodopsin-2 (ChR2) variants do not work well in adult *Drosophila* owing, at least in part, to low penetrance of blue light through the cuticle. Indeed, direct measurements *in vivo* indicated that the penetrance of blue light through the cuticle is much weaker (~ 1%) than that of longer wavelengths such as green or red light (5–10%) (Fig. 1a). Therefore, we created transgenic flies that express the recently developed red-shifted channelrhodopsins, C1V1(T/T) (Yizhar et al., 2011b) and ReaChR (Lin et al., 2013) under the control of the Gal4–upstream activating sequence (UAS) system, to test whether red-shifted light can penetrate the cuticle sufficiently to activate neurons expressing these channels.

We first compared the efficacy of different opsins to activate sugar-sensing gustatory receptor neurons (GRNs) that express the receptor Gr5a (Scott et al., 2001). Optogenetic activation of Gr5a neurons using ChR2 has previously been shown to trigger the proboscis extension reflex (PER) in *Drosophila* (Inagaki et al., 2012; Zhang et al., 2007). All of the blue light–sensitive opsin variants tested (ChR2 (refs. (Boyden et al., 2005; Nagel et al., 2003)), H134R (ref. (Nagel et al., 2005)) and C128T (ref. (Berndt et al., 2009))) induced PER behavior in response to photostimulation at 470 nm, although only H134R yielded responses in 100% of flies (Fig. 1b). Flies expressing ReaChR in Gr5a GRNs yielded robust PER responses to both red (627 nm) and green (530 nm) light. In contrast, flies expressing C1V1(T/T) did not exhibit PERs in response to either red or green light (Fig. 1b). Instead, they moved their proboscis slightly, albeit in a manner time locked to photostimulation, suggesting that C1V1(T/T) has only a weak ability to activate Gr5a GRNs.

Surprisingly, in flies expressing dTrpA1 in Gr5a GRNs, we did not observe any behavioral response at an ambient temperature known to activate the ion channel (32 °C) ((Hamada et al., 2008; Pulver et al., 2009) (Fig. 1b) or during gradual ramping to this temperature from 22 °C (data not shown). Interestingly, activation of dTrpA1 in Gr5a GRNs using heat pulses

from an infrared (IR) laser (Keene and Masek, 2012) has been reported to induce a PER. Upon continuous current injection, some neurons develop a depolarization block (Bianchi et al., 2012). We reasoned that if Gr5a neurons are continuously or gradually activated via TrpA1, they may undergo a rapid depolarization block that prevents PER behavior. Consistent with this idea, continuous illumination of Gr5a-ReaChR flies produced only a transient PER reaction (half-time for decay, 1.5 s), whereas pulsatile illumination (1 Hz, 100-ms pulse duration) evoked a train of PERs time locked to each light pulse (Fig. 1c).

Consistent with this result, electrophysiological recording of Gr5a GRNs revealed that pulsed light caused continuous bursts of spiking throughout the stimulation period (Fig. 1d,e) with short latencies (Fig. 1f). In contrast, spiking activity decayed exponentially during continuous light stimulation (half-time for decay, ~1.5 s; Fig. 1d,e). The rapid decay of both spiking and PER behavior during continuous activation of ReaChR (Fig. 1g; Pearson's correlation coefficient, $r = 0.96$) suggests that the former likely accounts for the latter.

Similar to the results obtained using continuous ReaChR activation, TrpA1 activation triggered only transient spiking in Gr5a GRNs, with a strong decay after several seconds (Fig. 1h). Together, these data may explain why PER responses were not induced by constitutive or gradual thermal activation in Gr5a-TrpA1–expressing flies (Fig. 1b). They also reconfirm the importance of pulsed activation of neurons to avoid depolarization block, as reported previously in other systems (Yizhar et al., 2011a) (but note that depolarization block does not occur in all neuronal subtypes (Pulver et al., 2009)).

Activation of CNS neurons with ReaChR

Only a few studies have reported successful elicitation of behavior in adult *Drosophila* by activating CNS neurons expressing blue light–sensitive opsins (de Vries and Clandinin, 2013; Zimmermann et al., 2009). To determine whether activation using ReaChR would be more effective, we directly compared the behavioral responses of flies expressing blue light– and red light–sensitive opsins in *GAL4* lines driving expression in different populations of CNS neurons. These lines included *hb9* (*exex*)-*GAL4* (Odden et al., 2002), whose activation

induces side walking and, at higher intensities, paralysis (loss of postural control and immobility); *Corazonin* (*Crz*)-*GAL4*, whose activation induces abdominal bending and ejaculation (Tayler et al., 2012); *fru*-*GAL4* (Stockinger et al., 2005), which labels ~1,500 neurons throughout the brain and whose activation in males induces mating behavior including wing extension (von Philipsborn et al., 2011) and abdominal bending, and at higher intensities, paralysis is observed; and P1-*GAL4*, a 'split' *GAL4* (Luan et al., 2006; Pfeiffer et al., 2010) driver generated from parental *GAL4* lines (Jenett et al., 2012) identified in a behavioral screen (E.D.H. and D.J.A., unpublished data) that is specifically expressed in ~16–20 male-specific P1 neurons and whose activation elicits wing extension in males in the absence of females (Pan et al., 2012; von Philipsborn et al., 2011). To facilitate the control and monitoring of light-induced behaviors in freely moving adult flies in a high-throughput, cost-effective and flexible manner, we developed a high-power LED–based activation system (Fig. 2a–c; Supplementary Fig. 1).

Strikingly, among all five opsins tested using these CNS drivers, ReaChR was the only one whose activation yielded robust behavioral phenotypes in a light-dependent manner (Fig. 2d). The evoked behaviors were not due to innate responses to light: control flies lacking UAS-ReaChR did not exhibit them in response to all the wavelengths tested (Fig. 2d). The fact that blue light–activated opsins yielded a behavioral response (PER) when expressed in GRNs but not in the CNS neurons tested here likely reflects the fact that the peripheral GRNs are located close to the cuticle, where blue light may penetrate more easily. Analysis of C1V1(T/T) expression in CNS neurons revealed that this opsin is expressed weakly in cell somata and not trafficked to arborizations, whereas ReaChR is strongly expressed in somata and is trafficked to arborizations as well (Supplementary Fig. 2a). This difference likely accounts for the different efficacies of the two red-shifted opsins in this system.

The peak of the ReaChR action spectrum (measured in cultured hippocampal neurons) is ~590 nm (Lin et al., 2013). The efficacy of ReaChR activation by different wavelengths in freely behaving flies will, however, reflect a combination of factors including cuticular penetration and intensity as well as proximity to peak sensitivity. To empirically determine

the optimal wavelength of light for behavioral assays, therefore, we compared the ability of blue (470-nm), green (530-nm), amber (590-nm) and red (627-nm) light to induce behavior in flies expressing ReaChR under the control of different CNS *GAL4* drivers. When not normalized for intensity, green LEDs had the strongest capacity to elicit ReaChR-dependent behaviors (Fig. 2d,f,g). In some cases (pIP10 neurons; see below), robust behavioral responses were detected only using green light and hardly at all using other wavelengths. Although amber light is closest to the peak of the ReaChR action spectrum, commercial LEDs of this wavelength are dimmer than the others and therefore did not elicit strong behavioral responses (Fig. 2f,g).

Although TrpA1-mediated activation of P1 neurons can elicit wing extension (Pan et al., 2012; von Philipsborn et al., 2011), in our direct comparison the fraction of solitary male flies showing a wing extension phenotype was much higher using ReaChR and green light than using TrpA1 (Fig. 2d). This suggests that the intensity of activation obtained using ReaChR (and green light) can be substantially stronger than that achieved using dTrpA1, without subjecting flies to the high temperatures necessary to activate the latter. Nevertheless, although green LEDs elicited the strongest behavioral responses, flies can see this wavelength, whereas their sensitivity to wavelengths >620 nm is much lower (Stavenga, 2002; Yamaguchi et al., 2010) (see, however, (Hanai et al., 2008)). Therefore, we used red LEDs whenever possible to avoid behavioral artifacts caused by strong visual stimulation.

To investigate whether the strength of a given ReaChR-dependent behavioral phenotype can be quantitatively tuned, we tested multiple frequencies and intensities of light pulses using the P1-*GAL4* driver (pulse width, 5 ms). There was a frequency-dependent increase in the fraction of flies showing wing extension as well as in the average number and duration of wing extension bouts per fly (Fig. 2e and Supplementary Fig. 2e), even when we corrected for the total duration of illumination (Supplementary Fig. 2f). The *hb9-GAL4* and *fru-GAL4* drivers also yielded an increase in the fraction of flies showing the respective behavioral responses as the intensity was increased, albeit over different ranges (Fig. 2f,g).

Together these data indicate that ReaChR can be used to tune behavioral phenotypes by varying the light intensity and/or pulse frequency, over a relatively broad dynamic range.

Probabilistic vs. deterministic control of wing extension

Previous studies of the neural circuitry underlying male courtship behavior in *Drosophila* have used neuronal activation methods, including P2X2 and TrpA1, to identify different neuronal subclasses that control courtship song (Clyne and Miesenbock, 2008; Kohatsu et al., 2011; Pan et al., 2012; von Philipsborn et al., 2011). In particular, studies using TrpA1 have described two neuronal classes in the central brain controlling this behavior: one, called P1 or pMP4, constitutes a population of interneurons (Kohatsu et al., 2011; Pan et al., 2012; von Philipsborn et al., 2011), and the other, called pIP10, constitutes a small group of descending neurons that project to the ventral nerve cord (von Philipsborn et al., 2011) (Fig. 3b). The presynaptic terminals of P1 neurons overlap with the dendrites of pIP10 neurons, which suggests that they may be synaptic partners (von Philipsborn et al., 2011); however, the difference, if any, between the roles of these neurons in controlling courtship song has not been apparent, as similar behaviors are evoked by TrpA1-mediated stimulation of both classes (von Philipsborn et al., 2011).

We used the time-resolved control of neuronal activation afforded by ReaChR to compare the temporal patterns of stimulation-evoked behavioral responses in P1 versus pIP10 neurons. To express ReaChR in the latter cells, we used an intersectional strategy combining a specific *GAL4* line (VT40556; (von Philipsborn et al., 2011)) with *fru-FLP* (Yu et al., 2010) and a UAS>mCherry>ReaChR transgene (where ">" denotes *FRT* sites, the target of Flp recombinase; see Supplementary Fig. 2b,c). Anatomical analysis using a Citrine reporter fused to the C terminus of ReaChR confirmed the restricted expression of ReaChR in flies of the appropriate intersectional genotype (Supplementary Fig. 2d).

Surprisingly, we found that the temporal dynamics of wing extension evoked by activation of P1 and pIP10 neurons were strikingly different. ReaChR-mediated activation of P1 neurons evoked wing extension in a probabilistic or stochastic manner: the initiation of wing

extension was not time locked to the onset of illumination but rather occurred with variable latencies throughout the stimulation period (17.7 ± 27.5 s (mean ± s.d.); Fig. 3a,c). The average duration of each bout was short (0.99 ± 0.48 s) relative to the duration of photostimulation (30 s). Finally, the termination of the behavior was not time locked to the termination of stimulation; rather, we observed persistent wing extension bouts in the intervals between photostimulation trials (Fig. 3a,e; Pearson's correlation coefficient between stimulation pattern and behavioral response, $r = 0.004$).

In contrast to the results observed with P1 neurons, activation of pIP10 neurons triggered robust wing extension in a deterministic manner (Fig. 3a). The onset of the behavior was strongly time locked to the onset of stimulation, with a very short latency (0.08 ± 0.04 s; Fig. 3a,c). Once initiated, wing extension continued throughout the photostimulation period and terminated, with few exceptions, with the end of photostimulation (Fig. 3a,d; Pearson's correlation coefficient between stimulation pattern and behavioral response, $r = 0.993$). With weaker intensities of illumination close to the wing extension response threshold (≤0.012 mW/mm^2), such responses were less efficiently evoked; but responses were still restricted to the photostimulation period, and no persistent behavior between trials was observed (Supplementary Fig. 3a).

These differences between P1 and pIP10 neurons in the temporal dynamics of ReaChR activation-evoked wing extensions do not reflect a higher sensitivity of pIP10 neurons relative to P1 neurons because the intensity dependence of pIP10-evoked wing extension by green light was almost identical to that of P1 neurons (Fig. 3f). Moreover, these properties were largely independent of illumination intensity (Figs. 4 and 5).

Social isolation modulates ReaChR-activated wing extension

The probabilistic or biasing nature of the wing extension responses elicited by ReaChR-mediated activation of P1 neurons suggested that these neurons might encode, or be modified by, state-dependent influences on male courtship behavior. Interestingly, social isolation of male flies for more than several days enhances courtship behavior, including singing, toward

females (Dankert et al., 2009). To investigate whether P1 neurons might be modulated by such experience, we first determined whether social isolation lowers the threshold for eliciting wing extension by using ReaChR-mediated stimulation of these neurons. Indeed, the intensity of red light that evoked wing extension in 50% of flies expressing ReaChR in P1 neurons was lower in males that were socially isolated for 7 d (single housed males, or SH) than in group-housed males (GH; Fig. 4). A similar effect was observed using green light (Supplementary Fig. 3b). For each of three different parameters measured, socially isolated flies exhibited significantly higher values than group housed flies (Fig. 4c). Thus, social isolation effectively 'tuned' the response to ReaChR activation of P1 neurons such that the probability of a wing extension response was increased. These data suggest that the increased sensitivity to ReaChR activation of wing extension occurs in P1 neurons themselves, or in a functionally downstream population.

Because pIP10 neurons are thought to be functionally downstream of P1 neurons (von Philipsborn et al., 2011) (Fig. 3b), we investigated whether ReaChR activation of wing extension via these descending neurons was also sensitive to social experience. Because red light was not strong enough to activate wing extension in male flies expressing ReaChR in pIP10 neurons, we used green light to trigger wing extension. Activation of pIP10 neurons using ReaChR did not reveal any differences between singly housed and group-housed flies in the efficiency with which photostimulation evoked wing extension behavior, even at lower intensities that evoked responses in only a subset of flies (Fig. 5). These data indicate that the enhanced sensitivity of ReaChR-evoked wing extension in singly housed flies using the P1-*GAL4* driver is likely to occur in P1 neurons themselves (or in other downstream neurons) rather than in pIP10 neurons. They also indicate that the sensitization of the P1 response by social isolation does not reflect a general increase in sensitivity among all neurons involved in wing extension behavior.

Functional calcium imaging combined with ReaChR activation

To examine directly whether social isolation enhances the sensitivity of P1 neurons to ReaChR activation, we performed calcium imaging experiments in isolated fly brains using

laser-scanning two-photon microscopy, taking advantage of the relative separation of the action spectrum peaks for ReaChR and GCaMP3.0 ((Tian et al., 2009); Fig. 6a). Notably, coexpression of GCaMP3.0 in P1 neurons together with ReaChR did not diminish the ability of the latter to mediate light-evoked wing extension in freely moving flies, a result indicating that the calcium-buffering effect of GCaMP3.0 does not interfere with this behavior (data not shown).

An amber LED (590 nm) was used for photostimulation during imaging experiments in order to maximize overlap with the peak of the ReaChR action spectrum. Excitation scanning caused an initial increase in baseline GCaMP3.0 fluorescence in fly brains coexpressing ReaChR in P1 neurons, even in the absence of amber light excitation of ReaChR (Fig. 6b). These increases were not observed in fly brains lacking UAS-ReaChR, a result implying that they reflect cross-activation of ReaChR by the GCaMP3.0 excitation beam (925 nm). Nevertheless, amber light still evoked a clear increase in the strength of GCaMP3.0 emissions over this background (Fig. 6b).

Using these conditions, we compared the GCaMP3.0 response of P1 neurons to ReaChR activation of these same neurons in brains from singly housed and group-housed flies. P1 neurons in SH fly brains showed larger ReaChR-evoked calcium influxes than did GH fly brains (Fig. 6b,c). Quantitative analysis of ReaChR-Citrine expression in these cells indicated that this difference was not due to higher levels of P1-*GAL4* expression in SH flies (Fig. 6d). Together these behavioral and imaging experiments suggest that the excitability of P1 neurons can be modulated by prior social experience. Attempts to monitor calcium transients in pIP10 neurons were precluded by the complex expression pattern and low level of GCaMP3 expression driven by this *GAL4* line.

2.4 Discussion

Here we describe a system for optogenetic activation of behavior in freely moving adult flies using ReaChR, a newly described red-shifted opsin (Lin et al., 2013). The strength of activation obtained using ReaChR, and the broad dynamic range of intensities and frequencies over which stimulation can be delivered, translates to a more quantitative and temporally controlled approach to investigating the neuronal control of behavior than that provided by available thermogenetic tools (but see (Keene and Masek, 2012)). The use of ReaChR with red light also reduces the confounding influence of strong visual stimulation that occurs when using blue light–activated opsins or with the temperature increases required by thermogenetic effectors. Finally, the ability to control activation using LEDs, rather than lasers (Keene and Masek, 2012; Lima and Miesenbock, 2005), permits a relatively inexpensive approach for large-scale, high-throughput screening of behaviors.

Using ReaChR to monitor both behavioral sensitivity and neuronal activation, we discovered that (i) P1 and pIP10 neurons control male courtship song in a state-like (probabilistic and persistent) and command-like (deterministic and time-locked) manner, respectively; and (ii) the effect of social isolation to increase male courtship behavior is mediated, at least in part, through an increase in the excitability of P1 neurons. It has been proposed, on the basis of anatomical data, that P1 neurons are part of a circuit integrating multimodal sensory cues that control courtship behavior (Yu et al., 2010). Our observations suggest that P1 neurons also integrate this information with the flies' history of social experience, in a manner that influences the probability that the flies will exhibit courtship behavior. To our knowledge, this represents the first observation of a neural correlate of social experience in *Drosophila*. Interestingly, we did not observe any evidence of persistent calcium transients in P1 neurons after photoactivation, which implies that the persistent wing extension triggered by P1 activation is mediated by other neurons. The mechanisms underlying the influence of social state on P1 excitability, and persistent activity, are interesting topics for future investigation.

Although ReaChR-based activation of behavior was effective in all the *GAL4* lines tested, the optogenetic toolkit in *Drosophila* could benefit from further engineering of red-shifted

opsins with a narrower action spectrum and faster kinetics, and also by development of red-shifted variants of inhibitory opsins. Together such tools would further enhance the applicability of optogenetics to neural circuit dissection in *Drosophila*.

2.5 Main figures

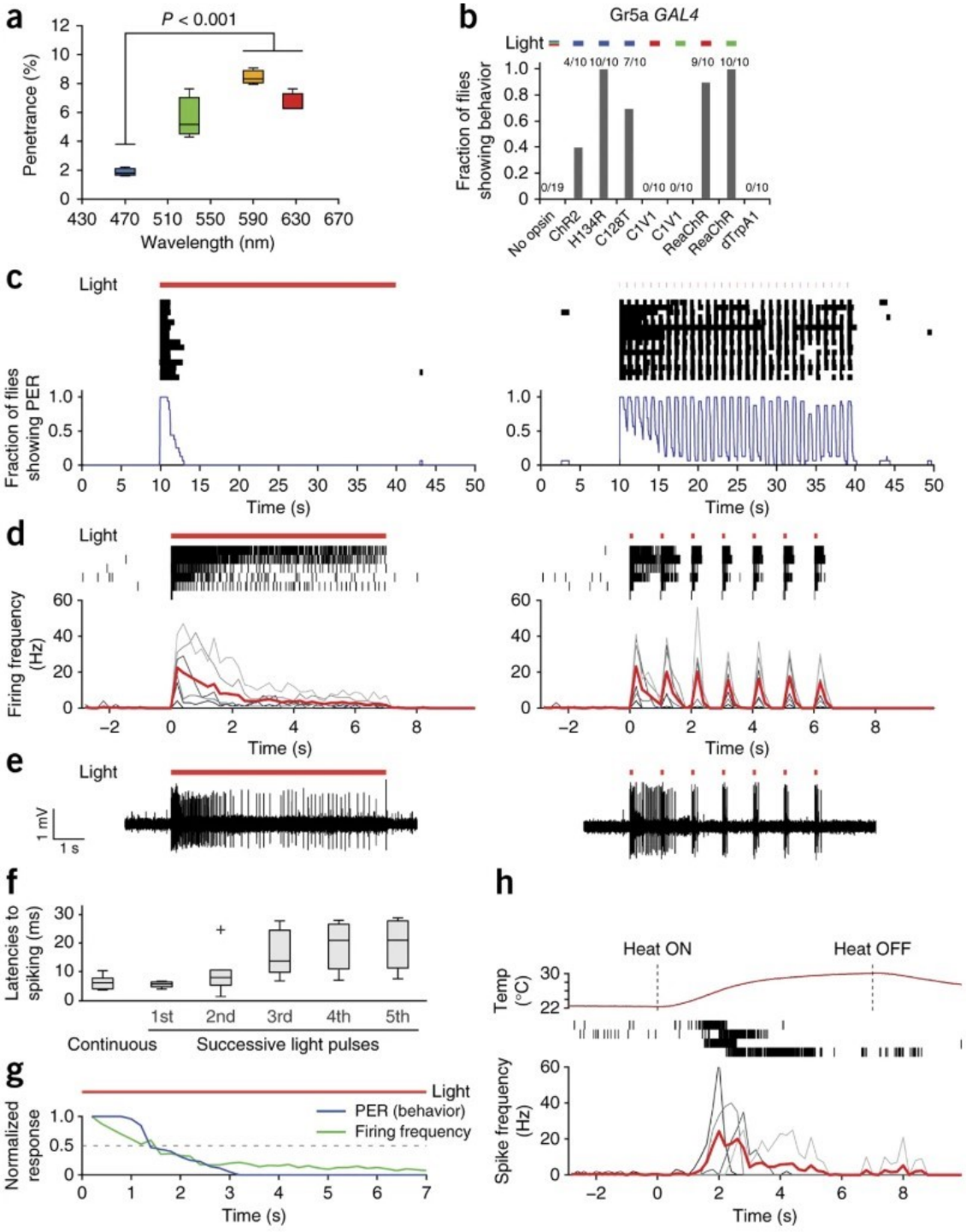

Figure 2.1: Optogenetic versus thermogenetic control of Gr5a GRNs.

(a) Penetrance of light through the adult fly cuticle. $n = 3$. $P = 0.0046$ for one-way ANOVA followed by *t*-test with Bonferroni correction ($P < 0.001$). (b) Fraction of flies showing PER triggered by different opsins expressed in Gr5a GRNs. Fractions indicate the number of responders out of the number of flies tested. Activation wavelengths are represented as blue (470 nm), green (530 nm) and red (627 nm) bars. For the no-opsin control, all the wavelengths were tested. (c–e) Behavioral (c) and electrophysiological (d,e) responses of flies expressing ReaChR in Gr5a GRNs. Red lines (c–e) represent the photostimulation pattern (627 nm, 1.1 mW/mm^2); pulsed photostimulation (right) was delivered at 1 Hz (100-ms pulse width). In c, raster plots show PER bouts, and blue curves show the fraction of flies showing PER (time bins: 1 s; $n = 16$). In d, raster plots show Gr5a GRNs spikes; the lower plots show average spiking rate (red) and spiking rates for individual flies (gray; time bins, 200 ms; $n = 6$). (e) Sample traces. (f) Latencies to first spike following photostimulation onset from d. Box plot whiskers represent 1.5× interquartile range of the lower and upper quartiles; box limits indicate lower quartile, median and upper quartile, from bottom to top; "+" indicates outlier data beyond the whiskers. (g) Overlay of normalized PER and firing frequencies during continuous photostimulation based on c,d. (h) Top, measured temperature change caused by a heat source placed near the labellum. Center, plots representing spikes in Gr5a GRNs expressing dTrpA1. Bottom, spiking responses plotted as in d; $n = 4$.

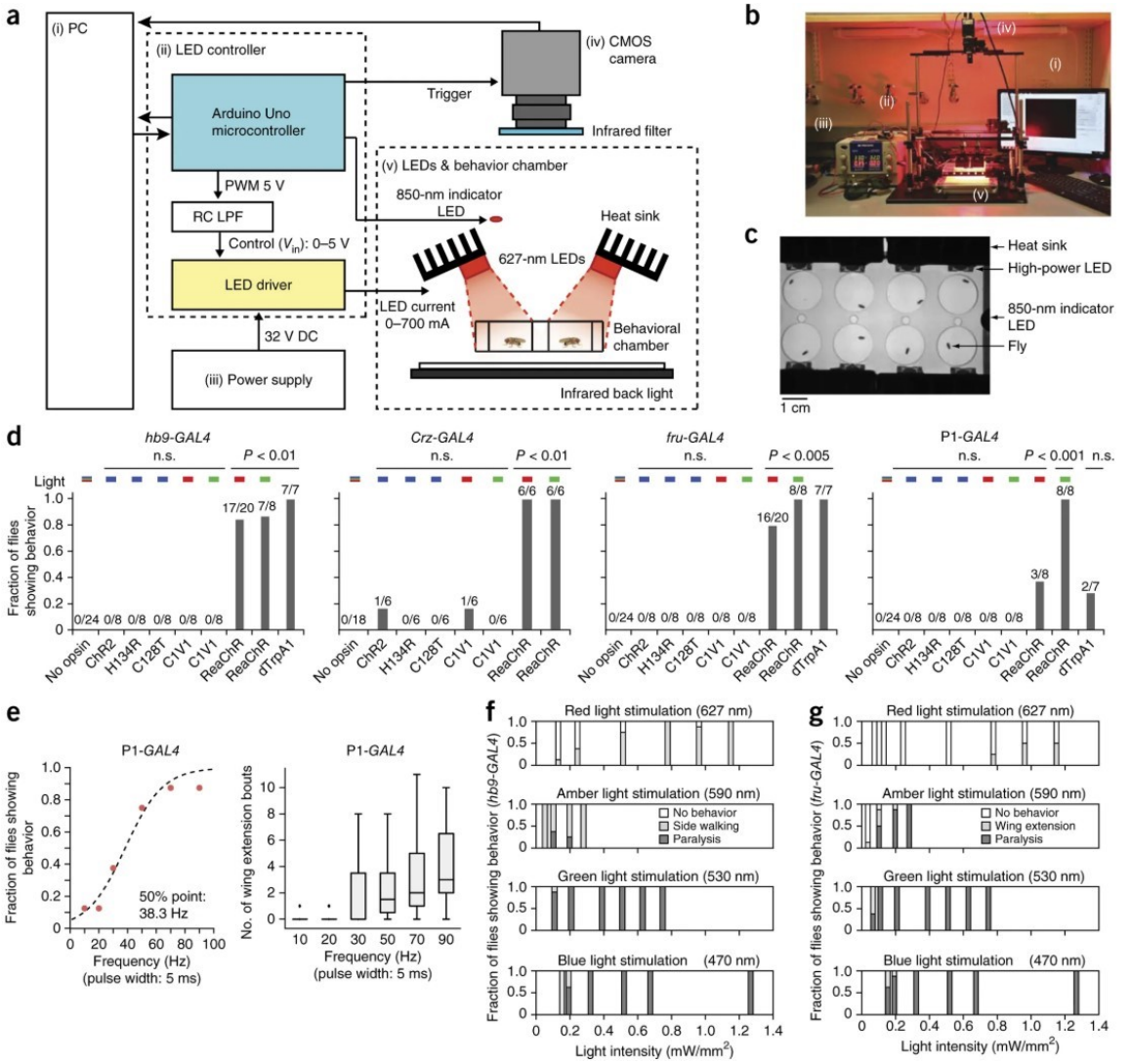

Figure 2.2: ReaChR enables light-dependent activation of CNS neurons in *Drosophila*.

(**a**,**b**) Experimental setup for high-power LED–based activation system. Each roman numeral in the diagram (**a**) corresponds to that in the photograph (**b**) (see Supplementary Fig. 1). PWM, pulse-width modulation; RC LPF, resistor-capacitor low-pass filter; CMOS, complementary metal-oxide semiconductor. (**c**) View from the CMOS camera. (**d**) Comparison of behavioral responses of flies expressing different channelrhodopsin variants in distinct CNS subpopulations. Plot properties are as in Figure 2.1b. "Fraction of flies showing behavior" indicates side-walking or knockout phenotype (*hb9-GAL4*), ejaculation (*Crz-GAL4*), wing extension or knockout (*fru-GAL4*), or wing extension (P1-*GAL4*). "No

opsin" is the empty promoter *GAL4* (BFP-*GAL4*) crossed with UAS-ReaChR. Flies showing any of the characteristic behaviors during 1 min of continuous photostimulation were scored as responders. *P* values represent Fisher's exact test with Bonferroni correction (comparing no-opsin control with each column). *P* values for significant columns in **d**, from left to right and each $\times 10^{-4}$, are 4.3, 56, 12, 77, 77, 13, 6.2, 12 and 6.2. n.s., not significant. (**e**) ReaChR-mediated activation of P1 neurons using different frequencies of red light pulses (627 nm, 1.1 mW/mm^2, 1 min) (P1-*GAL4*; UAS-ReaChR(attP40)). The fraction of flies showing wing extension during 1-min photostimulation trials was fitted by a sigmoidal function to calculate the 50% point. $n = 8$. Box plots properties are as in Figure 2.1f. (**f**,**g**) Fraction of flies exhibiting characteristic behaviors at different photostimulation intensities and wavelengths, in animals expressing *hb9-GAL4* (**f**) or *fru-GAL4* (**g**) and UAS-ReaChR. $n = 8$.

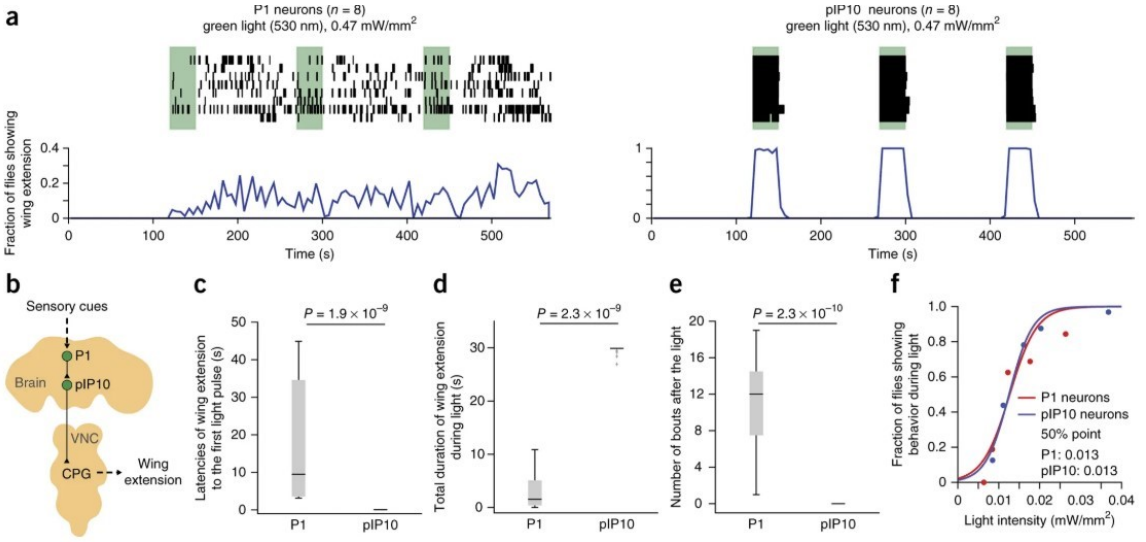

Figure 2.3: Probabilistic versus deterministic optogenetic control of courtship song.

(**a**) Activation of P1 neurons (P1-*GAL4*; UAS-ReaChR(VK5)) (left) and pIP10 neurons (VT40556/UAS>mCherry>ReaChR(attP40); *fru-FLP*) (right) with green light (530 nm, 0.47 mW/mm^2). Top, raster plot representing wing extension bouts (n = 8 flies per genotype). Green bars represent 30-s continuous photostimulation trials with 120-s intertrial intervals. Bottom, fraction of flies showing wing extension (time bins, 5 s). Note the different y-axis scales. P1 responses during trials 2 and 3 are more clearly phased to the onset of photostimulation at lower light intensities (Supplementary Fig. 3a). (**b**) Schematic illustrating neuronal circuit control of courtship song, simplified from (von Philipsborn et al., 2011). VNC, ventral nerve cord; CPG, central pattern generator. (**c**) Latency to first wing extension after onset of the first photostimulation. (**d**) Total duration of wing extension during photostimulation. (**e**) Number of wing extension bouts during 30 s following photostimulation termination. Plots in **c**–**e** are based on data in **a**. P values represent Mann-Whitney U tests. Box plots properties are as in Figure 2.1f. (**f**) Fraction of flies showing wing extension during a single photostimulation trial as a function of light intensity (green light: 530 nm, continuous, 30 s). The data were fitted by a sigmoidal function to calculate the 50% point. n = 32 for both P1 neurons and pIP10 neurons.

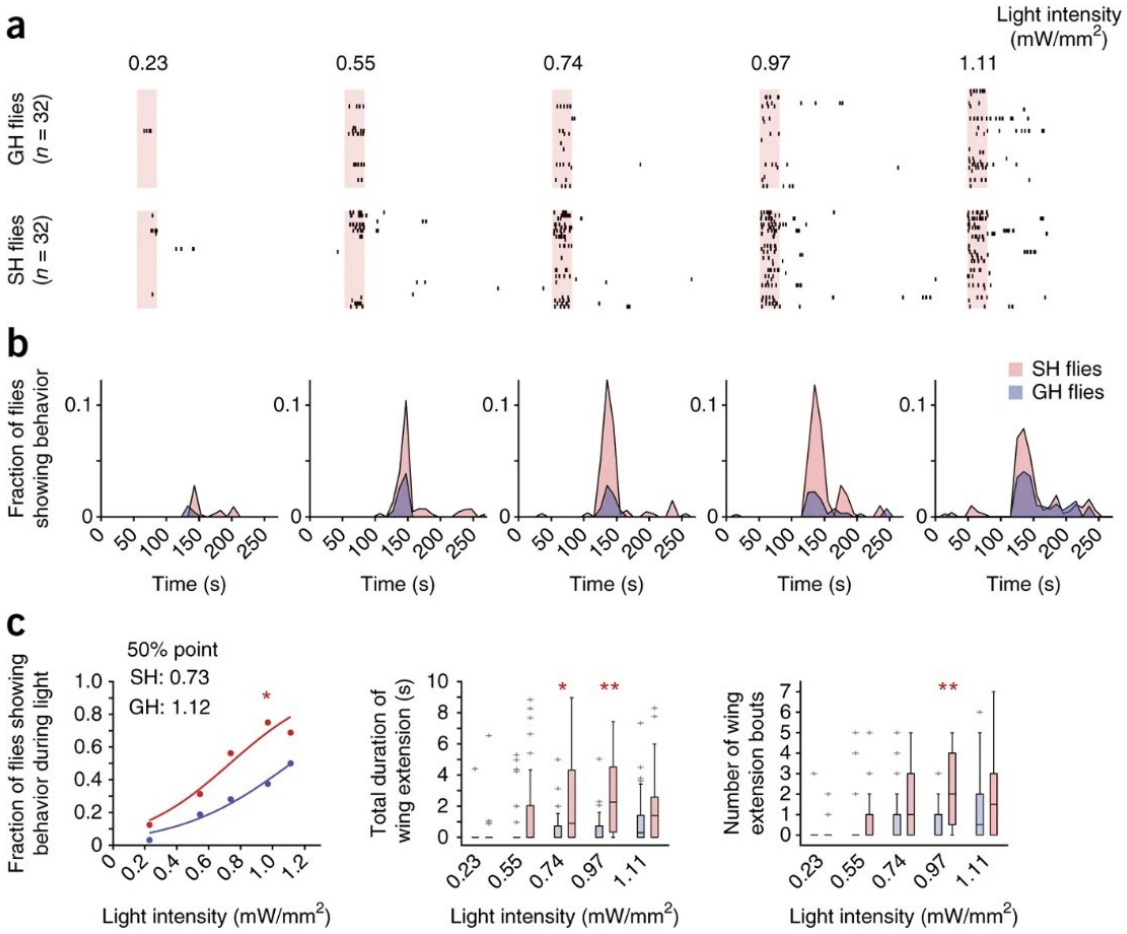

Figure 2.4: Social isolation lowers the threshold for ReaChR-activated male courtship behavior.

(**a**) Raster plots representing wing extension bouts from group-housed (GH) or singly housed (SH) flies expressing ReaChR in P1 neurons (P1-*GAL4*/UAS-ReaChR(VK5)). Flies were activated with different intensities of red light (627 nm). Light red bars in raster plots indicate photostimulation trials (30 s of continuous light), with different intensities indicated above the bars; $n = 32$ flies per intensity. (**b**) Fraction of flies showing wing extension based on the raster plots in **a**. Data were binned every 10 s. The time scale is the same in **a** and **b**. (**c**) Different parameters extracted from the raster plots in **a**. Properties of box plots are as in Figure 2.1f; "+" indicates outlier data larger than the upper whisker. *P* values were obtained from Friedman's test comparing SH and GH flies ($P = 6.3 \times 10^{-28}$) followed by

Fisher's exact test with Bonferroni correction comparing SH and GH flies at each intensity of light (*P = 0.01) (**c**, left); Kruskal-Wallis one-way ANOVA followed by Mann-Whitney U tests with Bonferroni correction (*P = 0.027 and **P < 0.005) (**c**, center and right); and Kruskal-Wallis one-way ANOVA $P = 6.4 \times 10^{-11}$ (**c**, center) and $P = 8.2 \times 10^{-12}$ (**c**, right).

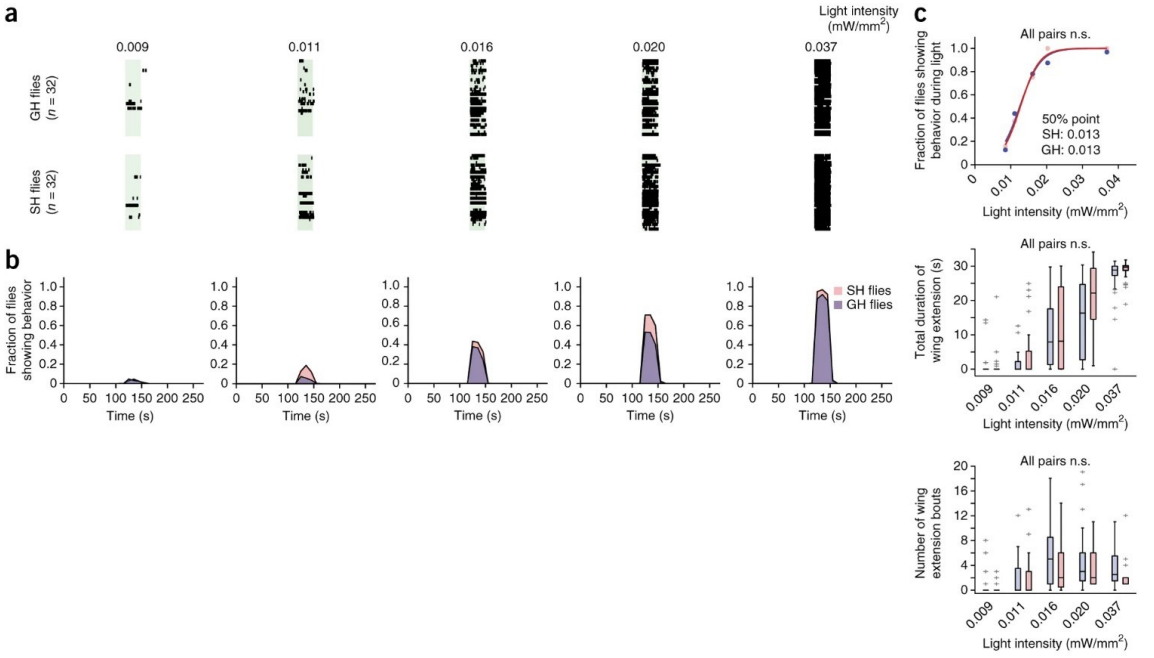

Figure 2.5: Optogenetic activation of pIP10 neurons is not modulated by social isolation.

(**a**) Raster plot representing wing extension bouts from group-housed (GH) or singly housed (SH) flies expressing ReaChR in pIP10 neurons (VT40556-*GAL4* (Bianchi et al., 2012)/UAS>mCherry>ReaChR(attP40); *fru-FLP*). Flies were activated with different intensities of green light (530 nm). Green bars indicate photostimulation trials (30 s of continuous light), with different intensities indicated above the bars. $n = 32$ flies per intensity. (**b**) Fraction of flies showing wing extension based on the raster plot in **a**. The time scale is the same in **a** and **b**. (**c**) Different parameters extracted from the raster plots in **a**. The GH data in the top of **c** (blue points) are the same as those used in Figure 2.3f and are replotted here for comparison purposes. Data were evaluated using Friedman's test comparing SH and GH flies followed by Fisher's exact test with Bonferroni correction comparing SH and GH at each light intensity (top) and using Kruskal-Wallis one-way ANOVA followed by Mann-Whitney *U* tests with Bonferroni correction (middle and bottom). All statistical tests yielded $P > 0.05$ (n.s., not significant). Properties of box plots are as in Figure 2.1f.

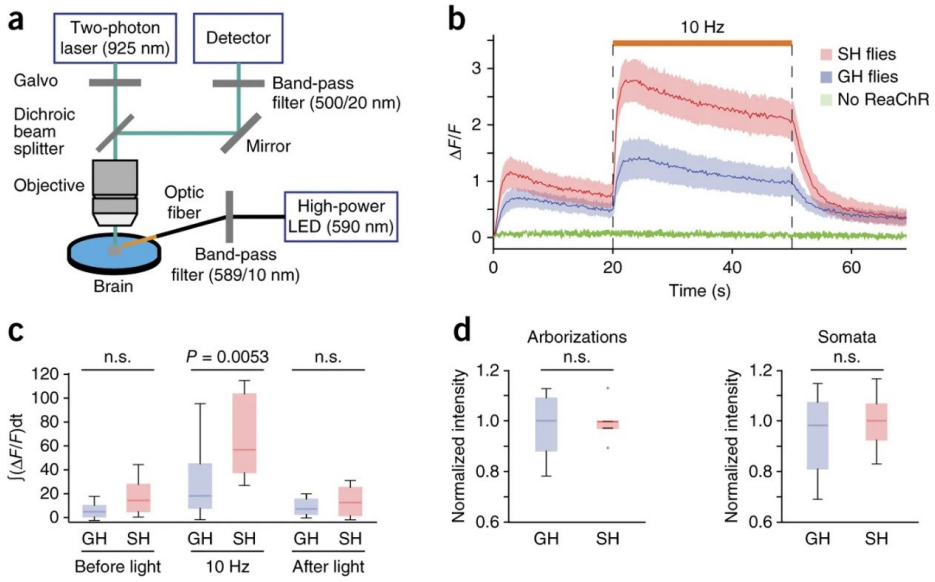

Figure 2.6: Functional calcium imaging of P1 neurons.

(**a**) Experimental setup for calcium imaging. (**b**) Responses of P1 neurons (Δ*F*/*F*, normalized fluorescence change) to ReaChR activation were monitored using two-photon laser-scanning microscopy. Flies expressing both ReaChR and GCaMP3 in P1 neurons (P1-*GAL4*/UAS-ReaChR(attP40); UAS-GCaMP3(VK5)) were singly housed (SH; $n = 11$) or group-housed (GH; $n = 16$) and their brains were imaged. Amber light (590 nm, 1.7 mW/mm^2) with a 5-ms pulse width was delivered at 10 Hz for 30 s (orange line above traces). GCaMP3.0 emissions were monitored in the arborizations of P1 neurons. Flies expressing GCaMP3.0 but not ReaChR in P1 neurons (P1-*GAL4*; UAS-GCaMP3(VK5)) were used as negative controls ($n = 3$). Solid red and blue lines represent average traces, and envelopes indicate s.e.m. (**c**) Quantification of fluorescence changes. ∫(Δ*F*/F)dt, integrated Δ*F*/*F* during 30 s of light activation. Data were analyzed from **b**. n.s., not significant. (**d**) Expression level of ReaChR at the arborizations and somata of P1 neurons were quantified using a Citrine tag fused to the C terminus of ReaChR. *P* values were obtained from Mann-Whitney *U* tests with Bonferroni correction. Box plots properties are as in Figure 2.1f.

2.6 Supplementary figures

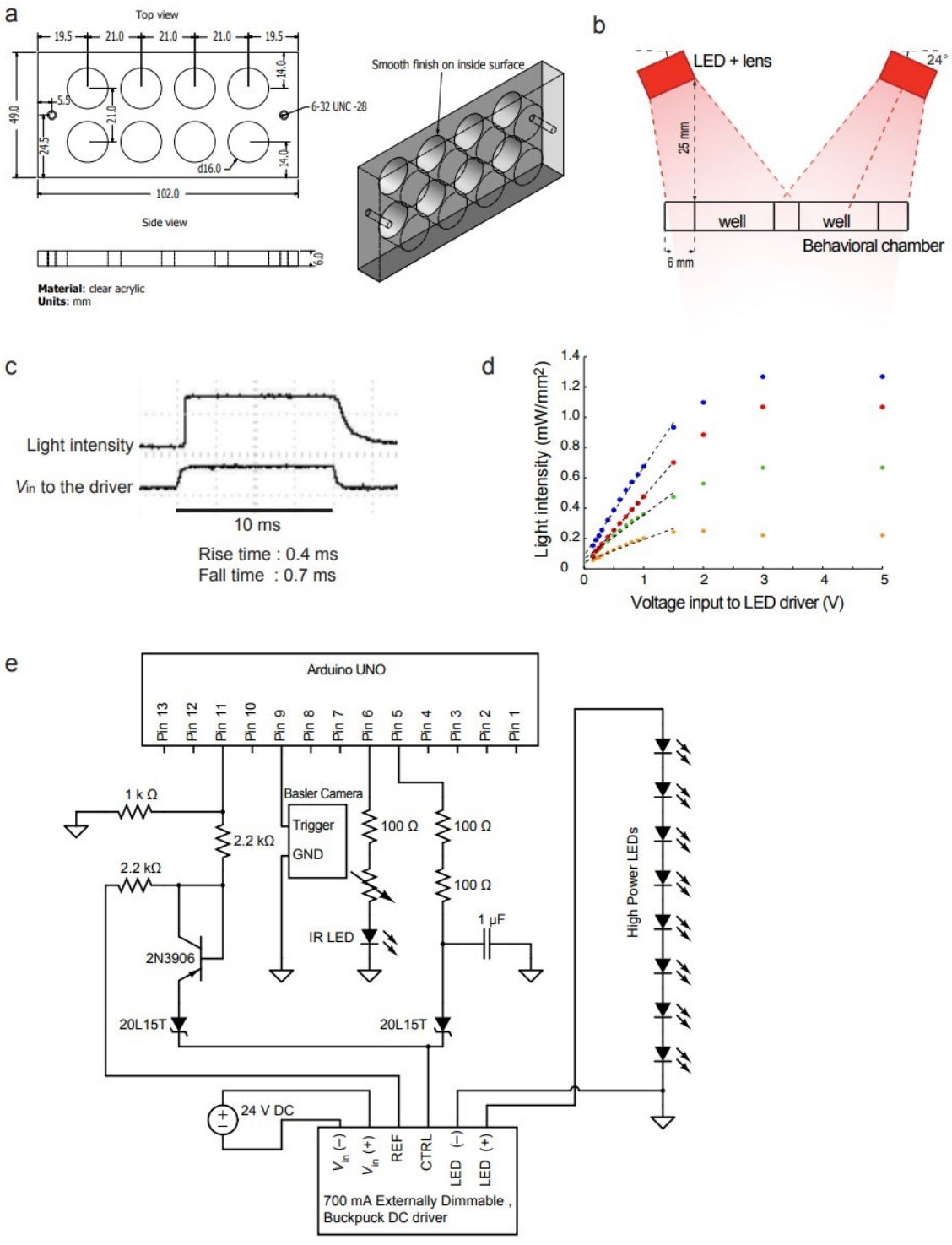

Supplementary Figure 2.1: Detail of the behavioral experimental setup.

(a) Design of the behavioral chamber. A top plate with holes to introduce flies into the chambers (not shown here), and a bottom plate (not shown here), are attached with screws to this behavioral chamber. (b) Alignment of LEDs with the behavioral chamber. Light beams are angled towards the center of the behavioral wells. Each LED delivers light to each well. (c) Light intensity of the LED and voltage input from the Arduino UNO board (Smart Projects, Italy) to the LED driver were simultaneously monitored. Start-up delay of LED is 0.4 msec and turn-off delay of LED is approximately 0.7 msec. (d) Relationship of light intensity inside the behavioral chamber and voltage input to the LED driver. Points with different color represent LEDs of different wavelengths (Red: 627 nm, Amber: 590 nm, Green: 530 nm, Blue: 470 nm). Dotted lines indicate linear dynamic ranges for each type of LED. (e) Electric circuit diagram for the LED controller. This circuit was built on a custom Arduino shield. With the Arduino program (downloadable from the online version of this paper), this electric circuit controls high power LEDs. Intensity, pulse width, pulse frequency, length of pulse train, and the number of and interval between repeated pulse trains are controllable for up to 8 of 700 mA LEDs in parallel.

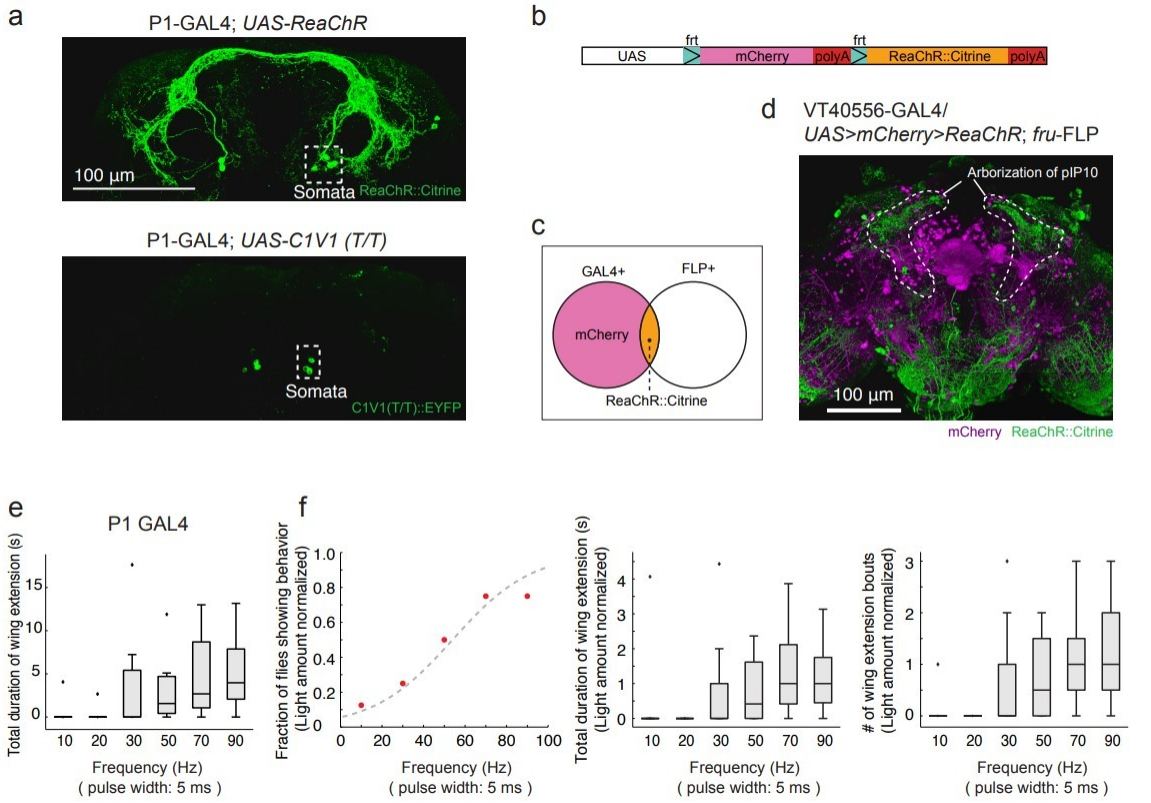

Supplementary Figure 2.2: Expression of ReaChR in the brain and ReaChR-based activation of behaviors with different frequencies.

(a) Expression and trafficking of ReaChR (top) and C1V1(T/T) (bottom) in P1 neurons in adult flies. Note that both opsins are expressed at cell somata (box with a white dotted line), but only ReaChR is trafficked to the arborizations. Both of the opsins are visualized with a citrine or YFP tag immunostained with anti-GFP antibody. (b) Design of the UASfrt-mCherry-frt-ReaChR transgene (Note that ReaChR is tagged with citrine). (c) Diagram representing the intersectional approach for labeling pIP10 neurons. (d) Representative confocal projection of whole-mount brain from VT40556 (GAL4) / UASfrt-mCherry-frt-ReaChR (UAS>stop>ReaChR) (attP40); fru-FLP flies. (e) Relationship between pulse stimulation frequencies and total duration of wing extensions in flies expressing ReaChR in P1 neurons (P1-GAL4; UAS-ReaChR (VK5)). Parameters are extracted from the same data used for Fig. 2e. Boxplot properties are as in Fig.2. (f) Relationships of frequencies of light

pulses and behavior in flies expressing ReaChR in P1 neurons, after normalization for the total amount of light delivered at different frequencies. For normalization purpose, behaviors during different durations of light activation were counted (first 60, 30, 20, 12, 8.57, and 6.67 sec during the activation for 10, 20, 30, 50, 70, 90 Hz, respectively). Parameters are extracted from the same data used for Fig. 2e. Boxplot properties are as in Fig. 2.

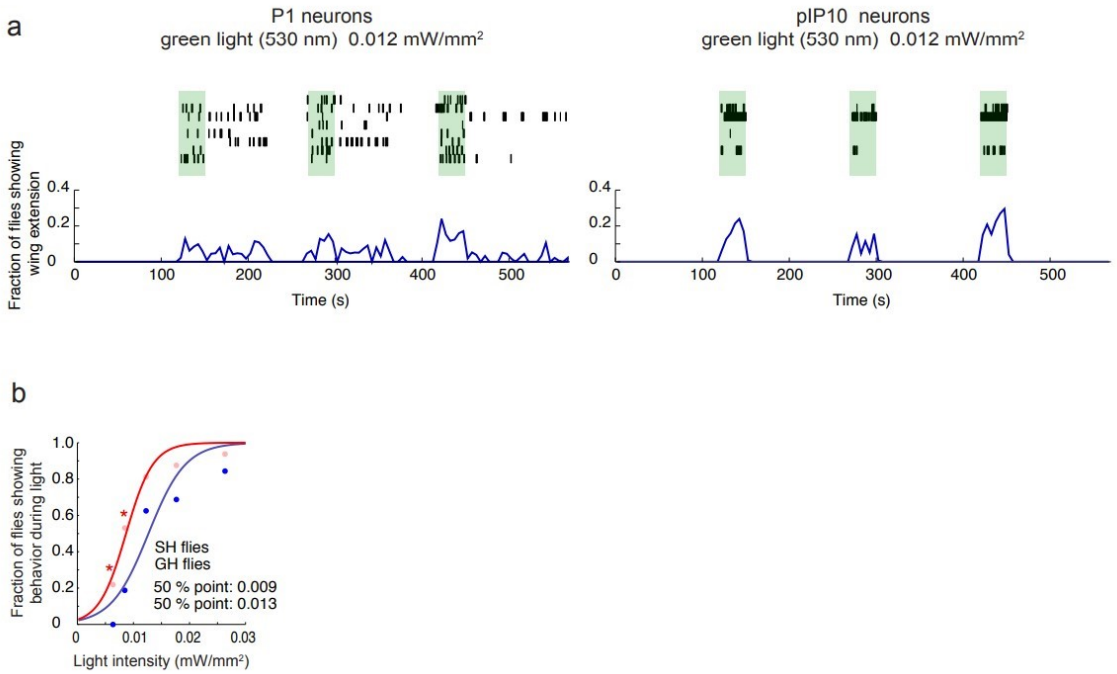

Supplementary Figure 2.3: ReaChR- based activation of P1 neurons.

(a) Activation of P1 neurons (P1-GAL4; UAS-ReaChR(VK5) (left) and pIP10 neurons (VT40556/UAS>stop>ReaChR (attP40); fru-FLP) (right) with green light (530 nm, 0.012 mW/mm2). Top: Raster plot representing wing extension bouts (n = 8 flies per genotype). Green bars represent 60 sec continuous photostimulation with 300 sec inter-trial intervals. Bottom: Fraction of flies showing wing extension (time bins: 5 sec). Note that regardless of photostimulation conditions (see also Figs. 3,4), ReaChR-based activation of P1 neurons triggers stochastic and persistent wing extensions. (b) Fraction of P1-GAL4; UAS-ReaChR(VK5) flies showing wing extension during a single photostimulation trial as a function of light intensity (green light: 530 nm, continuous, 30 sec). The data were fitted by a sigmoidal function to calculate the 50 % point. n = 32 for each intensity. (blue points) are the same as red point used in Fig. 3f, and are replotted here for purposes of comparison *: P < 0.05. P-values represent Friedman's test comparing SH vs. GH (P = 0.02) followed by Fisher's exact test with Bonferroni correction comparing SH vs. GH at each intensity of light.

2.7 Materials and methods

Construction of transgenic animals.

Plasmids were constructed by standard DNA cloning and PCR methods. All PCR reactions were performed using PrimeStar HS DNA polymerase (Takara). Following amplification, all sequences were verified by DNA sequencing.

UAS-ChR2(H134R)::EYFP-2A-ChR2(H134R)::EYFP. A DNA fragment containing the ChR2(H134R) coding sequence, kindly provided by K. Deisseroth, and an intervening F2A sequence (Donnelly et al., 2001; Inagaki et al., 2012) were amplified by PCR using primers (5F-EcoRI-chr2, 3R-2a-YFP, 5F-2a-Chr2, 3R-Xba-YFP, 5F-2a and 3R-2a) and subcloned into pUAST vector in a tandem manner using restriction enzymes. Several transgenic flies were created with different insertion sites. We picked the line that exhibited the strongest induction of PER when crossed to Gr5a-*GAL4*.

UAS-C1V1(T/T). A DNA fragment containing the coding sequence of C1V1(E122T/E162T)-TS-EYFP kindly provided by K. Deisseroth was amplified by PCR using primers (C1V1-f and C1V1-EGFP-r). This PCR product was subcloned into the vector pJFRC2 (Pfeiffer et al., 2010) using SLIC cloning (Li and Elledge, 2007). This vector was injected and integrated into attP40 and VK5 sites (Pfeiffer et al., 2010).

UAS-ReaChR, LexAop-ReaChR, UAS-FRT-*mCherry*-FRT-*ReaChR and LexAop*-FRT-*mCherry*-FRT-*ReaChR*. A DNA fragment containing the ReaChR::Citrine coding sequence was amplified by PCR using primers (ReaChR-f and ReaChR-citrine-r). This PCR product was subcloned into pJFRC2 and pJFRC19 (Pfeiffer et al., 2010) using SLIC cloning (Li and Elledge, 2007) for UAS- and LexAop-driven versions, respectively. For the version containing an *FRT*–mCherry–Stop-*FRT* cassette, the *FRT* sequences (GAAGTTCCTATTCTCTAGAAAGTATAGGAACTTC) and ReaChR DNA fragments were subcloned together into pJFRC2 and pJFRC19 using SLIC cloning (Li and Elledge,

2007). These vectors were injected and integrated into attP40, attP5 and VK5 sites (Pfeiffer et al., 2010).

Fly strains.

UAS-ChR2 (Schroll et al., 2006), UAS-dTrpA1 (Hamada et al., 2008), UAS-GCaMP3.0 (Tian et al., 2009), Gr5a-*GAL4* (Scott et al., 2001) and BDP-*GAL4* (Pfeiffer et al., 2008) (empty promoter *GAL4*: an enhancerless *GAL4* containing a *Drosophila* basal promoter) were generously provided by A. Fiala, P.A. Garrity, L.L. Looger, K. Scott and G.M. Rubin, respectively. *fru-GAL4* (Stockinger et al., 2005), *fru-FLP* (Yu et al., 2010) and VT40556 *GAL4* (von Philipsborn et al., 2011) were kindly provided by B.J. Dickson. *hb9-GAL4* was obtained from Bloomington Stock Center (BL #32555). *Crz-GAL4* (Tayler et al., 2012) and UAS-C128T (Inagaki et al., 2012) were previously created in the lab. These flies are available on request.

All experimental flies were maintained on a 12/12 h day-night cycle. Newly eclosed male flies were CO_2 anesthetized and allowed to recover for more than 3–7 d before behavioral tests at 25 °C. For dTrpA1 experiments, flies were raised at 18 °C. For experiments with Gr5a-*GAL4*, female flies were used; for all the other experiments, male flies were used.

Feeding of retinal.

All-*trans*-retinal powder (Sigma) was stored in −20 °C as a 40 mM stock solution dissolved in DMSO (×100). 400 µl of sugar-retinal solution (400 µM all-*trans*-retinal diluted in 89 mM sucrose) was directly added to surface of solid food in food vials when larvae were at the first or second instar stage. After collection of newly eclosed flies, they were transferred into a vial containing food with 400 µM all-*trans*-retinal (food was heated and liquefied to mix the retinal evenly in the food). We found that larval feeding is not necessary, but it was performed for all the experiments in this paper to be consistent.

Behavioral setup.

See Supplementary Figure 2.1 for details of the setup and the behavioral chamber. In brief, high-power LEDs mounted on heat sinks were placed above the behavioral chamber to provide an illumination source (Fig. 2a and Supplementary Fig. 1a,b). The range of available light intensities in our setup is approximately 0.001–1 mW/mm^2 (note that intensity ranges are different for different LEDs; see Supplementary Fig. 1d). LED units were designed to be switchable to facilitate testing of different photostimulation wavelengths. The LEDs were controlled by an externally dimmable LED driver (700 mA, externally dimmable, Buckpuck DC driver with leads), and its output was adjusted using custom software controlling an Arduino Uno board (Smart Projects). The Arduino digital PWM output was converted into analog voltage using an RC filter (electronic low-pass filter composed of resistor and capacitor; RC LPF in Fig. 2a) containing a 200-Ω resistor and 1-μF capacitor to control the output current of the LED driver. Fly behavior was monitored using a CMOS camera equipped with an IR long-pass filter to avoid detection of light from the high-power LEDs. IR back light was used to visualize the behaving flies. Video capture and LED control were time locked using the Arduino Uno board. To time-stamp photostimulation trials in the videos, we placed an IR indicator LED, whose illumination was synchronized to that of the photostimulation LEDs, in the field of view of the camera. The temperature inside the behavioral chamber was minimally affected by the high-intensity photostimulation: after illumination using the highest available intensities of blue, green or red LEDs (1.1, 0.67 and 1.27 mW/mm^2, respectively) for 1 min, the biggest change in ambient temperature, detected using a thermocouple inserted into the chamber, was 0.7 °C.

Behavioral experiments and quantification of behaviors.

For experiments to activate Gr5a-GRNs, nonstarved flies were mounted into 200-μl Pipetman tips as described previously (Inagaki et al., 2012). Mounted flies were placed beneath high-power LEDs, and PERs were monitored using a video camera. Mounted flies were not placed in the behavioral chamber but placed at the same location as the wells of behavioral chamber in Supplementary Figure 2.1b. Bouts of PER were counted manually. A bout was defined as beginning when flies start extending their proboscis and ending when

they retract the proboscis. Incomplete proboscis extensions were not counted. LEDs were used at maximum intensities in Figures 2.1b,c and 2.2d,e (red, 1.1 mW/mm^2; amber, 0.22 mW/mm^2; green, 0.67 mW/mm^2; blue, 1.27 mW/mm^2). For Figure 2.1b, 100-ms photostimulation trials (1 Hz) were delivered (three trials), and flies showing more than one PER during this activation period were counted as responders. Fly genotype: w^-; Gr5a-*GAL4*(II); GR5a-*GAL4*(III)/UAS-ReaChR(VK5) (Fig. 1b–g); w^-; Gr5a-*GAL4*(II)/UAS-dTrpA1(II); GR5a(III)-*GAL4*/UAS-dTrpA1(III) (Fig. 1h).

To activate Crz neurons (Fig. 2d), males expressing each opsin in *Crz-GAL4* neurons were mounted dorsal side down on a glass slide as previously described (Tayler et al., 2012). Flies were illuminated using the maximum available intensity of light for each type of LED, continuously for 1 min, while we monitored them from the ventral side using a video camera. The number of flies exhibiting ejaculation during light stimulation was manually counted.

For all other behavioral experiments, we used acrylic behavioral chambers (16-mm diameter) in a 2 × 4 array (Fig. 2 and Supplementary Fig. 1) to monitor fly behavior. Unless otherwise indicated, chambers were photostimulated using the maximum intensity available for each LED, for 1 min using continuous illumination, while we monitored them with the camera from above. The number of flies showing continuous side walking during stimulation using the *hb9-GAL4* driver was manually counted (Fig. 2d,f). *fru-GAL4* neurons were activated in the same manner, and flies showing wing extension or paralysis phenotypes were counted manually (Fig. 2d,g). Paralysis was defined as the cessation of locomotion and loss of postural control. Flies that showed a weaker behavioral phenotypes (HB9, side walk; Fru, wing extension) at the onset of photostimulation, but that were paralyzed before the 1-min stimulation was terminated, were counted as paralysis (Fig. 2f,g).

Wing extension evoked by activation of P1 or pIP10 neurons were tested in solitary males in the absence of female flies. The wing extension was manually scored (Figs. 2,3,4,5). Grooming (rapid wing movements while touching with hind leg) was excluded. A bout was defined as starting when flies begin to increase the wing angle and ending when they stop decreasing it.

In order to fit the data into a sigmoidal curve, sigmoid interpolation was performed. The sigmoid curves were defined as follows

$$F_{\text{behav}} = \frac{1}{1 + e^{-\alpha \log_2 \frac{X}{X_{50}}}}$$

where F_{behav} is the fraction of flies showing the behavior, X is the light intensity (Figs. 3f,4c and 5c) or frequency (Fig. 2e), X_{50} is the light intensity (Figs. 3f,4c and 5c) or frequency (Fig. 2e) where 50% of flies show the behavior, and α is the slope of the sigmoid curve.

On the basis of the experimentally measured quantities (X and F_{behav}), X_{50} and α were chosen to best fit the data. For all experimental data, polynomial curve fitting—which finds the coefficients that fit the data by the least-squares method—was calculated with Matlab (MathWorks). Goodness of fit was tested by two-way ANOVA between the sigmoidal curve and the actual PER response curve, which indicated a good fit for all cases ($P < 0.05$, two-way ANOVA). The X_{50} is shown as 50% point in the figures (Figs. 2.2e,3f,4c and 5c).

Measurement of light intensity.

A photodiode power sensor (S130VC, Thorlabs) was placed at the location of the behavioral chamber but in the absence of the chamber. The peak wavelength of each LED (red, 627 nm; amber, 590 nm; green, 530 nm; blue, 470 nm) was measured at different voltage inputs. Measurements were repeated four times and averaged. The baseline intensity of each wavelength before LED illumination was subtracted. Note that light intensity can drop during stimulation at high input voltages. In this study, intensity after 10 s of stimulation was measured.

Measurement of penetrance of different wavelengths of light through the fly cuticle.

The proboscis of a female adult fly was removed, and a 10-μm multimode optic fiber (NA, 0.1; Thorlabs) was inserted into the brain through the window. The amount of light entering

the optic fiber inside or outside the fly was measured using a power meter (Model 1931, Newport). Penetrance was calculated as the amount of light that entered the optic fiber inside the fly divided by the amount of light measured outside the fly. The long axis of the optic fiber was always aligned with the light source. Different wavelengths of high power LEDs (470 nm, 530 nm, 590 m, 627 nm) were used as light sources.

Fly histology.

All fixation and staining procedures were performed at 4 °C in PBS unless otherwise specified. Dissected brains were fixed in 4% formaldehyde in PEM (0.1 M PIPES, pH 6.95, 2 mM EGTA, 1 mM $MgSO_4$) for 2 h. After three 15-min rinses with PBS, brains were incubated with primary antibodies overnight. Following three 15 min rinses with PBS, brains were incubated with secondary antibody overnight. Following three 15-min rinses, brains were incubated in 50% glycerol in PBS for 2 h and cleared with Vectashield (Vector Labs). All procedures were performed at 4 °C. A FluoView FV1000 Confocal laser scanning biological microscope (Olympus) with a 30×/1.05-NA silicone oil objective (Olympus) was used to obtain confocal serial optical sections. The antibodies used for Supplementary Figure 2.2a,d were anti-GFP, rabbit polyclonal antibody unconjugated (A11122, Invitrogen) and Alexa Fluor 488 donkey anti-rabbit IgG(H+L) (A11008, Invitrogen). Both of the antibodies were diluted to 1/300. Expression of mCherry in Supplementary Figure 2.2d was monitored using native fluorescence without antibody staining.

FluoRender software (Wan et al., 2009) (http://www.sci.utah.edu/software/13-software/127-fluorender.html) was used to make 3D image reconstructions. To measure the expression levels of ReaChR::Citrine in P1 neurons in Figure 2.6d, the native fluorescence of Citrine in different specimens was monitored using the same intensity of laser power (470 nm) and PMT voltage. Signal intensity was quantified in ImageJ (http://rsbweb.nih.gov/ij/).

Calcium imaging.

Two-photon imaging was performed on an Ultima two-photon laser-scanning microscope (Prairie Technology) with an imaging wavelength of 925 nm (Fig. 6). To filter out autofluorescence of the brain and light from the amber stimulation LED (for ReaChR activation), we used a 500/20 nm (center wavelength/bandwidth) band-pass filter (Chroma) in the emission pathway to detect the GCaMP3 fluorescence. With this laser and filter setting, fluorescence emissions from the Citrine tag (on ReaChR) were not detectable by our PMT. This was confirmed by examination of P1-GAL4;UAS-ReaChR::Citrine flies (the flies without GCaMP3.0), which exhibited no fluorescence signal under our imaging conditions. Therefore, the detected fluorescence signals are purely from GCaMP3.0. The scanning resolution was 128 × 128 pixels, dwell time per pixel was 8 μsec and the optical zoom was 4×. The scanning speed was ~10 Hz. The excitation intensity of the two-photon laser was varied among samples depending on the level of GCaMP3.

In both cases, a 40×/0.80-NA water-immersion objective (Olympus) was used for imaging. A high-power amber LED (590 nm) collimated with an optic fiber (M590F1, Thorlabs) was used as a light source to activate ReaChR. To narrow the bandwidth of the LED output, we connected the optic fiber to a fiber optic filter holder (World Precision Instruments) equipped with 589/10 nm (center wavelength/bandwidth) band-pass filter (Edmund optics). A 200-μm core multimode optic fiber (NA, 0.39; FT200EMT, Thorlabs) was used to deliver the light from the fiber optic holder to the brain. One side of the optic fiber was custom-made to be a bare tip (Thorlabs) and was dipped into the saline imaging bath and placed 430 μm away from the brain. A 10×/0.30-NA water-immersion objective (Olympus) was used to locate the brain and align the optic fiber. The distance between brain and the fiber was measured with an objective micrometer (Olympus). We set the light intensity to be 170 μW at the tip of optic fiber. Thus, at a distance of 430 μm from the tip of a 0.39-NA optic fiber, the light power is calculated to be approximately 1.7 mW/mm^2 at the brain surface (the size of the light spot should be approximately 0.10 mm^2 at the brain). In addition to the PMT used to monitor GCaMP emissions, we used another PMT to monitor the 590-nm ReaChR activation light. This was to ensure that the intensities of 590-nm light were comparable between samples.

To prepare the brain for imaging, we used an *ex vivo* prep. After briefly anesthetizing a fly on ice, the brain was dissected out using a sharp forceps into a 35-mm plastic Petri dish (35 3001, Falcon) containing *Drosophila* imaging saline (108 mM NaCl, 5 mM KCl, 2 mM $CaCl_2$, 8.2 mM $MgCl_2$, 4 mM $NaHCO_3$, 1 mM NaH_2PO_4, 5 mM trehalose, 10 mM sucrose, 5 mM HEPES, pH 7.5) (Wong et al., 2002). The fat body, air sacs and esophagus were gently removed to give a clear view of the brain and to minimize its movement. The brains were attached to the bottom of the plate by static. The saline was changed once after dissection to remove debris. Calcium imaging was performed within 10–15 min after the dissection to ensure that the brains were healthy.

Electrophysiology.

The tip recording method was used to record the electrophysiological responses of labellar taste neurons (Hodgson et al., 1955). Briefly, the fly was mounted and immobilized for recording by inserting a pulled glass capillary (BF150-86-10, Sutter Instruments) from the dorsal surface of the thorax to the tip of the labellum, passing through the cervical connective and the head. The mounting glass capillary was filled with recording solution (7.5 g/L NaCl, 0.35 g/L KCl, 0.279 g/L $CaCl_2 \cdot 2H_2O$ and 11.915 g/L HEPES (Sigma-Aldrich)) and served as a ground electrode. Another glass capillary, pulled to a tip diameter of 10–20 μm and filled with 30 mM tricholine citrate (TCC; Sigma-Aldrich), as an electrolyte, was used for recording the electrophysiological responses of the gustatory neurons innervating this sensillum. All the recordings were obtained from L7 sensilla. The recordings were made using a MultiClamp 700B amplifier and Digidata 1440A A/D converter (Molecular Devices). The recorded data were sampled at a rate of 10 kHz, filtered (band-pass filter between 100 Hz and 3 kHz) and stored on a PC hard drive using Clampex 10 software (Molecular Devices). The data were analyzed by sorting the action potentials and measuring their frequency within the indicated time windows using Clampfit software (Molecular Devices).

For PER activation experiments, a high-power amber LED (590 nm) collimated with an optic fiber (M590F1, Thorlabs) was used as a light source to activate ReaChR. For delivering light to the labellum, a 200-μm core multimode optic fiber with bare end (NA, 0.39; Thorlabs)

was used. The distance of optic fiber from the labellum was set to be 540 μm using a micrometer. The estimated light intensity at the labellum was approximately 1.0 mW/mm^2.

To activate TrpA1 (Fig. 1h), we used a custom-made heat source. In brief, the heat source is a small piece of thermistor (2K Bead Thermistor, Fenwal) that emits heat in proportion to the electrical current passed through it. The distance of the heat source from the labellum was set to be 540 μm using a micrometer. The temperature at this distance was measured using a thermocouple (Omega) (top panel in Fig. 1h).

2.8 Reference

Berndt, A., Yizhar, O., Gunaydin, L.A., Hegemann, P., and Deisseroth, K. (2009). Bi-stable neural state switches. Nat Neurosci *12*, 229-234.

Bianchi, D., Marasco, A., Limongiello, A., Marchetti, C., Marie, H., Tirozzi, B., and Migliore, M. (2012). On the mechanisms underlying the depolarization block in the spiking dynamics of CA1 pyramidal neurons. J Comput Neurosci *33*, 207-225.

Boyden, E.S., Zhang, F., Bamberg, E., Nagel, G., and Deisseroth, K. (2005). Millisecond-timescale, genetically targeted optical control of neural activity. Nat Neurosci *8*, 1263-1268.

Clyne, J.D., and Miesenbock, G. (2008). Sex-specific control and tuning of the pattern generator for courtship song in Drosophila. Cell *133*, 354-363.

Dankert, H., Wang, L., Hoopfer, E.D., Anderson, D.J., and Perona, P. (2009). Automated monitoring and analysis of social behavior in Drosophila. Nat Methods *6*, 297-303.

de Vries, S.E., and Clandinin, T. (2013). Optogenetic stimulation of escape behavior in Drosophila melanogaster. J Vis Exp.

Donnelly, M.L., Hughes, L.E., Luke, G., Mendoza, H., ten Dam, E., Gani, D., and Ryan, M.D. (2001). The 'cleavage' activities of foot-and-mouth disease virus 2A site-directed mutants and naturally occurring '2A-like' sequences. J Gen Virol *82*, 1027-1041.

Fenno, L., Yizhar, O., and Deisseroth, K. (2011). The development and application of optogenetics. Annu Rev Neurosci *34*, 389-412.

Gordon, M.D., and Scott, K. (2009). Motor control in a Drosophila taste circuit. Neuron *61*, 373-384.

Hanai, S., Hamasaka, Y., and Ishida, N. (2008). Circadian entrainment to red light in Drosophila: requirement of Rhodopsin 1 and Rhodopsin 6. Neuroreport *19*, 1441-1444.

Hodgson, E.S., Lettvin, J.Y., and Roeder, K.D. (1955). Physiology of a primary chemoreceptor unit. Science *122*, 417-418.

Inagaki, H.K., Ben-Tabou de-Leon, S., Wong, A.M., Jagadish, S., Ishimoto, H., Barnea, G., Kitamoto, T., Axel, R., and Anderson, D.J. (2012). Visualizing neuromodulation in vivo: TANGO-mapping of dopamine signaling reveals appetite control of sugar sensing. Cell *148*, 583-595.

Jenett, A., Rubin, G.M., Ngo, T.T., Shepherd, D., Murphy, C., Dionne, H., Pfeiffer, B.D., Cavallaro, A., Hall, D., Jeter, J.*, et al.* (2012). A GAL4-driver line resource for Drosophila neurobiology. Cell Rep *2*, 991-1001.

Keene, A.C., and Masek, P. (2012). Optogenetic induction of aversive taste memory. Neuroscience *222*, 173-180.

Kohatsu, S., Koganezawa, M., and Yamamoto, D. (2011). Female contact activates male-specific interneurons that trigger stereotypic courtship behavior in Drosophila. Neuron *69*, 498-508.

Li, M.Z., and Elledge, S.J. (2007). Harnessing homologous recombination in vitro to generate recombinant DNA via SLIC. Nat Methods *4*, 251-256.

Lima, S.Q., and Miesenbock, G. (2005). Remote control of behavior through genetically targeted photostimulation of neurons. Cell *121*, 141-152.

Lin, J.Y., Knutsen, P.M., Muller, A., Kleinfeld, D., and Tsien, R.Y. (2013). ReaChR: a red-shifted variant of channelrhodopsin enables deep transcranial optogenetic excitation. Nat Neurosci *16*, 1499-1508.

Luan, H., Peabody, N.C., Vinson, C.R., and White, B.H. (2006). Refined spatial manipulation of neuronal function by combinatorial restriction of transgene expression. Neuron *52*, 425-436.

Luo, L., Callaway, E.M., and Svoboda, K. (2008). Genetic dissection of neural circuits. Neuron *57*, 634-660.

Nagel, G., Brauner, M., Liewald, J.F., Adeishvili, N., Bamberg, E., and Gottschalk, A. (2005). Light activation of channelrhodopsin-2 in excitable cells of Caenorhabditis elegans triggers rapid behavioral responses. Curr Biol *15*, 2279-2284.

Nagel, G., Szellas, T., Huhn, W., Kateriya, S., Adeishvili, N., Berthold, P., Ollig, D., Hegemann, P., and Bamberg, E. (2003). Channelrhodopsin-2, a directly light-gated cation-selective membrane channel. Proc Natl Acad Sci U S A *100*, 13940-13945.

Odden, J.P., Holbrook, S., and Doe, C.Q. (2002). Drosophila HB9 is expressed in a subset of motoneurons and interneurons, where it regulates gene expression and axon pathfinding. J Neurosci *22*, 9143-9149.

Pan, Y., Meissner, G.W., and Baker, B.S. (2012). Joint control of Drosophila male courtship behavior by motion cues and activation of male-specific P1 neurons. Proc Natl Acad Sci U S A *109*, 10065-10070.

Pfeiffer, B.D., Jenett, A., Hammonds, A.S., Ngo, T.T., Misra, S., Murphy, C., Scully, A., Carlson, J.W., Wan, K.H., Laverty, T.R.*, et al.* (2008). Tools for neuroanatomy and neurogenetics in Drosophila. Proc Natl Acad Sci U S A *105*, 9715-9720.

Pfeiffer, B.D., Ngo, T.T., Hibbard, K.L., Murphy, C., Jenett, A., Truman, J.W., and Rubin, G.M. (2010). Refinement of tools for targeted gene expression in Drosophila. Genetics *186*, 735-755.

Pulver, S.R., Pashkovski, S.L., Hornstein, N.J., Garrity, P.A., and Griffith, L.C. (2009). Temporal dynamics of neuronal activation by Channelrhodopsin-2 and TRPA1 determine behavioral output in Drosophila larvae. J Neurophysiol *101*, 3075-3088.

Schroll, C., Riemensperger, T., Bucher, D., Ehmer, J., Voller, T., Erbguth, K., Gerber, B., Hendel, T., Nagel, G., Buchner, E.*, et al.* (2006). Light-induced activation of distinct modulatory neurons triggers appetitive or aversive learning in Drosophila larvae. Curr Biol *16*, 1741-1747.

Scott, K., Brady, R., Jr., Cravchik, A., Morozov, P., Rzhetsky, A., Zuker, C., and Axel, R. (2001). A chemosensory gene family encoding candidate gustatory and olfactory receptors in Drosophila. Cell *104*, 661-673.

Stavenga, D.G. (2002). Colour in the eyes of insects. J Comp Physiol A Neuroethol Sens Neural Behav Physiol *188*, 337-348.

Stockinger, P., Kvitsiani, D., Rotkopf, S., Tirian, L., and Dickson, B.J. (2005). Neural circuitry that governs Drosophila male courtship behavior. Cell *121*, 795-807.

Suh, G.S., Ben-Tabou de Leon, S., Tanimoto, H., Fiala, A., Benzer, S., and Anderson, D.J. (2007). Light activation of an innate olfactory avoidance response in Drosophila. Curr Biol *17*, 905-908.

Tayler, T.D., Pacheco, D.A., Hergarden, A.C., Murthy, M., and Anderson, D.J. (2012). A neuropeptide circuit that coordinates sperm transfer and copulation duration in Drosophila. Proc Natl Acad Sci U S A *109*, 20697-20702.

Tian, L., Hires, S.A., Mao, T., Huber, D., Chiappe, M.E., Chalasani, S.H., Petreanu, L., Akerboom, J., McKinney, S.A., Schreiter, E.R.*, et al.* (2009). Imaging neural activity in worms, flies and mice with improved GCaMP calcium indicators. Nat Methods *6*, 875-881.

Venken, K.J.T., Simpson, J.H., and Bellen, H.J. (2011). Genetic Manipulation of Genes and Cells in the Nervous System of the Fruit Fly. Neuron *72*, 202-230.

Wan, Y., Otsuna, H., Chien, C.B., and Hansen, C. (2009). An interactive visualization tool for multi-channel confocal microscopy data in neurobiology research. IEEE Trans Vis Comput Graph *15*, 1489-1496.

Wong, A.M., Wang, J.W., and Axel, R. (2002). Spatial representation of the glomerular map in the Drosophila protocerebrum. Cell *109*, 229-241.

Yamaguchi, S., Desplan, C., and Heisenberg, M. (2010). Contribution of photoreceptor subtypes to spectral wavelength preference in Drosophila. Proc Natl Acad Sci U S A *107*, 5634-5639.

Yizhar, O., Fenno, L.E., Davidson, T.J., Mogri, M., and Deisseroth, K. (2011a). Optogenetics in neural systems. Neuron *71*, 9-34.

Yizhar, O., Fenno, L.E., Prigge, M., Schneider, F., Davidson, T.J., O'Shea, D.J., Sohal, V.S., Goshen, I., Finkelstein, J., Paz, J.T.*, et al.* (2011b). Neocortical excitation/inhibition balance in information processing and social dysfunction. Nature *477*, 171-178.

Zhang, W., Ge, W., and Wang, Z. (2007). A toolbox for light control of Drosophila behaviors through Channelrhodopsin 2-mediated photoactivation of targeted neurons. Eur J Neurosci *26*, 2405-2416.

Zimmermann, G., Wang, L.P., Vaughan, A.G., Manoli, D.S., Zhang, F., Deisseroth, K., Baker, B.S., and Scott, M.P. (2009). Manipulation of an innate escape response in Drosophila: photoexcitation of acj6 neurons induces the escape response. PLoS One *4*, e5100.

C h a p t e r 3

Neurons that Function within an Integrator to Promote a Persistent Behavioral State in Drosophila

Jung Y, Kennedy A, Chiu H, Mohammad F, Claridge-Chang A, Anderson DJ. "Neurons that Function within an Integrator to Promote a Persistent Behavioral State in Drosophila". *Neuron*. 2019 Nov 5;. doi: 10.1016/j.neuron.2019.10.028.

3.1 Summary

Innate behaviors involve both reflexive motor programs and enduring internal states, but how these responses are coordinated by the brain is not clear. In *Drosophila*, male-specific P1 interneurons promote courtship song, as well as a persistent internal state that prolongs courtship and enhances aggressiveness. However, P1 neurons themselves are not persistently active. Here we identify pCd neurons as persistently active, indirect P1 targets that are required for P1-evoked persistent courtship and aggression. Acute activation of pCd neurons alone is inefficacious, but enhances and prolongs courtship or aggression promoted by female cues. Brief female exposure induces a persistent increase in male aggressiveness, an effect abrogated by interruption of pCd activity. pCd activity is not sufficient but necessary for persistent physiological activity, implying an essential role in a persistence network. Thus, P1 neurons coordinate both command-like control of courtship song, and a persistent internal state of social arousal mediated by pCd neurons.

3.2 Introduction

Animal behaviors triggered by specific sensory cues evolve over multiple time-scales, from rapid reflex reactions to more enduring responses accompanied by changes in internal state (Tinbergen, 1951; Bargmann, 2012). The former allow quick survival reactions, while the latter afford time to integrate contextual and other influences on behavioral decisions. How these reflexive and integrative pathways are coordinated by neural circuits remains

poorly understood. One useful feature of integrative responses is that they allow behaviors to persist on time-scales beyond the duration of the triggering sensory stimulus (Anderson and Adolphs, 2014). Studies in *C. elegans* have identified neuromodulatory circuits involving serotonin and PDF, which control persistent states of roaming vs. dwelling associated with exploration vs. exploitation of food resources (Anderson and Adolphs, 2014). In mice, transient activation of agouti-related peptide (AgRP) –expressing neurons in the arcute nucleus of the hypothalamus promotes persistent food-seeking behavior, an effect mediate by neuropeptide Y (NPY) signaling (Chen *et al.*, 2016; Chen *et al.*, 2019). Transient activation of steroidogenic factor 1 (SF1) neurons in the dorsomedial/central portion of the ventromedial hypothalamus (VMHdm/c) promotes persistent defensive behaviors (Kunwar *et al.*, 2015). However the circuit-level mechanisms underlying these persistent effects are not well understood.

In *Drosophila melanogaster*, male-specific P1 interneurons (Yamamoto and Koganezawa, 2013) are activated by female-specific pheromones (Kohatsu *et al.*, 2011; Clowney *et al.*, 2015; Kallman *et al.*, 2015), and control male courtship behaviors such as singing (Pan *et al.*, 2011; von Philipsborn *et al.*, 2011), as well as internal states that regulate aggression (Hoopfer *et al.*, 2015), mating (Kohatsu and Yamamoto, 2015; Zhang *et al.*, 2016), feeding (Zhang *et al.*, 2018b) and sleep (Chen *et al.*, 2017) (reviewed in Ref. (Auer and Benton, 2016)). Artificial stimulation of P1 neurons in solitary males can trigger rapid-onset courtship song (Pan *et al.*, 2011; von Philipsborn *et al.*, 2011; Inagaki *et al.*, 2014). Nevertheless, singing persists for minutes after stimulation offset (Bath *et al.*, 2014; Inagaki *et al.*, 2014; Clowney *et al.*, 2015). Similarly, the effect of P1 activation to promote inter-male aggressiveness endures for minutes after photostimulation offset (Hoopfer, 2016; Watanabe *et al.*, 2017).

In contrast to these persistent behavioral effects, optogenetically evoked P1 physiological activity, measured via calcium imaging in live, head-fixed flies, returns to baseline in tens of seconds (Inagaki *et al.*, 2014; Hoopfer *et al.*, 2015) (although it has been reported to persist in brain explants (Zhang *et al.*, 2018a)). These data suggest that persistent behavioral states evoked by P1 stimulation are not encoded in P1 neurons

themselves, but rather in one or more of their downstream targets. We therefore sought to identify such persistently activated P1 targets, and to understand their functional role in the encoding of persistent behavioral states.

3.3 Result

To search for P1 follower cells exhibiting persistent responses, we expressed the red-shifted opsin Chrimson (Klapoetke *et al.*, 2014) in P1^{a}-split GAL4 neurons (Hoopfer *et al.*, 2015; Anderson, 2016; Hoopfer, 2016), and a calcium indicator (GCaMP6s (Chen *et al.*, 2013)) in ~2,000 Fruitless (Fru)-LexA (Mellert *et al.*, 2010) neurons (Figure 3.1A). Optogenetic stimulation was calibrated to activate P1 cells at a level comparable to that evoked in these cells by female abdomen touching in the same preparation. Fru^{+} cells activated by P1 stimulation were identified by volumetric imaging (30 4-μm optical sections covering a 250 μm x 250 μm x 120 μm volume; Figure 3.S1D, E). On average, we monitored activity of 191 Fru^{+} cell somata and identified ~37 cells per fly that responded to P1 stimulation ($\geq$2/3 trials evoking a peak $\Delta F/F$ response >4σ above baseline; Figure 3.S1F), in 14 distinct brain regions. Different putative P1 follower cells showed different response durations, in a continuous distribution ranging from those similar to P1 (τ~15 s; see Methods) to those lasting much longer (Figure 3.1B, Figure S3.1G, I). We used several criteria to select cells for further study: 1) median tau value > 5-fold that of P1 (τ>~75 s); 2) persistent P1 responses detected in >75% of tested flies (n=12); 3) >2 cells/fly per hemibrain; 4) cells genetically accessible using specific GAL4 drivers.

We identified several putative persistent P1 follower (PPF) cells, which met the first criterion. These neurons were present in ~5 distinct clusters, each containing ~1-3 PPF cells, within a relatively small brain region (see Figure 3.1A. Cells in one such cluster, PPF1 (Figure 3.1B, #6) exhibited a median τ~83 s (Figure S3.1G, H). Cells in three other clusters including PPF2 (Figure 3.1B, #3), showed a median τ>~75, but failed to meet the

second and third criteria. Another cluster in addition to PPF1 met all 3 criteria, but was not genetically accessible.

To gain specific genetic access to PPF1 neurons, we first examined the anatomy of these cells by combining P1 stimulation-evoked GCaMP imaging with photo-activatable GFP (PA-GFP) labeling of responding cells (Datta *et al.*, 2008). We generated a nuclear-localized GCaMP (NLS-GCaMP6s) to prevent cytoplasmic GCaMP signal from obscuring PA-GFP fluorescence (Figure 3.1C1). NLS-GCaMP6s also detected persistent responses to P1 stimulation in PPF1 cells (Figure 3.1C2). We then focused a 720 nm two-photon laser on the identified PPF1 cells, and revealed their projection pattern via diffusion of activated PA-GFP (Datta *et al.*, 2008) (Figure 3.1C3). By comparing the morphology of PPF1 neurons with Fru-MARCM (Cachero *et al.*, 2010; Chiang *et al.*, 2011) and Gal4 line image databases (Jenett *et al.*, 2012), we identified two Gal4 drivers, R41A01 and R21D06, which labeled morphologically similar neurons (Figure 3.1C4, D; Figure S3.2A-D). To verify that R41A01 and R21D06 indeed label PPF1 neurons, we performed functional imaging in R41A01>GCaMP6s or R21D06>GCaMP6s flies, and confirmed persistent responses to P1 activation in PPF1 somata (Figure 3.1E and Figure S3.2C); whether such persistent responses are present in all neurites is difficult to ascertain. Interestingly, these neurons exhibited stepwise integration of P1 input (Figure 3.1E); however repeated P1 stimulation trials (as done in volume imaging, 30 trials, Figure 3.1B) sensitized PPF1 neurons (Figure S3.3).

Gal4 line R41A01 labels a cell cluster called pCd, previously reported to play an important role in female sexual receptivity (Zhou *et al.*, 2014). Analysis of marker expression indicated that pCd cells are cholinergic neurons (Diao *et al.*, 2015) that express both Fru and Dsx (Figure S3.2F-I), two sex-determination factors that label neurons involved in male courtship and aggression (Manoli *et al.*, 2005; Stockinger *et al.*, 2005; Rideout *et al.*, 2007; Kimura *et al.*, 2008; Pan *et al.*, 2011; Yamamoto and Koganezawa, 2013). pCd neurons project densely to the superior-medial protocerebrum (SMP), while extending an additional long fiber bundle ventrally to innervate the dorsal region of the subesophageal zone (SEZ; Figure 3.1D). Double labeling of pCd neurons with

somatodendritic (Denmark-RFP (Nicolai *et al.*, 2010)) and pre-synaptic (Syt-GFP (Zhang *et al.*, 2002)) markers revealed that their SMP projections are mostly dendritic, while their pre-synaptic terminals are located in the SMP and the SEZ (Figure S3.4D). Registration of P1 pre-synaptic labeling with pCd somatodendritic labeling in a common brain template failed to reveal clear overlap (Figure S3.4G-I), and application of the GFP Reconstitution Across Synaptic Partner (GRASP (Feinberg *et al.*, 2008)) technique failed to detect close proximity between P1 and pCd neurons (Figure S3.4J-R), suggesting that functional connectivity between these cells is unlikely to be monosynaptic.

pCd neuronal activity is required for P1-induced persistent social behaviors

To test whether P1-evoked persistent social behaviors require pCd activity, we silenced the latter using R41A01-LexA>LexAop-Kir2.1 while activating $P1^{a}$-split GAL4 neurons using UAS-Chrimson. In solitary males (Figure 3.2A), silencing pCd neurons dramatically reduced persistent wing extension evoked by Chrimson activation of P1 cells (Figure 3.2B vs. 2C, green shading; 2D). Importantly, time-locked wing-extension during photostimulation was unaffected (Figure 3.2B-D, gray shading). Persistent aggression evoked by P1 activation in pairs of males (Hoopfer *et al.*, 2015; Watanabe *et al.*, 2017) (Figure 3.2E, F) was also strongly reduced by silencing pCd neurons (Figure 3.2G, H, blue shading), while wing-extension during photostimulation was unaffected. This result was confirmed using a more specific R41A01∩R21D06 intersectional split-GAL4 driver (Figure S3.2D) to silence pCd neurons, and R15A01-LexA to activate P1 cells (Figure S3.5). Thus pCd activity is required for enduring, but not for time-locked, behavioral responses to P1 activation.

pCd neurons amplify and prolong, but do not trigger, social behaviors

We next investigated the effect on behavior of optogenetically stimulating pCd neurons. Interestingly, optogenetic activation of pCd neurons in solitary flies had no visible effect, in contrast to optogenetic activation of P1 neurons (Inagaki *et al.*, 2014; Clowney *et al.*, 2015; Hoopfer *et al.*, 2015) (Figure 3.3A, B). Persistent internal states can change an animal's behavioral response to sensory cues. We reasoned that if pCd neurons promote

such a persistent internal state, then their optogenetic activation, while insufficient to evoke behavior on its own, might nevertheless suffice to modify the behavioral response of the flies to an external social stimulus. To test this, we examined the effect of pCd stimulation on the behavioral response of males to female cues (Figure 3.3D). Activation of pCd neurons in the presence of a dead female dramatically elevated courtship behavior during photostimulation, and this effect persisted for several minutes after stimulus offset (Figure 3.3B vs. 3E, pCd>Chrimson; Figure 3C, F, pCd).

Activation of pCd neurons in pairs of non-aggressive group-housed male flies did not promote aggression, unlike P1 activation (Hoopfer *et al.*, 2015) (Figure 33.G-I). But in the presence of a dead female, which produced increased baseline aggression in male flies (Lim *et al.*, 2014), activation of pCd neurons significantly enhanced fly aggressiveness after photostimulation, an effect not observed in photostimulated controls (Figure 3.3J-L). Thus, unlike P1 activation, which can substitute for the effect of dead females to trigger courtship or aggression, pCd activation alone cannot do so (Figure 3.3B-C, H-I). However pCd neuron activation can enhance and extend the effect of a dead female to promote these social behaviors.

pCd neurons are required for sustained courtship and aggressive drive

Given that pCd neuronal activity is required for optogenetic P1 activation-evoked social behavior (Figure 3.2), we next investigated its requirement during natural social behavior. Silencing pCd neurons significantly increased the latency to copulation (Figure 3.4A, B). To examine the effect of silencing on courtship *per se*, without rapid progression to copulation, we tested males in the presence of a freeze-killed virgin female, which induced robust unilateral wing-extensions (UWEs; courtship song (Tauber and Eberl, 2003)). In controls (BDP-GAL4> Kir2.1 or GFP), the fraction of flies exhibiting UWEs was relatively constant across the 15 min assay (Figure 3.4C, BDP, gray and red lines). However in pCd>Kir2.1 flies, UWEs declined significantly during that interval, in comparison to pCd>GFP controls (Figure 3.4C, pCd, red line, green vs blue shading).

We next performed parallel experiments for aggression. Single-housed (SH) male flies will fight on food in the absence of females (Wang *et al.*, 2008; Lim *et al.*, 2014), and the intensity of fighting escalates over time (Figure 3.4D, BDP). However in SH pCd>Kir2.1 flies, aggression did not escalate over time, although initial levels of lunging were similar to controls (Figure 3.4D, pCd, blue line, green vs. blue shading). These data demonstrate a requirement for pCd neurons in escalated aggression, independent of any influence from females. Importantly, in both assays, silencing pCd neurons did not impair initiation of social behavior, consistent with the inability of pCd optogenetic stimulation to trigger these behaviors (Figure C, D); rather it influenced their amplitude and kinetics.

The effect of pCd silencing on courtship vs. aggression was subtly different: in the former case, silencing pCd neurons caused UWEs to steadily decline over time, whereas during aggression, natural escalation failed to occur (Figure 3.4C vs. 4D, pCd, red vs. blue lines). To investigate whether a common mechanism could explain both phenotypes, we asked whether both data could be jointly fit by a "leaky integrator" model (Chaudhuri and Fiete, 2016). Such models formalize classical "hydraulic" theories of behavioral drive (Lorenz and Leyhausen, 1973), in which the instantaneous level of activity in a neural integrator circuit determines either the rate or type of an animal's behavior; here, we sought to fit the time-evolving rate of UWEs (Figure 3.4E), or of lunging (Figure 3.4F). Our leaky integrator model assumed that flies received sensory input from conspecifics with a rate constant R, and that the activity of the neural circuit integrating conspecific sensory cues decayed from its initial condition to steady-state with a "leak" rate constant T (min^{-1}).

The behavioral data in each assay were well fit by models in which the only free parameter allowed to vary by genotype was T (Figure 3.4E-G). For UWEs, in control flies the relatively flat line reflects the fact that the initial rate of behavior is high, and already close to the steady-state where "fill" and "leak" rates are equal (Figure 3.4H, left). In contrast, the faster decline of UWEs in pCd>Kir2.1 flies (Figure 3.4E) was best fit by an increase in T (Figure 3.4G, red bars). During aggression, control flies exhibit escalation (Figure 3.4F, BDP>Kir2.1) because the initial rate of aggression is low, and the sensory input rate constant R is greater than T for this behavior (Figure 3.4I, left). Increasing T in

pCd>Kir2.1 flies therefore converts aggression to a relatively flat line (Figure 3.4F; 4I, right). Thus, the superficially different courtship vs. aggression phenotypes caused by silencing pCd neurons can be explained by a common mechanism, whereby inhibition of pCd neurons increases the leak rate constant of a neural integrator, which may control a state of social arousal or drive (Anderson and Adolphs, 2014; Anderson, 2016).

pCd neurons display neural integrator properties

We next investigated whether pCd neurons display integrator properties at the level of their physiology. The observation that they exhibit stepwise summation of P1 input (Figure 3.1E, Figure S3.3A) is consistent with this idea. Surprisingly, repeated direct stimulation of PPF1 neurons did not exhibit such summation, and evoked faster-decaying responses (median τ~13.4 s) than evoked by indirect P1 activation (median τ~83 s), indicating that persistent activity cannot be triggered cell autonomously (Figure 3.5A). However, pCd function might be necessary, although not sufficient, for persistent activity (Figure 3.5B, right). If so, then persistent pCd activity should not recover from transient inhibition performed during the decay phase following P1 stimulation (Guo *et al.*, 2017; Inagaki *et al.*, 2019). Alternatively, if pCd cells simply "inherit" persistence passively from an upstream input (Figure 3.5B, left), their persistent P1 response should recover following transient inhibition. We therefore stimulated P1 neurons (5 s) while imaging from pCd cells, and after a short delay (25 s) briefly (~10 s) inhibited pCd activity using the green light-sensitive inhibitory opsin GtACR1 (Mohammad *et al.*, 2017) and 2-photon spiral scanning (Rickgauer and Tank, 2009) at 1070 nm to restrict inhibition to pCd cells (Figure 3.5E, F and Methods).

Actuation of GtACR1 in pCd neurons following P1 stimulation caused a rapid, ~68% decrease in $\Delta F/F$ signal, which did not recover to control levels following the offset of inhibition, but rather remained flat (Figure 3.5G2, blue shaded area, solid vs. dashed line and Figure 3.5H, pCd, green bar). This effect is not due to irreversible damage to pCd neurons by photo-inhibition, since reactivation of P1 neurons following transient pCd inhibition reliably re-evoked pCd persistent activity, and multiple cycles of P1 stimulation

with or without GtACR1 actuation could be performed with consistent results (Figure S3.6A-B, pCd). Furthermore, 2-photon spiral scanning at 1070 nm of pCd neurons lacking GtACR1 had no effect (Figure 3.5G3), confirming that the decrease in GCaMP signal is due to inhibition of activity by GtACR1 and not to 2-photon irradiation. As the experiment was originally performed using Fru-LexA to label pCd cells, we confirmed the result using a pCd-specific driver (Figure S3.6C-E, blue shading).

As an additional control, we also performed the same manipulation on PPF2 neurons, another $FruM^{+}$ population located near pCd (Figure 3.5C), which also showed persistent responses to P1 activation (Figure 1B, #3; Figure 3.5D, PPF2). In this case, following GtACR inhibition PPF2 activity quickly recovered to the level observed at the equivalent time-point in controls without 1070 nm photo-inhibition (Figure 3.5G5, 5H, PPF2 and Figure S3.6B, PPF2). Thus, PPF2 activity is not required continuously to maintain a persistent response to P1 activation. In contrast, persistence in pCd neurons requires their continuous activity. However the fact that persistent activity cannot be evoked by direct stimulation of pCd neurons alone suggests that persistence likely requires co-activation of a network comprised of multiple neurons.

pCd neurons are required for an effect of females to persistently enhance male aggressiveness

The foregoing data indicated that pCd neurons are required to maintain a P1 activation-triggered persistent internal state, which prolongs wing extension in solitary males and promotes aggression when male flies encounter another male. We next asked whether pCd neurons are similarly required for a persistent internal state triggered by naturalistic cues. Since P1 neurons are activated by female cues (reviewed in ref. (Auer and Benton, 2016)), we examined the influence of transient female exposure on male aggressive behavior. Previous studies have demonstrated that females can enhance inter-male aggression (ref. (Lim, 2014; Lim *et al.*, 2014) and see Figure 3.3H vs. K), but whether this effect can persist following the removal of females was not clear. To investigate this, we pre-incubated individual male flies for 5 min with or without a live female, and then gently transferred

them into an agarose-covered arena to measure their aggression (Figure 3.6A). Male flies pre-incubated with a female showed significantly higher levels of lunging than controls (Figure 3.6B), indicating a persistent influence of female exposure to enhance aggressiveness.

We next asked whether this persistent influence requires continuous pCd activity. To do this, male flies expressing GtACR1 in pCd neurons were pre-incubated with females, and briefly photostimulated with green light during the aggression test (Figure 3.6C). Transient inhibition of pCd neurons abrogated the effect of female pre-exposure to enhance aggression (Figure 3.6D), mirroring the effect of such transient inhibition to disrupt persistent physiological activity in these cells (Figure 3.5G2). Thus, continuous pCd neuron activity is required to maintain a persistent behavioral state change induced by female presentation. Importantly, this effect was not observed when P1 neurons were transiently silenced using GtACR, although such silencing of P1 cells did transiently disrupt male courtship towards females (Figure S3.7), as previously reported (Zhang *et al.*, 2018a).

Individual pCd neurons respond to both P1 stimulation and the aggression-promoting pheromone cVA

The foregoing experiments indicated that when males are removed from the presence of females and confronted with another male, their behavior switches from courtship to aggression. To investigate whether pCd neurons themselves might also play a role in the detection of male cues that trigger this behavioral switch, we investigated whether they can respond to 11-cis Vaccenyl Acetate (cVA), a male-specific pheromone that has been shown to promote aggression (Wang and Anderson, 2010) (Figure 3.7A). Notably, cVA has already been shown to activate pCd cells in females (Zhou *et al.*, 2014), where the pheromone promotes sexual receptivity. Although other pheromones have been shown to promote male aggression in *Drosophila*, such as 7-tricosene (Wang *et al.*, 2011), the non-volatility of that compound made it difficult to deliver in a controlled manner to walking flies in our imaging preparation (Figure 7B) without physically disturbing them.

To do this, we imaged pCd activity using GCaMP6s in flies exposed to the following stimuli at 5 minute intervals: 10 s of P1 activation; cVA vapour presentation; or P1 stimulation (10 s) followed 30 s later by cVA (Figure 3.7C). Among pCd neurons persistently activated by P1 stimulation (Figure 3.7C1), only half responded to cVA alone (defined as >2σ above baseline; Figure 3.7C2). However, delivery of cVA 30 s after P1 stimulation (i.e., during the persistent phase of the response) yielded cVA responses (>2σ above post-P1 activity) in 90% of the pCd cells (Figure 3.7C3). Moreover, peak cVA responses were significantly greater following P1 activation, than in flies exposed to the pheromone on its own (median increase 1.8-fold; Fig. 3.7D, E). Thus, individual pCd neurons that are activated by P1 stimulation in males can also respond to cVA (Figure 3.7A), and this response is enhanced during the persistent phase of the P1 response.

3.4 Discussion

Optogenetic activation of P1 neurons evokes both courtship song, in a reflexive manner (Bath *et al.*, 2014; Inagaki *et al.*, 2014), and a persistent internal state of social arousal or drive (Anderson, 2016) that promotes aggression in the presence of a conspecific male (Hoopfer *et al.*, 2015; Watanabe *et al.*, 2017). Here we have identified a population of indirect persistent P1 follower cells, called pCd neurons (Zhou *et al.*, 2014), whose activity is necessary for P1-triggered persistent aggression. pCd neurons are also necessary for persistent UWEs triggered by P1 activation, on a time scale outlasting P1 activity (as measured in separate imaging experiments). An earlier study (Zhang *et al.*, 2018a) reported that P1 activity is continuously required during male courtship following initial female contact, but did not distinguish whether this requirement reflected continuous stimulation of P1 cells by non-contact-dependent female-derived cues (e.g., motion cues (Kohatsu and Yamamoto, 2015; Auer and Benton, 2016)), or a true fly-intrinsic persistent response. In contrast, the use of transient optogenetic stimulation here clearly demonstrates persistent fly-intrinsic responses. Nevertheless, we cannot exclude that persistent P1 activity may occur during natural courtship bouts (Zhang *et al.*, 2018a). Importantly, however, we show that pCd but not P1 neurons are required for a persistent increase in aggressive state induced by transient female pre-exposure (Figure 3.6D). Together, these data suggest that

pCd neurons participate in a network that may encode a persistent memory of a female, which can be combined with the detection of an opponent male at a later time to elicit aggression (Hoopfer *et al.*, 2015; Anderson, 2016). The observation that P1 neuron activation enhances pCd responses to cVA, an aggression-promoting pheromone (Wang and Anderson, 2010), is consistent with this idea.

The effect of females to promote inter-male aggression are well-known and widespread throughout the animal kingdom (Homer, 850 B.C.; Lorenz, 1966). This effect is typically attributed to increases in circulating steroid hormones, such as testosterone or estrogen (Wingfield *et al.*, 1990; Archer, 2006; Sobolewski *et al.*, 2013), or to the effects of neuromodulators such as neuropeptides or biogenic amines (Gobrogge *et al.*, 2007). Our data provide evidence that neural circuit dynamics involving persistent activity may also play a role in the effect of social experience with females to enhance male aggressiveness, in *Drosophila*. Whether such mechanisms also operate in mammalian systems where female exposure promotes aggressiveness (Remedios *et al.*, 2017), remains to be determined.

Our physiological data suggest that pCd neurons are part of a circuit that temporally integrates P1 input to yield a slow response that decays over minutes (Figure 3.1E). The fact that transiently silencing pCd neurons using GtACR irreversibly interrupts this slow response argues that it indeed reflects persistent pCd activity, and not simply persistence of GCaMP6s fluorescence. It is likely that this integrator circuit comprises additional neurons, including non-Fru-expressing neurons. Evidently, P1 neurons activate this circuit in parallel with a "command" network, including pIP10 descending interneurons (von Philipsborn *et al.*, 2011; Ding *et al.*, 2019), that triggers rapid-onset courtship behavior. These results illustrate how acute and enduring responses to sensory cues may be segregated into parallel neural pathways, allowing behavioral control on different time scales, with different degrees of flexibility (Figure 3.7F). The incorporation of parallel neural pathways that allow behavioral responses to stimuli to be processed on multiple timescales may represent an important step in the evolution of behavior, from simple

stimulus-response reflexes to more integrative, malleable responses (Anderson and Adolphs, 2014; Gibson *et al.*, 2015; Bach and Dayan, 2017).

Recently, Zhang et al reported a role for pCd neurons in a recurrent circuit with NPF neurons that accumulates mating drive under conditions of extended sexual deprivation in *Drosophila* males (Zhang *et al.*, 2019). In agreement with our results, Zhang et al found that constitutive silencing of pCd neurons partially reduces mating behavior. However, they also reported that acute activation of these neurons has no effect on courtship, and that behavioral effects are only observed following 12 hrs of continuous thermogenetic stimulation of these cells (Zhang *et al.*, 2019). In contrast, we observed a clear effect of acute (30s) pCd stimulation to promote courtship, but only when males are provided with a source of female cues (Fig. 3.3D-F). Our data demonstrating a requirement for pCd neurons in aggression enhanced by 5 min of female pre-exposure (Fig. 3.6D) indicate that these cells regulate persistent internal states triggered by exposure to ecologically relevant stimuli, on a time-scale orders of magnitude shorter than those required for homeostatic influences on mating (Zhang *et al.*, 2019). Whether NPF neurons are involved in this aggression-promoting function of pCd neurons remains to be determined; we previously reported a weak effect of NPF neuron stimulation to enhance aggression (Asahina *et al.*, 2014), while another group reported that silencing of NPF neurons increased aggression (Dierick and Greenspan, 2007).

Our observations raise several new and interesting questions for future investigation. First, what cells provide direct synaptic inputs to pCd neurons, and what is the connectional relationship of these cells to P1 neurons? Second, the fact that pCd activity is necessary but not sufficient to trigger persistence suggests that other cells likely contribute to the integrator circuit; what are these cells (Figure 3.7F, Y, Z)? Finally, how is persistence encoded, and what is the role of pCd neurons in determining its duration? The data presented here provide insight into the complex networks that underlie behavioral temporal dynamics (Crickmore and Vosshall, 2013; Zhang *et al.*, 2018a) in *Drosophila*, and offer a useful point-of-entry to this fascinating problem.

3.5 Main figures

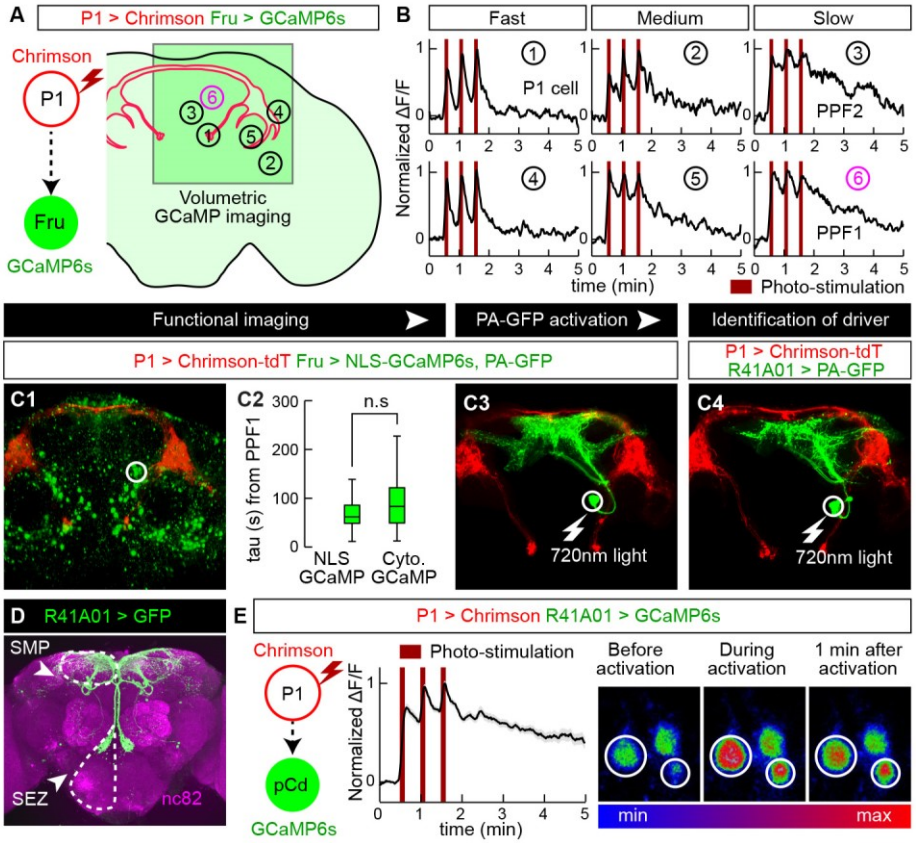

Figure 3.1. Identification of P1 follower cells with long-lasting responses.

(A) Experimental schematic. Green square indicates imaging field containing different putative P1 follower cells (numbered circles). (B) Representative GCaMP6s traces (normalized ΔF/F); numbers correspond to cells in (A). PPF1 cells (⑥) are pCd neurons. 655 nm light (10 Hz, 10 ms pulse-width, 25 s inter-stimulation interval) was delivered for Chrimson stimulation (dark red bars). (C1-4) Identification of GAL4 driver labeling PPF1 (pCd) neurons (See Figure S2A for details). (C1) LexAop-NLS-GCaMP expressed in Fru-LexA neurons; white circle, PPF1 somata. (C2) Comparison between NLS GCaMP6s and Cytoplasmic GCaMP6s. Decay constants (tau) were calculated by curve fitting (See Figure S1I and Methods for details). n=32 trials, 11 cells from 7 flies (NLS GCaMP), 77 cells from 12 flies (Cytoplasmic GCaMP). Statistical significance in this and in all other figures

(unless otherwise indicated) was calculated using a Mann-Whitney U-test. Boxplots throughout show the median (center line), 25th and 75th percentiles (box), and 1.5 times the interquartile range (whiskers). Outliers were defined as data points falling outside 1.5x the interquartile range of the data, and were excluded from plots for clarity, but not from statistical analyses. (C3) PPF1 projections revealed by Fru-LexA>PA-GFP activation (Datta *et al.*, 2008). (C4) PPF1 neurons labeled by R41A01-LexA>PA-GFP. Non-PPF1 PA-GFP and NLS-GCaMP basal fluorescence have been masked for clarity. All images in C1, C2, and C4 are maximum intensity z-projections of 2-µm optical sections acquired by 2-P imaging. (D) Central brain R41A01 Gal4 neurons revealed by UAS-myr::GFP reporter. Superior medial protocerebrum (SMP) and sub-esophageal zone (SEZ) are indicated by dashed outlines. (E) LexAop-GCaMP6s response of pCd neurons labeled by R41A01-LexA following P1-Gal4/UAS-Chrimson stimulation (see Supp. Table 1 for genotypes). Left, schematic; middle, normalized ΔF/F trace (n=23 trials, 15 cells from 10 flies; mean±sem); right, fluorescent images taken before, during, and 1 minute after P1 activation (averaged over 5 frames). White circles indicate two responding cells.

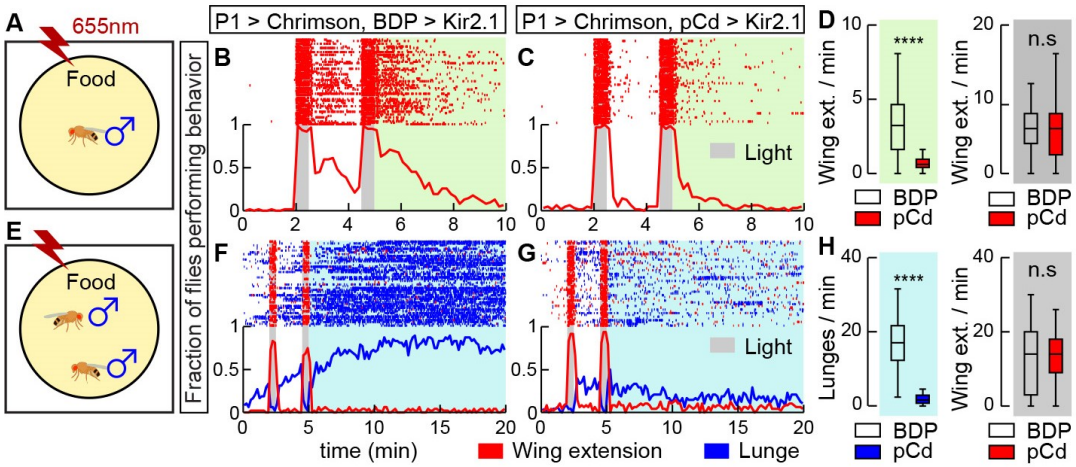

Figure 3.2. Activity of pCd neurons is required for P1-induced persistent behaviors.

(A) Schematic (approximately to scale). Chrimson activation at 655 nm (Inagaki *et al.*, 2014) was performed in solitary males on food. (B, C) Behavior of flies during (gray shading) and after (green shading) P1[a] (Hoopfer *et al.*, 2015; Anderson, 2016) neuronal activation, either without (B; BDP is enhancerless LexA control driver), or with (C; pCd-LexA) Kir2.1-mediated (Baines *et al.*, 2001) inhibition of pCd neurons. Grey bars, 30 s photostimulations (40 Hz, 10 ms pulse-width) at 2 min intervals. Upper: Wing extension raster plot (red ticks). Lower: fraction of flies performing wing extensions (red line) in 10 s time bins. n=62 (B), 63 (C). (D) Wing extension frequency per fly after (green shading) or during (grey shading) photostimulation. **** $P < 0.0001$. (E) As in (A), but using male pairs. (F, G) Plot properties as in (B, C). Grey bars, 30 s photostimulation periods (2 Hz, 10 ms pulse-width) at 2 min intervals. Upper: raster plot showing wing extensions (red ticks) and lunges (blue ticks). Lower: fraction of flies performing wing extensions (red line) or lunges (blue line) in 20 s time bins. n=48 for each genotypes. (H) Lunge frequency after photostimulation (light blue shading, left), and wing extension frequency during photostimulation (grey shading, right). Lunging during, and wing extension after photostimulation were $\leq$ 1 event/min and are omitted for clarity. Statistics as in (D).

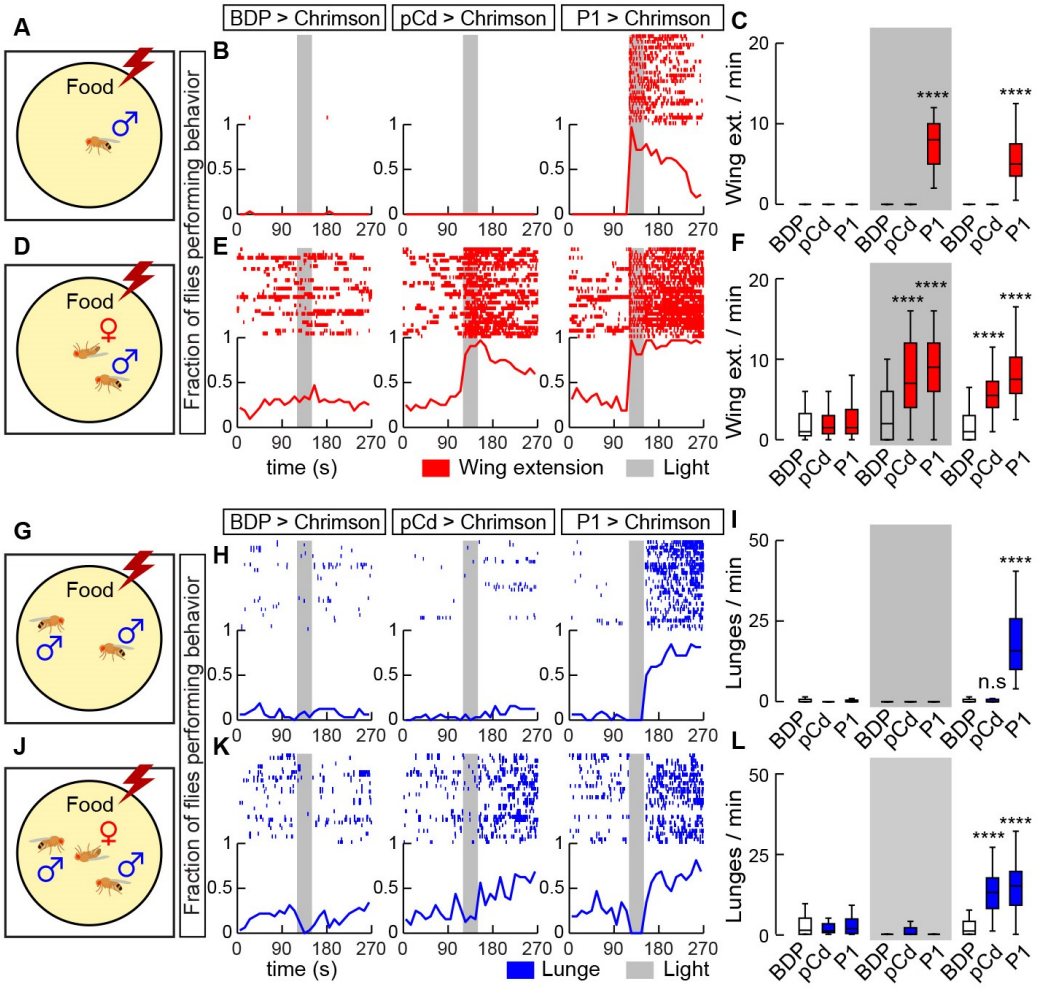

Figure 3.3. Activation of pCd neurons amplifies and extends male social behaviors induced by female cues.

(A, D, G, and H), experimental schematics illustrating optogenetic activation of pCd neurons in solitary males (A-F) or pairs of group-housed males (G-L), tested without (A-C, G-I) or with (D-F, J-L) a dead female. Raster plots and fraction of flies performing behaviors (red and blue lines, 10 s time bins) are shown in (B, E, H, and K). Plot properties same as in Figure 2. Grey bars, 30 s Chrimson activation at 655 nm (10 Hz, 10 ms pulse-width). Quantification and statistical tests shown in (C, F, I, and L). n=32 flies each. Statistical test used was a Kruskal-Wallis test. **** Dunn's corrected $P < 0.0001$ for between-genotype comparisons. Courtship data are omitted in (H, K) for clarity.

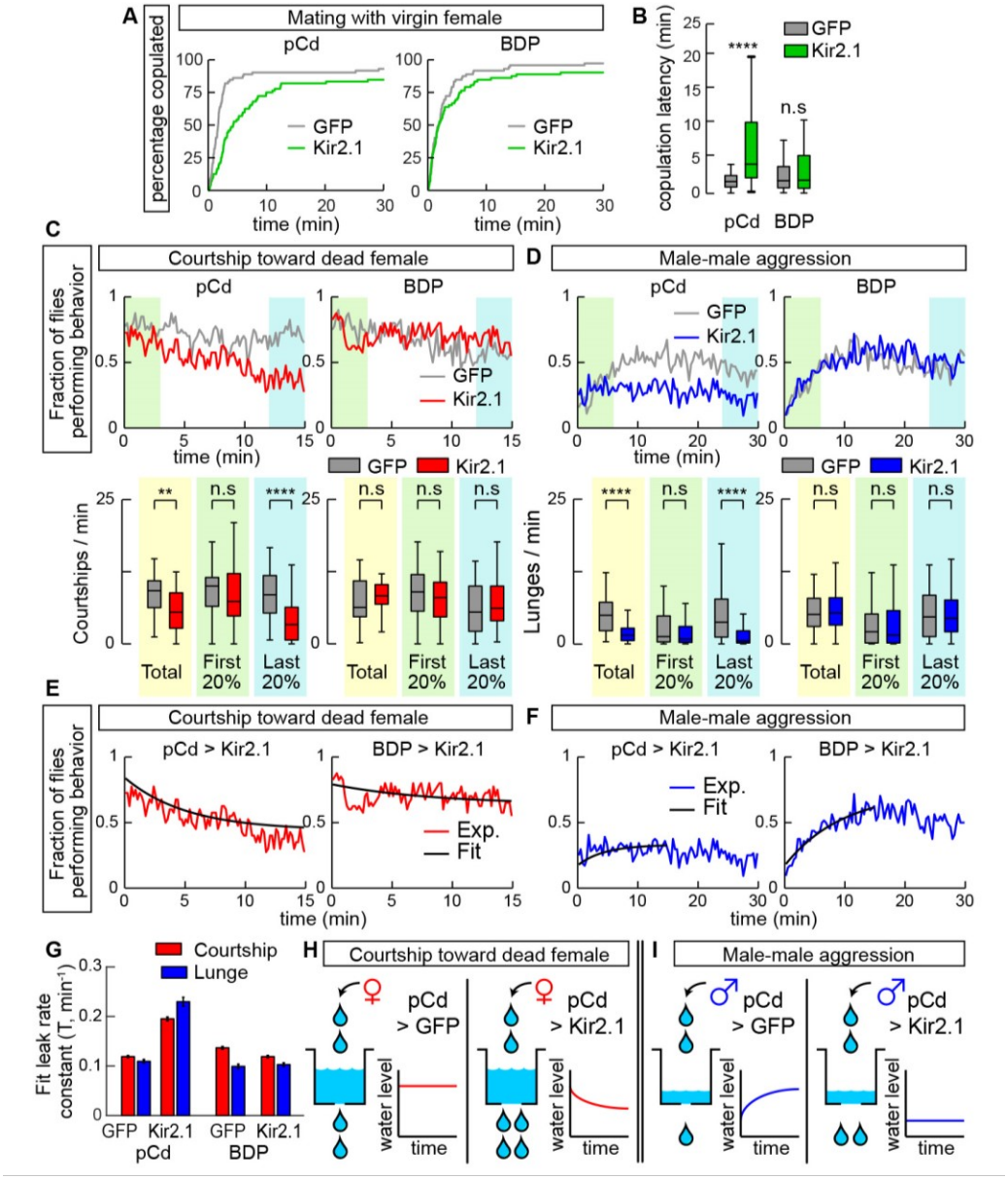

Figure 3.4. Inhibition of pCd neurons increases copulation latency and reduces endurance of naturally occurring social behaviors.

(A) Individual males of the indicated genotypes were paired with a live wild-type virgin female. Cumulative percentage of flies that copulated over 30 min is shown. (B) Quantification and statistical tests for copulation latency. **** $P < 0.0001$ for between-genotype comparisons (Mann-Whitney U-test). (C) Solitary male flies were incubated with

a dead female and courtship (unilateral wing extension bouts, UWEs) measured over 15 min. Left panels show experimental (pCd>Kir2.1, red line) and responder control (UAS-GFP, grey line) flies, right panels show enhancerless driver controls (BDP-Gal4; red and grey lines). Upper: fraction of flies performing behavior in 10 s time bins. Lower: number of UWE bouts per min per fly over entire 15 min observation (yellow shading), first (green shading) and last (blue shading) 20% (3 min) of the interval. n=40 flies per genotype. ** $P < 0.01$, **** $P < 0.0001$. (D) Pairs of single-housed males monitored over 30 min. Plot properties and statistical tests same as in (C), except blue color indicates lunging. Fraction of flies performing behavior was binned in 20 s time intervals. n=64 flies per genotypes. (E, F) Curve fitting of (E) courtship data from (C), or (F) lunging data from (D). Black lines show exponential fit curve for each experiment. Goodness of fit (MSE): courtship; 0.0042 (pCd>GFP), 0.0051 (pCd>Kir2.1), 0.0056 (BDP>GFP), 0.0058 (BDP>Kir2.1); Aggression; 0.0028 (pCd>GFP), 0.0031 (pCd>Kir2.1), 0.0045 (BDP>GFP), 0.0029 (BDP>Kir2.1). (G) Leak rate constants derived from curve fitting in (E, F); note that both courtship and lunging in pCd>Kir2.1 flies are best fit by assuming increased leak constants, relative to genetic controls. (H, I) Illustration of modeling results. Water level represents level of activity in a hypothetical leaky integrator driving behavior (Lorenz and Leyhausen, 1973). Inhibition of pCd activity with Kir2.1 increases leak rate constant of the integrator.

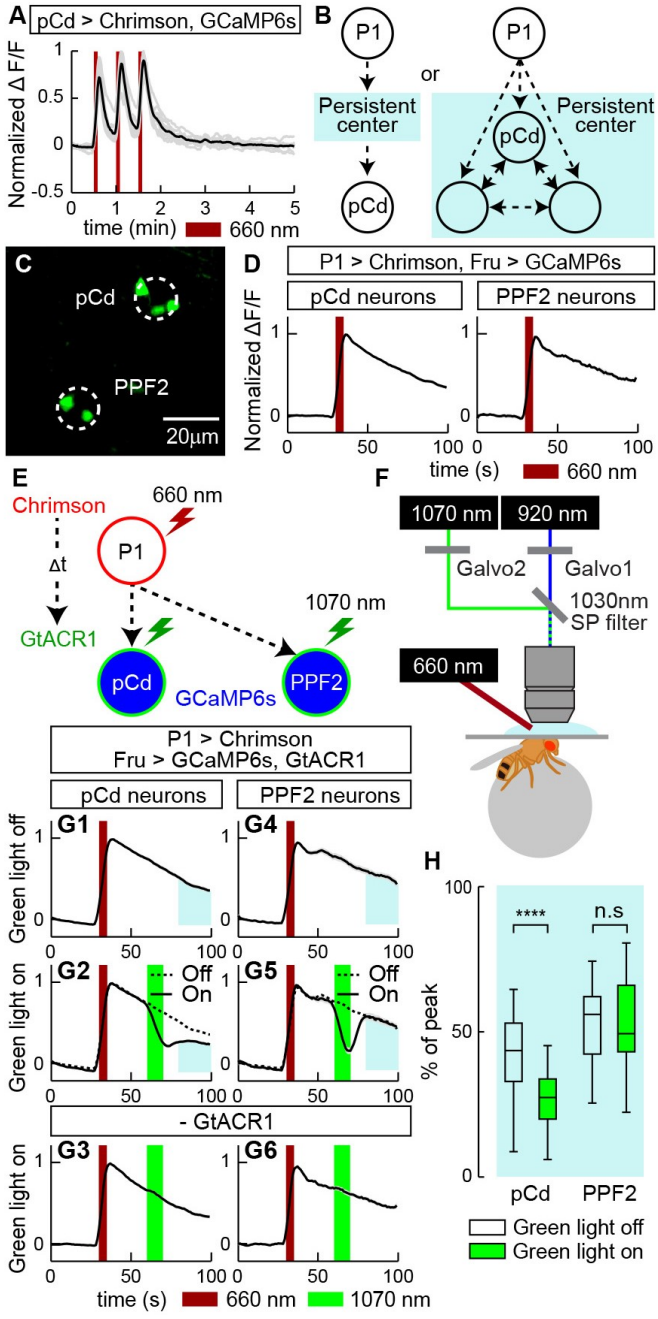

Figure 3.5. pCd neuronal activity is required for physiological persistence.

(A) pCd response to direct optogenetic stimulation is not persistent. Gray lines depict individual pCd cell responses (n=27 from 9 flies), black line shows the mean for all cells. Dark red bars, Chrimson stimulation (655 nm light (10 Hz, 10 ms pulse-width, 25 s inter-

stimulation interval). (B) Schematic illustrating alternatives tested by the experiment in (E-H). Light blue shading depicts hypothetical persistence-encoding network ("center"). If pCd neurons simply inherit persistence passively from the center (left), then persistence should rebound following transient pCd silencing. If persistence does not rebound, it implies that pCd activity is required for the center to maintain persistence (right). (C) Representative two-photon image showing cell body locations of pCd and PPF2 neurons expressing Fruitless>GCaMP6s in vivo. Dashed white circles indicate spiral scanning area for GtACR actuation in (E-H). Maximum intensity projection of 5 x 4 μm optical sections, averaged over 10 frames. (D) Normalized ΔF/F traces from pCd (left, n=36 trials from 8 flies), and PPF2 (right, n=29 trials from 5 flies) neurons upon P1 activation. Mean±sem. Dark red bar indicates P1 photostimulation (5 s, 10 Hz, 10 ms pulse-width, 660 nm LED). (E) Experimental schematic. pCd or PPF2 neuron cell bodies are locally photo-inhibited with GtACR1 (~10 s, spiral scanning, see Methods for details) after a delay (Δt, 25 s) following P1 activation (5 s). (F) Schematic illustrating imaging setup with 1070 nm 2-photon laser for GtACR1 photo-inhibition, and 920 nm 2-photon laser for in vivo GCaMP imaging. (G) Normalized ΔF/F from pCd neurons (G1-G3), and PPF2 neurons (G4-G6) with GtACR actuation (green bars) applied during P1-induced persistent phase. G1 and G4: without photo-inhibition; G3 and G6, 1070 nm irradiation without GtACR1 expression. Dashed lines in G2 and G5 are mean of G1 and G4 traces, respectively. n=36 trials from 8 flies for pCd neurons, and 16 (5 flies) for PPF2 neurons. n=40 (8 pCd flies), 29 (6 PPF2 flies) for genetic controls. Mean±sem. (H) Normalized area under the curve (blue shaded regions in (G)) after photo-inhibition. **** $P < 0.0001$.

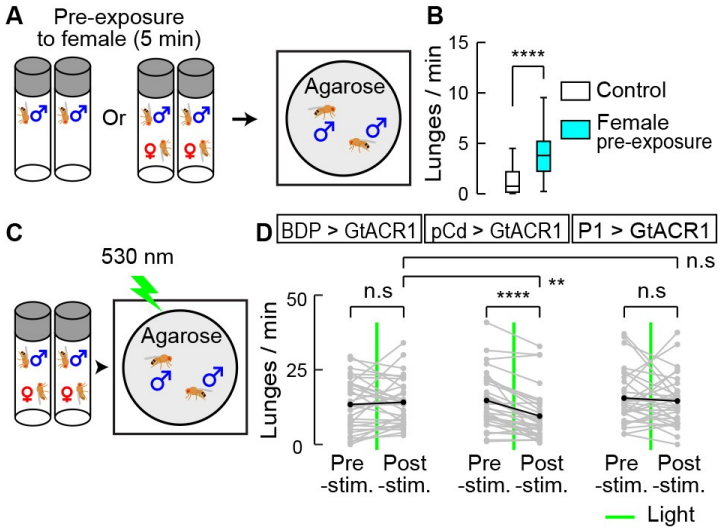

Figure 3.6. Role of pCd neurons in a female-induced enhancement of male aggressiveness.

(A) Schematic illustrating female induced inter-male aggression experiment. Single-housed male flies were pre-incubated in vial with or without (control) a virgin female for 5 min. Subsequently, pairs of pre-incubated males were placed in behavioral arenas with an agarose substrate. (B) Lunge frequency per fly after pre-incubation without (white) or with (blue) a female. n=32 flies each. Statistical test used was a Mann-Whitney U-test. **** $P < 0.001$. (C) Schematic of experimental design. (D) Lunge number before (pre-stim.) and after (post-stim.) GtACR1-mediated neural silencing. Green lines depict exposure to green light (530 nm, 10 Hz, 10 ms pulse-width) for 10 s. Gray points show lunge frequencies for individual flies, and black points show mean values. Statistical tests used were Wilcoxon signed test (within fly comparison) and Kruskal-Wallis test (between genotype comparison). ** Dunn's corrected $P < 0.01$, **** $P < 0.0001$

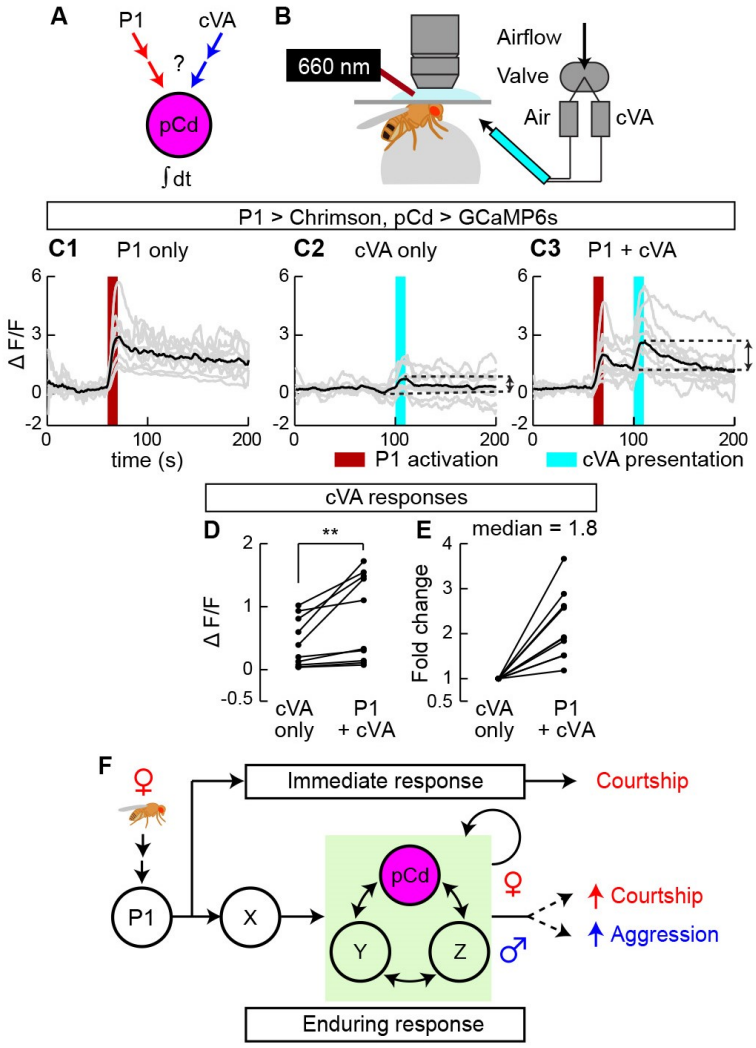

Figure 3.7. P1 activation of pCd neurons enhanced their responsiveness to cVA.

(A) Schematic illustrating experimental design. (B) In vivo GCaMP imaging. P1 neurons were optogenetically activated (660 nm LED), and cVA (or air) was delivered using an olfactometer synchronized and controlled by the imaging acquisition software. (C) GCaMP responses (ΔF/F) to cVA of pCd neurons exhibiting persistent responses to P1 photostimulation (C1, dark red bar, 10 s, 10 Hz, 10 ms pulse-width). cVA alone (C2, cyan bar) or 30 s after a second (10 s) P1 stimulation (C3) were delivered 3 min apart in random order (Methods). Gray lines depict trial-averaged individual pCd cell responses (2-3 trials/cell, n=10 cells from 7 flies) and black lines show the mean for all cells. Double-headed

arrows in (C2 and C3) indicate intervals for cVA responses calculated in (D, E). (D) Individual pCd cell responses (ΔF/F) to cVA presented alone ("cVA only") or 30 s after a 10 s P1 stimulation ("P1+cVA"). Statistical test used was a Wilcoxon signed-rank test. ** $P < 0.01$. (E) Fold change of pCd responses to cVA presentation after P1 stimulation, compared to cVA delivered alone. Data normalized to ΔF/F without P1 stimulation. (F) Models for how P1 and pCd neurons regulate immediate and enduring social behaviors.

3.6 Supplementary figures

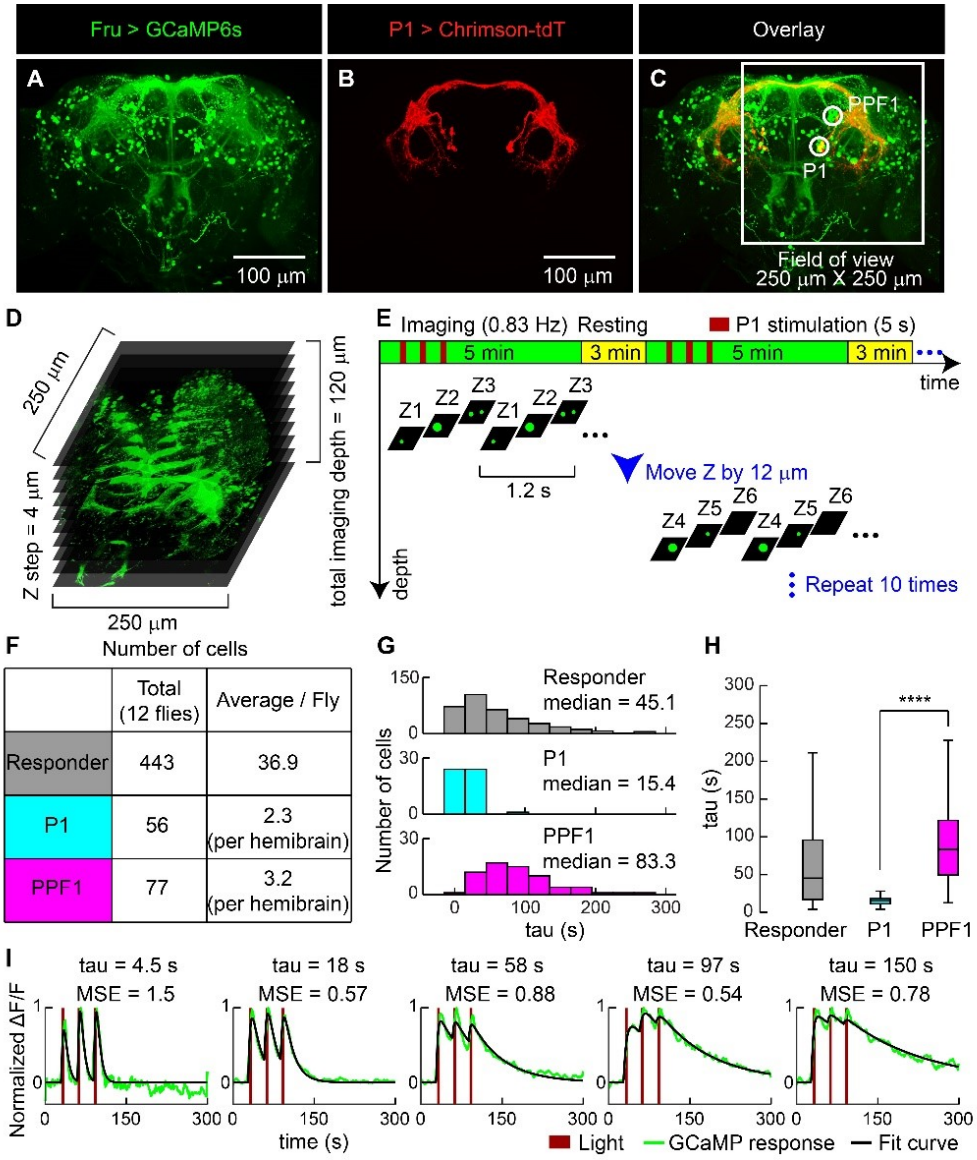

Figure S3.1. Volumetric functional GCaMP imaging to identify persistent P1 follower cells, related to Figure 1.

(A-C) Maximum intensity confocal stacks showing projection patterns of Fruitless (A) and P1[a] (B) neurons (Hoopfer *et al.*, 2015; Anderson, 2016) expressing GCaMP6s and Chrimson-tdT, respectively; (C), overlay. (D, E) Schematics illustrating functional connectomics strategy. Responses to P1[a] photostimulation (3 x 5 s pulses) from multiple

Fru>GCaMP6s cells in each imaging plane (250 x 250 μm^2) were recorded during ten 5 min trials, at multiple z-depths (4 μm/z-step) covering 120 μm. (F) Number of Fruitless$^+$ cells that responded to P1^a activation. PPF1 cells were identified anatomically in high-resolution images acquired following P1 stimulation trials, using 40 mM KCl-containing saline to increase baseline GCaMP6s signals. Red channel (Chrimson-tdTomato) was used to identify P1 neurons, and cell body position and primary projection pattern were used to identify PPF1 neurons. P1 and PPF1 were visible in both hemi-brains of all specimens, but some responder cells on the lateral side appeared only in one hemi-brain (see Field of view marked in (C)). (G) Histogram of τ (tau, decay constant of a model exponential fit to observed neural ΔF/F traces) for all responder cells (top, grey), P1 cells (middle, light blue), and PPF1 neurons (bottom, magenta). (H) Quantification and statistical test for τ. Statistical test used was a Mann-Whitney U-test. **** $P < 0.0001$. τ from 80% of the total identified cells (MSE $\leq$2.06, 354 cells) were used for the plot (G) and quantification and statistical test (H). (I) Representative examples of GCaMP responses and τ for different responder cells. Dark red lines indicate Chrimson activation at 660 nm (3 stimulations, 5 s each, 10 Hz, 10 ms pulse-width, 25 s inter-stimulation interval).

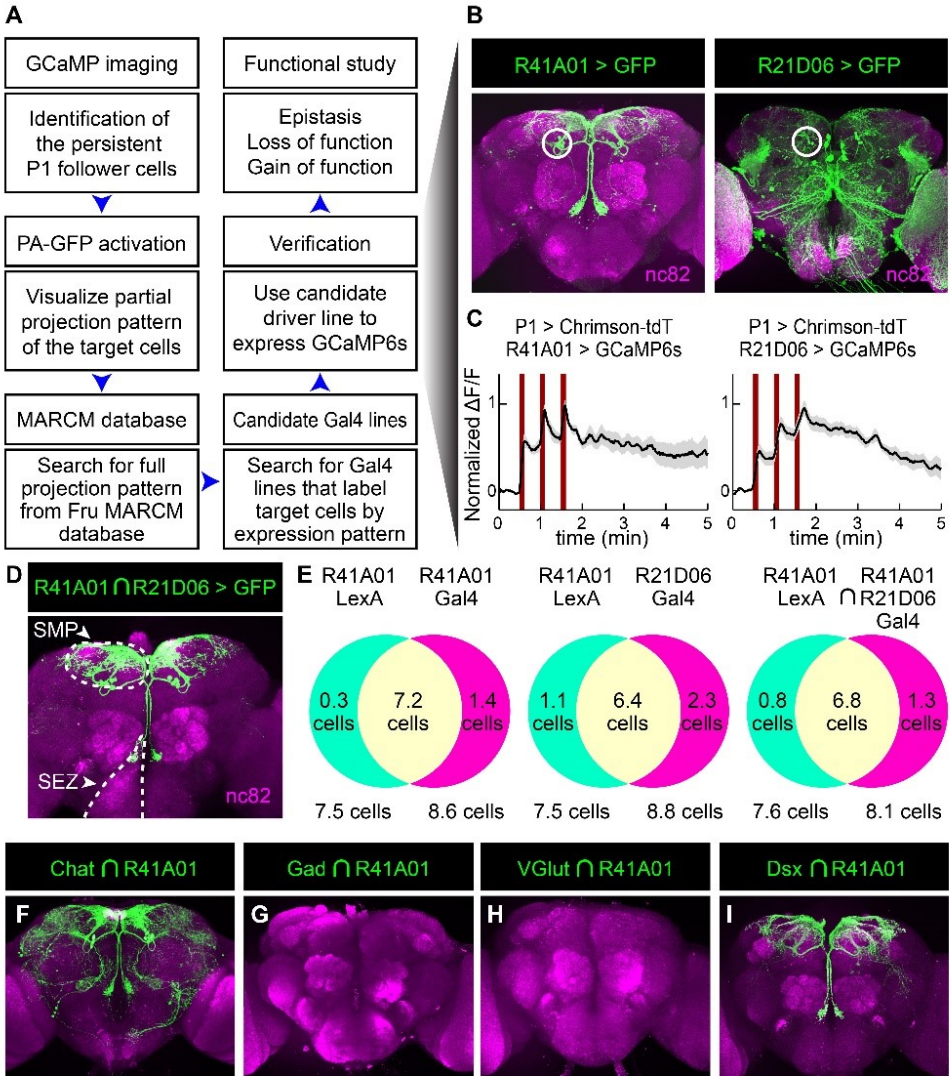

Figure S3.2. Gaining genetic access to PPF1 neurons and molecular phenotype of pCd neurons, related to Figure 1.

(A) Flowchart of the protocol for identifying specific Gal4 lines labeling PPF1 neurons. (B) Anatomy of two Gal4 lines, R41A01 (left) and R21D06 (right) that label PPF1 neurons. Maximum-intensity projection (z-stack) of confocal 2-µm optical sections. (C) Functional imaging of putative PPF1 neuronal cell bodies labeled by R41A01-LexA (left) and R21D06-LexA (right). Traces represent normalized ΔF/F response to P1 stimulation (dark red bars, 3 repeats of 5 s stimulation, 10 Hz, 10 ms pulse-width, 25 s inter-stimulation interval), and were obtained from cell bodies within the white circles indicated in (B).

Mean±sem, n=7 (4 flies) for R41A01, and 9 (4 flies) for R21D06. (D) Anatomy of split-Gal4 intersection between R41A01-AD and R21D06-DBD in the male brain. SMP and SEZ are indicated with white dashed line. (E) Quantification of pCd cell numbers (per hemibrain) labeled by two different reporters, UAS>tdTomato and LexAop>GFP, in flies co-expressing the indicated GAL4 or LexA drivers. Green=GFP positive, Red=tdTomato positive, Yellow=double positive. Area of Venn diagram not scaled to number of cells. n=12 hemibrains per test. (F-I) Anatomy of split intersection between R41A01-AD and Chat-DBD (Diao *et al.*, 2015) (F), Gad1-AD and R41A01-DBD (G), R41A01-AD and VGlut-DBD (H), and R41A01-AD and dsx-DBD. Maximum-intensity projection of confocal 2-µm optical sections.

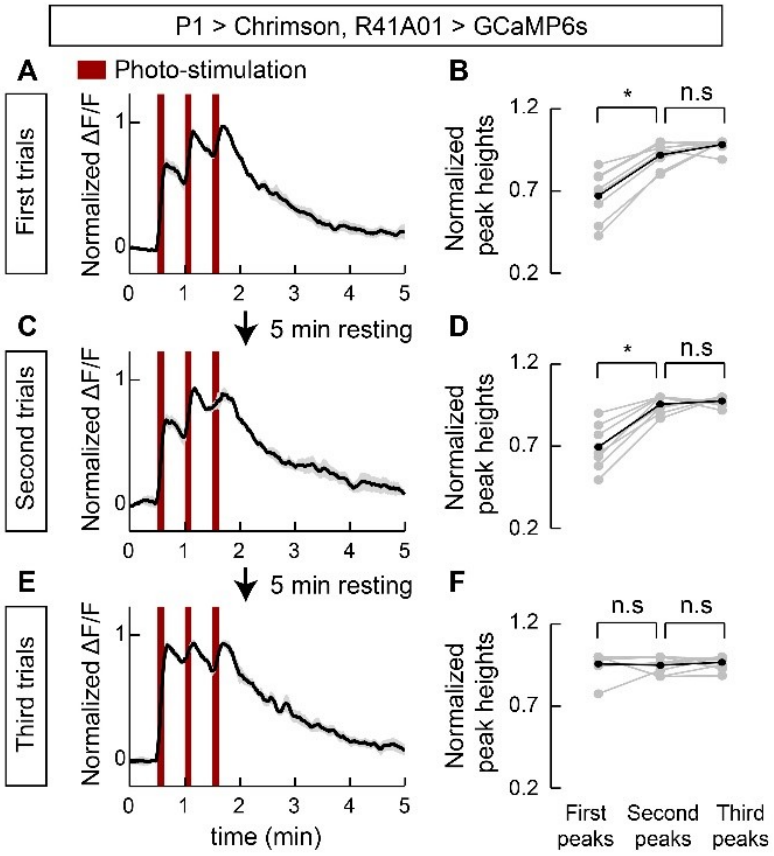

Figure S3.3. Integration of repeated P1 input by pCd neurons, related to Figure 1.

(A, C, E) Normalized GCaMP response of pCd neurons to optogenetic stimulation of P1 neurons. Mean±sem. n=8 cells, 6 flies. (B, D, F) Normalized peak heights during each P1 stimulation. Statistical test used was Wilcoxon signed test with correction for multiple comparisons. * $P < 0.05$

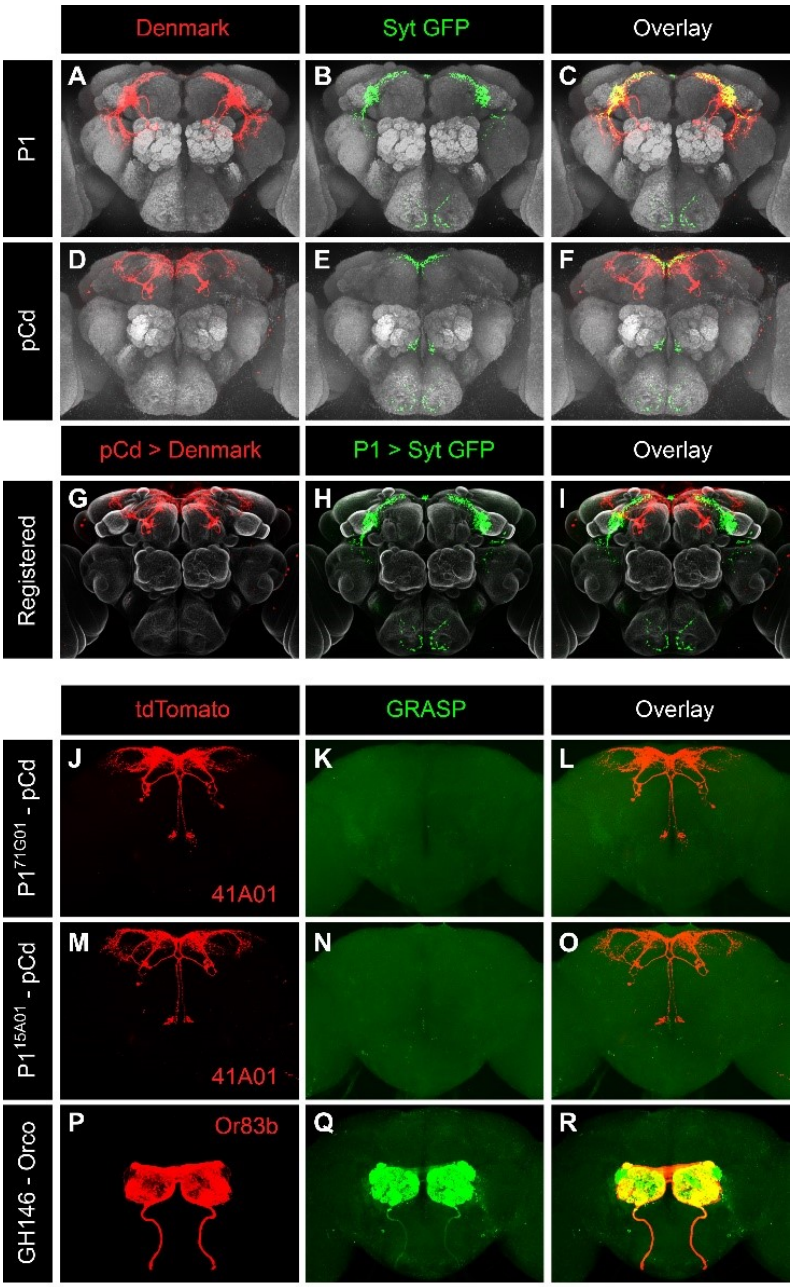

Figure S3.4. Anatomic relationship between P1 and pCd neurons, related to Figure 1.

(A-F) Input and output region of the P1 and pCd neurons visualized by double-labeling with somatodendritic marker (Denmark, red) and pre-synaptic marker (Syt-GFP, green). (G-I). Co-registered images showing somatodendritic region of pCd neurons and pre-synaptic region of P1 neurons. Note that yellow regions in (I, "Overlay") are not observed

when the image is rotated and viewed from a different angle, indicating a lack of overlap. (J-R) GRASP (Feinberg *et al.*, 2008) experiments performed between R41A01 (pCd driver) and either of two P1 drivers, 71G01 (J-L) and 15A01 (M-O), or between GH146 and Orco as a positive control (P-R). tdTomato was expressed in one of the putative synaptic partners, R41A01 (J and M) or Orco (P), to mark fibers for detailed analysis. No positive GRASP signal is observed between pCd and either of the 2 P1 drivers (J-O).

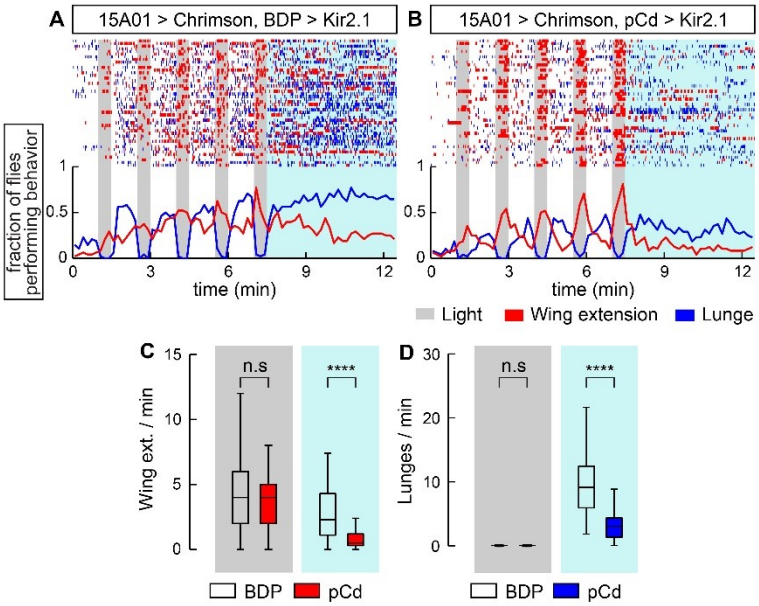

Figure S3.5. Inhibition of pCd neurons with R41A01∩R21D06 Split-Gal4 reduces P1-induced social behaviors, related to Figure 2.

(A, B) Top: raster plot showing wing extensions (red ticks), and lunges (blue ticks) in pair of males. In this experiment, a single driver 15A01-LexA (Hoopfer *et al.*, 2015; Watanabe *et al.*, 2017) was used to activate P1 neurons, while a split GAL4 driver (Figure S2D) was used to inhibit pCd neurons, complementing the genetic strategy used in Figure 2 in which a split-Gal4 was used to activate P1 neurons, while R41A01-LexA was used to inhibit pCd neurons (see Table 1 for genotypes). Bottom: fraction of flies performing unilateral wing extensions (red lines), and lunges (blue lines) in 10 s time bins. Gray bars indicate Chrimson activation (5 repeats of 30 s stimulation, continuous light, 60 s inter-stimulation interval). n= 48 flies per genotype. (C, D) Quantification and statistical tests for unilateral wing extensions (C) and lunges (D) during P1 stimulation (gray shading) and after photostimulation (blue shading), without (open boxes, BDP) or with (red boxes) silencing of pCd neurons using Kir2.1 . **** $P < 0.0001$ for between-genotype comparisons (Mann-Whitney U-test). Note that both wing-extensions and aggression are suppressed by pCd silencing during the post-P1 stimulation period.

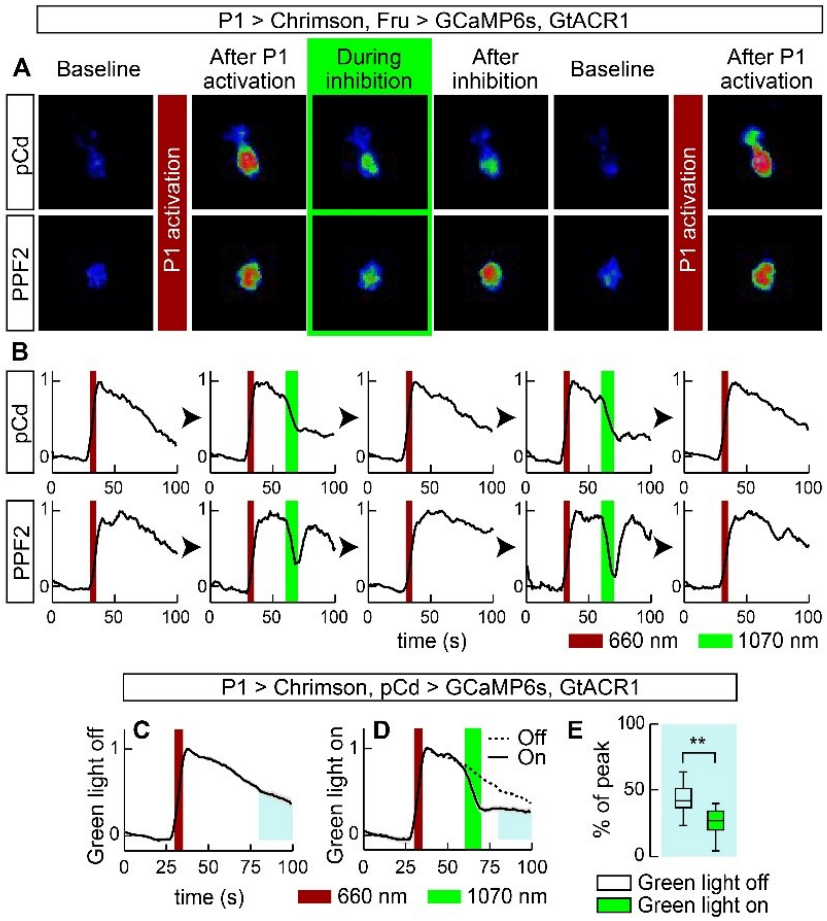

Figure S3.6. Multiple cycles of P1 stimulation and GtACR1 actuation, and inhibition of pCd neurons following P1 stimulation labeled by a pCd-specific driver, related to Figure 5.

(A) Representative GCaMP fluorescent images of pCd (*upper*) and PPF2 neurons (*lower*) at different time points following Chrimson-mediated P1 stimulation (wide-field LED actuation at 660 nm), and cell-restricted GtACR-mediated pCd or PPF2 inhibition (2-photon spiral scanning actuation at 1070 nm). pCd and PPF2 neurons both respond to P1 stimulation, and their response endures following offset of P1 photostimulation ("After P1 activation"). GCaMP signals in pCd neurons rapidly decrease upon photo-inhibition ("During inhibition", green outline), and do not recover 10 s following offset of GtACR actuation ("After inhibition"). In contrast, PPF2 activity recovers after photo-inhibition.

pCd and PPF2 neurons were reliably reactivated by a second cycle of P1 stimulation after following GtACR-mediated inhibition. Images shown are averaged over 5 frames. (B) Representative GCaMP trace (normalized ΔF/F) from individual trials. Multiple cycles of P1 stimulation with or without GtACR1 actuation did not change the initial responses of pCd and PPF2 neurons to P1 stimulation. Dark red bar indicates Chrimson activation at 660 nm (5 s, 10 Hz, 10 ms pulse-width), and green bar indicates GtACR1 actuation (~10 s, spiral scanning) 25 s after Chrimson activation. (C) GCaMP6s response of pCd neurons (normalized ΔF/F) labeled with the driver R41A01-LexA (pCd^{R41A01}) to P1 stimulation (dark red bar) without GtACR1 actuation. (D) GCaMP6s response of pCd^{R41A01} to P1 stimulation with GtACR1 actuation. n=10 trials from 3 flies (C, D). Dark red bar indicates Chrimson activation at 660 nm (5 s, 10 Hz, 10 ms pulse-width), and green bar indicates GtACR1 actuation (~10 s, spiral scanning) 25 s after Chrimson activation. (E) Normalized area under the curve after photo-inhibition (blue shaded area in (C, D)). Statistical test used was a Mann-Whitney U-test. ** $P < 0.01$. This experiment confirms the result reported in Figure 7, in which Fru-LexA was used to express GCaMP6s and pCd neurons were identified morphologically.

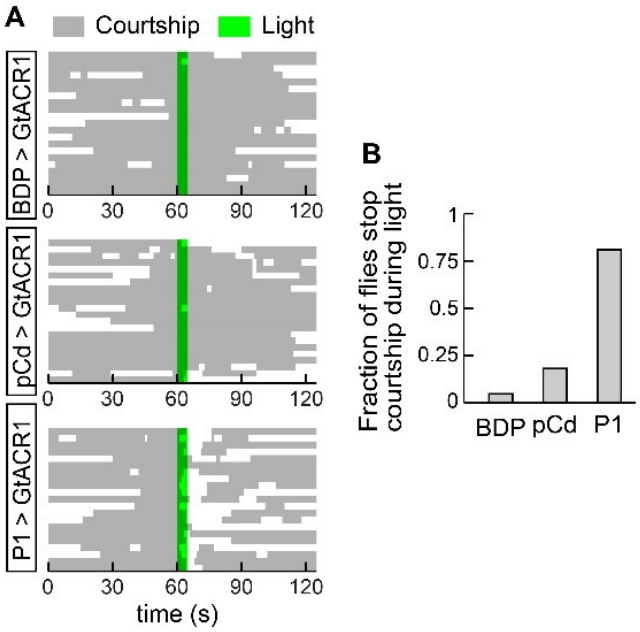

Figure S3.7. Transient inhibition of P1 neurons interrupt ongoing courtship behavior toward dead female, related to Figure 6.

(A) Raster plot showing courtship toward dead female (gray). Note that "courtship" metric used here incorporates multiple behavioral actions, following the definition used by Zhang et al. (Zhang *et al.*, 2018a), and thereby differs from the wing extension metric used in other figures (see Methods for details). Green line indicates GtACR1 stimulation (530 nm, 10 Hz, 10 ms pulse-width) for 10 s. n=21 for BDP and P1 > GtACR1, and 22 for pCd > GtACR1. (B) Fraction of flies stop on-going courtship behaviors during light stimulation.

Supplemental Table 1. Genotypes

Figure	Male genotype
Figure 1A, B	w-, *10xUAS-IVS-Syn21-Chrimson::tdT3.1-SV40 (attp18), 13xLexAop2—Syn21-OpGCaMP6s-p10 (su(Hw)attp8)* ; *15A01-AD (attp40)/+* ; *71G01-DBD (attp2)/Fru-LexA*
Figure 1C1-3	w-, *13xLexAop2-IVS-Syn21-mPA-p10 (su(Hw)attp8)* ; *15A01-AD (attp40)/13xLexAop2-IVS-Syn21-NLS-OpGCaMP6s-scalloped-NLS-p10 (su(Hw)attp5)* ; *71G01-DBD (attp2), 10xUAS-IVS-Syn21-Chrimson::tdT3.1-SV40 (su(Hw)attp1)/Fru-LexA*
Figure 1C4	w-, *13xLexAop2-IVS-Syn21-mPA-p10 (su(Hw)attp8)* ; *15A01-AD (attp40)/13xLexAop2-IVS-Syn21-NLS-OpGCaMP6s-scalloped-NLS-p10 (su(Hw)attp5)* ; *71G01-DBD (attp2), 10xUAS-IVS-Syn21-Chrimson::tdT3.1-SV40 (su(Hw)attp1)/41A01-LexA::p65 (attp2)*
Figure 1D	w- ; +/+ ; *41A01-Gal4 (attp2)/10xUAS-IVS-myr::GFP (attp2)*
Figure 1E	w-, *10xUAS-IVS-Syn21-Chrimson::tdT3.1-SV40 (attp18), 13xLexAop2—Syn21-OpGCaMP6s-p10 (su(Hw)attp8)* ; *15A01-AD (attp40)/+* ; *71G01-DBD (attp2)/41A01-LexA::p65 (attp40, attp2, or VK00027)*
Figure 2B, F	w- ; *15A01-AD (attp40)/BDP-LexA::p65 (attp40)* ; *71G01-DBD (attp2), 10xUAS-IVS-Syn21-Chrimson::tdT3.1-SV40 (su(Hw)attp1)/13xLexAop2-IVS-Kir2.1::eGFP (VK00027)*
Figure 2C, G	w- ; *15A01-AD (attp40)/41A01-LexA::p65 (attp40)* ; *71G01-DBD (attp2), 10xUAS-IVS-Syn21-Chrimson::tdT3.1-SV40 (su(Hw)attp1)/13xLexAop2-IVS-Kir2.1::eGFP (VK00027)*
Figure 3B, E, H, K BDP>Chrimson	w- ; *BDP-AD (attp40)/20xUAS-IVS-Syn21-Chrimson::tdT3.1-SV40 (su(Hw)attp5)* ; *BDP-DBD (attp2)/+*
Figure 3B, E, H, K P1>Chrimson	w- ; *15A01-AD (attp40)/20xUAS-IVS-Syn21-Chrimson::tdT3.1-SV40 (su(Hw)attp5)* ; *15A01-DBD (attp2)/+*
Figure 3B, E, H, K pCd>Chrimson	w- ; *41A01-AD (attp40)/20xUAS-IVS-Syn21-Chrimson::tdT3.1-SV40 (su(Hw)attp5)* ; *21D06-DBD (attp2)/+*
Figure 4A-D pCd > GFP	w- ; *41A01-AD (attp4)/+* ; *21D06-DBD (attp2)/10xUAS-IVS-syn21-GFP-p10 (attp2)*
Figure 4A-D pCd > Kir2.1	w- ; *41A01-AD (attp4)/+* ; *21D06-DBD (attp2)/10xUAS-IVS-Kir2.1::eGFP (attp2)*
Figure 4A-D BDP > GFP	w- ; *BDP-AD (attp4)/+* ; *BDP-DBD (attp2)/10xUAS-IVS-syn21-GFP-p10 (attp2)*

Figure 4A-D BDP > Kir2.1	w- ; *BDP-AD (attp4)/+* ; *BDP-DBD (attp2)/10xUAS-IVS-Kir2.1::eGFP (attp2)*
Figure 5A	w- ; *20xUAS-Syn21-OpGCaMP6s-p10 (su(Hw)attp5)/41A01-AD (attp40)* ; *10xUAS-IVS-Syn21-Chrimson::tdT3.1-SV40 (su(Hw)attp1)/21D06-DBD (attp2)*
Figure 5C, G1, G2, G4, G5	w-, *10xUAS-IVS-Syn21-Chrimson::tdT3.1-SV40 (attp18), 13xLexAop2—Syn21-OpGCaMP6s-p10 (su(Hw)attp8)* ; *15A01-AD (attp40)/13xLexAop2-IVS-GtACR1::eYFP-SV40 (attp40)* ; *71G01-DBD (attp2)/Fru-LexA*
Figure 5D, G3, G6	Same as Fig. 1A
Figure 6B	Canton S (+/+ ; +/+ ; +/+)
Figure 6D BDP>GtACR1	w- ; *BDP-AD (attp40)/+* ; *BDP-DBD (attp2)/ 20xUAS-IVS- GtACR1::eYFP-SV40 (attp2)*
Figure 6D pCd>GtACR1	w- ; *41A01-AD (attp40)/+* ; *21D06-DBD (attp2)/ 20xUAS-IVS- GtACR1::eYFP-SV40 (attp2)*
Figure 6D P1>GtACR1	w- ; *15A01-AD (attp40)/+* ; *71G01-DBD (attp2)/ 20xUAS-IVS- GtACR1::eYFP-SV40 (attp2)*
Figure 7C	w-, *10xUAS-IVS-Syn21-Chrimson::tdT3.1-SV40 (attp18), 13xLexAop2—Syn21-OpGCaMP6s-p10 (su(Hw)attp8)* ; *15A01-AD (attp40)/+* ; *71G01-DBD (attp2)/41A01-LexA::p65 (attp2, or VK00027)*
Figure S1	Same as Fig. 1A
Figure S2B left	Same as Fig. 1D
Figure S2B right	w- ; +/+ ; *21D06-Gal4 (attp2)/10xUAS-IVS-myr::GFP (attp2)*
Figure S2C left	Same as Fig. 1E
Figure S2C right	w-, *10xUAS-IVS-Syn21-Chrimson::tdT3.1-SV40 (attp18), 13xLexAop2—Syn21-OpGCaMP6s-p10 (su(Hw)attp8)* ; *15A01-AD (attp40)/+* ; *71G01-DBD (attp2)/21D06-LexA::p65 (attp2)*
Figure S2D	w- ; *41A01-AD (attp40)/+* ; *21D06-DBD (attp2)/10xUAS-IVS-myr::GFP (attp2)*
Figure S2E left	w- ; *10xUAS-IVS-NLS-tdTomato (VK00022)/+* ; *41A01-LexA::p65 (VK00027), 13xLexAop2-IVS-NLS-GFP (VK00040)/41A01-Gal4 (attp2)*
Figure S2E middle	w- ; *10xUAS-IVS-NLS-tdTomato (VK00022)/+* ; *41A01-LexA::p65 (VK00027), 13xLexAop2-IVS-NLS-GFP (VK00040)/21D06-Gal4 (attp2)*
Figure S2E right	w- ; *10xUAS-IVS-NLS-tdTomato (VK00022)/41A01-AD (attp40)* ; *41A01-LexA::p65 (VK00027), 13xLexAop2-IVS-NLS-GFP (VK00040)/21D06-DBD (attp2)*
Figure S2F	w-,*10xUAS-IVS-myr::GFP (su(Hw)attp8)* ; *41A01-AD (attp40)/+* ; *Chat-DBD/+*
Figure S2G	w-,*10xUAS-IVS-myr::GFP (su(Hw)attp8)* ; *Gad1-AD/+* ; *41A01-DBD (attp2)/+*
Figure S2H	w-,*10xUAS-IVS-myr::GFP (su(Hw)attp8)* ; *41A01-AD (attp40)/+* ; *VGlut-DBD/+*

Figure S2I	w-,*10xUAS-IVS-myr::GFP (su(Hw)attp8)* ; *41A01-AD (attp40)/+* ; *Dsx-DBD/+*
Figure S3	Same as Fig. 1E
Figure S4A-C	w- ; *15A01-AD (attp40)/+* ; *71G01-DBD (attp2)/UAS-Denmark, UAS-Syt-eGFP*
Figure S4D-F	w- ; *41A01-AD (attp40)/+* ; *21D06-DBD (attp2)/UAS-Denmark, UAS-Syt-eGFP*
Figure S4J-I	w-, *13xLexAop2-IVS-myr::tdTomato (attp18)* ; *41A01-LexA (attp40)/LexAop-CD4::spGFP11* ; *71G01-Gal4 (attp2)/UAS-CD4::spGFP1-10*
Figure S4M-O	w-, *13xLexAop2-IVS-myr::tdTomato (attp18)* ; *41A01-LexA (attp40)/LexAop-CD4::spGFP11* ; *15A01-Gal4 (attp2)/UAS-CD4::spGFP1-10*
Figure S4P-R	w-, *13xLexAop2-IVS-myr::tdTomato (attp18)* ; *GH146-Gal4/LexAop-CD4::spGFP11* ; *Or83b-LexA/UAS-CD4::spGFP1-10*
Figure S5A	w- ; *BDP-AD (attp40)/13xLexAop2-IVS-CsChrimson::mVenus (attp40)* ; *BDP-DBD (attp2)/15A01-LexA::p65 (attp2), UAS-Kir2.1::eGFP*
Figure S5B	w- ; *41A01-AD (attp40)/13xLexAop2-IVS-CsChrimson::mVenus (attp40)* ; *21D06-DBD (attp2)/15A01-LexA::p65 (attp2), UAS-Kir2.1::eGFP*
Figure S6A, B	Same as Fig. 5C
Figure S6C-E	w-, *10xUAS-IVS-Syn21-Chrimson::tdT3.1-SV40 (attp18), 13xLexAop2—Syn21-OpGCaMP6s-p10 (su(Hw)attp8)* ; *15A01-AD (attp40)/13xLexAop2-IVS-GtACR1::eYFP-SV40 (attp40)* ; *71G01-DBD (attp2)/41A01-LexA (attp2 or VK00027)*
Figure S7	Same as Fig. 6D

Insertion sites: attp18 (X), su(Hw)attp8 (X), su(Hw)attp5 (2R), VK00022 (2R), attp40 (2L), VK00040 (3R), VK00027 (3R), su(Hw)attp1 (3R), attp2 (3L).

Females: always wild-type Canton S (+/+ ; +/+ ; +/+)

Supplemental Table 2. Statistics

Figure	Statistical test	Comparisons	Identifiers	p-values
Figure 1C2	Mann-Whitney U-test	NLS vs Cyto. GCaMP	n.s	0.15
Figure 2D left	Mann-Whitney U-test	BDP vs pCd	****	9.5e-13
Figure 2D right	Mann-Whitney U-test	BDP vs pCd	n.s	0.82
Figure 2H left	Mann-Whitney U-test	BDP vs pCd	****	3.6e-16
Figure 2H right	Mann-Whitney U-test	BDP vs pCd	n.s	0.11
Figure 3C during photo-stimulation	Kruskal-Wallis test Dunn's correction	BDP vs pCd	n.a	not applicable
		BDP vs P1	****	2.5e-13
Figure 3C after photo-stimulation	Kruskal-Wallis test Dunn's correction	BDP vs pCd	n.a	not applicable
		BDP vs P1	****	4.4e-13
Figure 3F during photo-stimulation	Kruskal-Wallis test Dunn's correction	BDP vs pCd	****	6.6e-06
		BDP vs P1	****	1.5e-07
Figure 3F after photo-stimulation	Kruskal-Wallis test Dunn's correction	BDP vs pCd	****	2.5e-06
		BDP vs P1	****	6.4e-09
Figure 3I after photo-stimulation	Kruskal-Wallis test Dunn's correction	BDP vs pCd	n.s	0.58
		BDP vs P1	****	1.3e-11
Figure 3L after photo-stimulation	Kruskal-Wallis test Dunn's correction	BDP vs pCd	****	3.0e-08
		BDP vs P1	****	7.9e-08
Figure 4B pCd	Mann-Whitney U-test	pCd>GFP vs pCd>Kir2.1	****	9.9e-07
Figure 4B BDP	Mann-Whitney U-test	BDP>GFP vs BDP>Kir2.1	n.s	0.4036
Figure 4C left total	Mann-Whitney U-test	pCd>GFP vs pCd>Kir2.1	**	0.0017
Figure 4C left first 20%	Mann-Whitney U-test	pCd>GFP vs pCd>Kir2.1	n.s	0.46
Figure 4C left last 20%	Mann-Whitney U-test	pCd>GFP vs pCd>Kir2.1	****	6.7e-06

Figure 4C right total	Mann-Whitney U-test	BDP>GFP vs BDP>Kir2.1	n.s	0.38
Figure 4C right first 20%	Mann-Whitney U-test	BDP>GFP vs BDP>Kir2.1	n.s	0.18
Figure 4C right last 20%	Mann-Whitney U-test	BDP>GFP vs BDP>Kir2.1	n.s	0.30
Figure 4D left total	Mann-Whitney U-test	pCd>GFP vs pCd>Kir2.1	****	6.4e-09
Figure 4D left first 20%	Mann-Whitney U-test	pCd>GFP vs pCd>Kir2.1	n.s	0.26
Figure 4D left last 20%	Mann-Whitney U-test	pCd>GFP vs pCd>Kir2.1	****	3.6e-07
Figure 4D right total	Mann-Whitney U-test	BDP>GFP vs BDP>Kir2.1	n.s	0.56
Figure 4D right first 20%	Mann-Whitney U-test	BDP>GFP vs BDP>Kir2.1	n.s	0.74
Figure 4D right last 20%	Mann-Whitney U-test	BDP>GFP vs BDP>Kir2.1	n.s	0.79
Figure 5H pCd	Mann-Whitney U-test	Light on vs Light off	****	6.1e-06
Figure 5H PPF2	Mann-Whitney U-test	Light on vs Light off	n.s	0.87
Figure 6D within genotype	Wilcoxon signed-rank test	BDP>GtACR1	n.s	0.80
		pCd>GtACR1	****	6.79e-06
		P1>GtACR1	n.s	0.49
Figure 6D between genotype	Kruskal-Wallis test	BDP vs pCd	**	0.0070
	Dunn's correction	BDP vs P1	n.s	1
Figure 6D	Wilcoxon signed-rank test	cVA only vs P1+cVA	**	0.0020
Figure S1H	Mann-Whitney U-test	P1 vs PPF1	****	6.2e-18
Figure S3B	Wilcoxon signed-rank test	1^{st} vs 2^{nd}	*	0.011
	Dunn's correction	2^{nd} vs 3^{rd}	n.s	0.15
Figure S3D	Wilcoxon signed-rank test	1^{st} vs 2^{nd}	*	0.011
	Dunn's correction	2^{nd} vs 3^{rd}	n.s	0.65
Figure S3F	Wilcoxon signed-rank test	1^{st} vs 2^{nd}	n.s	1

	Dunn's correction	2nd vs 3rd	n.s	0.65
Figure S5C during photo-stimulation	Mann-Whitney U-test	BDP vs pCd	n.s	0.56
Figure S5C after photo-stimulation	Mann-Whitney U-test	BDP vs pCd	****	2.4e-06
Figure S5D during photo-stimulation	Mann-Whitney U-test	BDP vs pCd	n.s	0.37
Figure S5D after photo-stimulation	Mann-Whitney U-test	BDP vs pCd	****	2.8e-09
Figure S8C	Mann-Whitney U-test	Light on vs Light off	**	0.0091

3.7 Materials and methods

Rearing conditions. Flies were reared under standard conditions at 25°C and 55% humidity, on a 12 h light/12 h dark cycle. 2-5 days old virgin females were used to cross with different male stocks. The density of experimental flies (-5 pupae/cm^2) was controlled by limiting the number of parents; crosses with too high or too low a density of progeny were discarded. Male flies were collected 0-2 days after eclosion and reared either individually (single-housed) or at 18 flies (group-housed) per vial for 5-6 days before the behavioral assays. Newly eclosed males were excluded from collection. For optogenetic experiments, eclosed males were reared in the dark with food containing 0.4 mM all-*trans*-retinal (Sigma-Aldrich, St. Louis, MO). For two-color optogenetic experiments, flies were reared in the dark from larval stage. Virgin females provided during behavioral tests were reared at high density (30 flies per vial) for 2-3 days. Flies carrying Gal4 and UAS-opsin transgenes were maintained in the dark to prevent uncontrolled activation of the opsins.

METHODS DETAILS

Generation of transgenic fly lines The following lines were generated in this study. *R41A01-LexA (vk00027* and *attp2)*, *R41A01-AD (attp40)*, and *R41A01-DBD (attp2)* were constructed based on the methods described in ref (Pfeiffer *et al.*, 2008) . R41A01 enhancer fragment was amplified from genomic DNA based on sequences in ref. (Adams *et al.*, 2000). The primers used for amplification were designed based on recommendations in the Janelia FlyLight project and Bloominton Drosophila Stock Center (https://bdsc.indiana.edu/stocks/gal4/gal4_janelia.html). For making *LexAop2-NLS-GCaMP6s (su(Hw)attp5)*, two nuclear localization signal (NLS) peptides, one from SV40 and the other from the *Drosophila* gene *scalloped,* were used. SV40-NLS (ccaaagaagaaaaggaaggta) was fused to the 5' end, and the scalloped-NLS (agaaccaggaagcaagtcagttcgcacatccaagtgctggctcgccgtaaactccgcgagatc) was fused to the 3' end of the codon-optimized GCaMP6s. A DNA fragment containing syn21-SV40-NLS-GCaMP6s-scalloped-NLS was ligated into pJFRC19-13LexAop2-IVS-myr::GFP-sv40 (Addgene plasmid # 26224) via XhoI and XbaI restriction enzyme sites. The sv40 terminator in the pJFRC19 was replaced with p10 terminator via XbaI and FseI sites. To generate

LexAop2-GtACR1 flies, the GtACR1 Drosophila-codon-optimized sequence (Mohammad *et al.*, 2017) was subcloned into pJFRC19-13LexAop2-IVS-myr::GFP-sv40 (Addgene plasmid # 26224) plasmid. The GtACR1::eYFP fragment was swapped with the myr::GFP fragment using XhoI and Xba1.

Two-photon GCaMP imaging. Calcium imaging was performed using a custom-modified Ultima two-photon laser scanning microscope (Bruker). The primary beam path was equipped with galvanometers driving a Chameleon Ultra II Ti:Sapphire laser (Coherent) and used for GCaMP imaging (920 nm). The secondary beam path was equipped with separate set of galvanometers driving a Fidelity-2 Fiber Oscillator laser (Coherent) for GtACR1 actuation (1070 nm). The two lasers were combined using 1030 nm short-pass filter (Bruker). GCaMP emission was detected with photomultiplier-tube (Hamamatsu). Images were acquired with an Olympus 40x, 0.8 numerical aperture objective (LUMPLFLN) equipped with high-speed piezo-z (Bruker). All images acquisition was performed using PrairieView Software (Version 5.3). For fast volume imaging (Figure 1A, B and Figure S1), three 4-µm optical sections were collected at 180 X 180 pixel resolution with a frame rate ~0.83 Hz. All of the other images were acquired at 256 X 256 pixel resolution with a frame rate 1 Hz. Saline (108 mM NaCl, 5 mM KCl, 4 mM $NaHCO_3$, 1 mM NaH_2PO_4, 5 mM trehalose, 10 mM sucrose, 5 mM HEPES, 0.5 mM $CaCl_2$, 2 mM $MgCl_2$, pH=7.5) was used to bathe the brain during functional imaging. Saline containing 90 mM KCl was added for high-resolution z stack after functional imaging to verify cell identity in Figure S1.

To prepare flies in vivo imaging, 6-8 days old flies were anesthetized on a cold plate and mounted on a thin plastic plate with wax. The wings, all legs, antenna, and arista were kept intact, wax-free, and free to move. Saline was added on the top side of the plate to submerge the fly head. A hole in the posterior-dorsal side of the head was opened using sharp forceps. Animals were then placed beneath the objective, and a plastic ball supported with air was positioned under the fly. The conditions inside of the imaging setup were maintained similar to the rearing conditions (25°C and 55% humidity). The flies were habituated for 30 min, and their behaviors were observed from the side using Point Grey Flea3 camera mounted with 0.5x-at-94 mm Infinistix lens fitted with a bandpass IR filter (830 nm, Edmund Optics) to block the two photon imaging laser and optogenetic stimulation lights. Animals that

exhibited no movement, strenuous movement, and prolonged abdomen bending during and after habituation were discarded.

Chrimson activation during calcium imaging was performed as described in ref(Inagaki *et al.*, 2014). A deep red (660 nm) fiber-coupled LED (Thorlab) with band-pass filter (660 nm, Edmund Optics) was used for light source to activate Chrimson. A 200 μm core multimode optic fiber placed 200 μm away from the brain was used to deliver 10 Hz, 10 ms pulse-width light. The light intensity at the tip of optic fiber was set to be 39.2 μW. For two photon GtACR1 actuation, 1070 nm laser (Fidelity-2, Coherent) was delivered by galvanometers to a circular area with diameter =~15 μm containing 1-3 cell bodies in focus for ~10 s by spiral scanning (10 μm/pixel, 45.24 ms/repeat, 220 repeats). Galvanometers were re-calibrated weekly using a slide glass coated with thin layer of fluorescent dye. Field of view was adjusted in order to keep the spiral scanning area near the center of the imaging field. cVA was presented by directing a continuous airstream (80 mL/min) through a 4 mm diameter Teflon tube directed at the fly's antennae. A custom-designed solenoid valve controller system was used to redirect the airstream between a blank cartridge and one containing cVA or Ethanol (solvent control). To make odour cartridges, 10 μL of undiluted cVA (Cayman Chemicals, 20 mg/mL) or Ethanol were placed on filter papers, and dried for 3 min to remove solvent before inserted into 15 mL pre-cleaned vials (Sigma-Aldrich).

Labeling neurons with Photoactivation after GCaMP imaging. Photoactivation experiments were performed in vivo using spiral scanning as described above. To perform GCaMP imaging and PA-GFP activation simultaneously, two Chameleon Ultra II Ti:Sapphire lasers (Coherent), one set at 920 nm and the other at 710 nm, are combined using 760 nm long pass filter (Bruker). Cell bodies of pCd neurons were identified by functional imaging using NLS-GCaMP6s, and a three-dimensional region of photoactivation was defined. The defined region of photoactivation was photoactivated by two cycles of spiral scanning (diameter =~7.5 μm, 45.24 ms/repeat, 20 repeats, 150 ms inter-repeat-intervals) separated by 20 min interval to allow diffusion of photoactivated PA-GFP molecules to the projections. 20 min after second cycle of the spiral scanning, 3-dimensional images were acquired at 1024 X 1024 pixel resolution. To reduce the fly's movement and residual GCaMP signal, cold saline containing 1mM EDTA was perfused until the end of image acquisition.

tdTomato signals and photoactivated PA-GFP signals were imaged simultaneously at 940 nm. Non-PPF1 PA-GFP and NLS-GCaMP basal fluorescence have been masked for clarity and z stack were created (Figure 1C3 and C4) using Fluorender (Wan *et al.*, 2009) and Fiji (Schindelin *et al.*, 2012; Schneider *et al.*, 2012) software.

Immunohistochemistry. Brains from 7-to-10-day-old adult files were dissected and stained as previously described(Watanabe *et al.*, 2017). The primary antibody mixture consisted of 1:1000 rabbit anti-GFP (Thermo Fisher Scientific, Cat#A11122), 1:1000 chicken anti-GFP (Aves Lab, Cat#GFP-1010), 1:100 mono-clonal (for GRASP experiment, Figure S4J-R) mouse anti-GFP (Sigma-Aldrich, Cat#G6539), 1:1000 rabbit anti-DsRed (Takara Bio, Cat#632496), 1:50 mouse anti-Brochpilot nc82 (Developmental Studies Hybridoma Bank), and 10% normal goat serum (Sigma-Aldrich) in PBST. Secondary antibodies used were 1:1000 goat anti-rabbit-Alexa488 (Thermo Fisher Scientific, Cat#A11008), 1:1000 goat anti-chicken-Alexa488 (Thermo Fisher Scientific, Cat#A11039), 1:1000 goat anti-mouse-Alexa488 (Thermo Fisher Scientific, Cat#A11001), 1:1000 goat anti-rabbit-Alexa568 (Thermo Fisher Scientific, Cat#A11011), and 1:1000 goat anti-mouse-Alexa633 (Thermo Fisher Scientific, Cat#A21050).

Confocal stacks were obtained with Fluoview FV1000 or FV3000 (Olympus). Fiji (Schindelin *et al.*, 2012; Schneider *et al.*, 2012) and Fluorender (Wan *et al.*, 2009) software was used to create z stack images. For brain registration (Figure S4G-I), the two images shown in Figure S4B and D are registered to T1 template brain (Yu *et al.*, 2010) using CMTK registration tools (Jefferis *et al.*, 2007).

Behavioral assay. Temperature and humidity of the room for behavioral assay was set to 25°C and 55%, respectively. All naturally occurring behavior assays were performed between 2:00pm to 7:00pm. Optogenetically-induced behaviors were not performed at specific times. All the behavior assays except mating assay (Figure 4A, B) were performed in 8-well acrylic chamber (16 mm diameter x 10 mm height, modified from ref. (Inagaki *et al.*, 2014), and side of the each well was coated with aInsect-a-Slip (Bioquip Products). Temperature probe (Vktech) was inserted into one side of the chamber to accurately monitor the chamber temperature. The clear top plates were coated with Sigmacote (Sigma-Aldrich), and the floor of the arenas was composed of clear acrylic covered with food (2.5% (w/v)

sucrose and 2.25% (w/v) agarose in apple juice). Flies were introduced into the chambers by gentle aspiration using a mouth pipette, and the chambers were placed under the behavioral setup. Flies were allowed to acclimate to the chamber under the camera without disturbance for 90 s before the recording. Fly behaviors were recorded at 30 Hz using Point Grey Flea3 camera mounted with Fujinon lens (HF35HA-1B) fitted with a long pass IR filter (780 nm, Midwest Optical Systems). Camera was located ~0.5 m above the chamber, and IR backlighting (855 nm, SmartVision Lights) was used for illumination from beneath the arena. Optogenetic activation was performed as described previously (Inagaki *et al.*, 2014). Briefly, a 655 nm 10 mm Square LED (Luxeon Star) was used to deliver 0.48 mW/mm^2 light for 30 seconds. For dead female presentation (Figure 3D-F and J-L, Figure 4C, and Figure S7), 2-5 day old wild-type Canton S virgin females were freeze-killed, and affixed in the middle of the arena with UV curable glue. The ventral end of the female abdomen was glued to prevent copulation.

For the female induced aggression assay (Figure 6A-D), single-housed male flies were transferred individually into empty vials containing a virgin female, and allowed to freely interact with the female for ~5 min. After this pre-exposure period, the male flies were gently transferred to the behavior arena covered with 2.25% (w/v) agarose in dH_2O, instead of fly food. For GtACR1 stimulation (Figure 6C, D), a 530 nm 10 mm Square LED (Luxeon Star) was used to deliver 117 $\mu W/mm^2$ light for 10 seconds. Male flies that initiated copulation during the 5 min pre-exposure period were not tested.

For the mating assay (Figure 4A, B),12-well two-layer chambers in which the layers were separated by a removable aluminum film. 2-5 day old wild-type Canton S virgin females were introduced into the lower layers, and males of a particular genotype were introduced in the upper layers. Flies were allowed to acclimate to the chamber for 90 s as described above before removing film. Behavior recording started right after film was removed.

QUANTIFICATION AND STATISTICAL ANALYSIS

Imaging data analysis. All data analysis was performed in MATLAB (MathWorks). ROIs (region of interest) corresponding to individual cell bodies were manually selected and fluorescence signal from the ROIs were smoothed with a moving average (window =5

frames). For volume imaging (Figure 1A, B and Figure S1), a single focal plane in which we observed the highest ΔF/F was used for each cell. Normalized ΔF/F values for each trials were calculated by dividing ΔF/F by the maximum ΔF/F. The average signal before photostimulation was used as F0 to calculate the ΔF/F, and cells with peak ΔF/F responses < 4σ above baseline more than 1/3 trials were excluded. Decay constants (tau) were fit to minimize mean-squared error between observed ΔF/F traces and a five-parameter model of cell responses to optogenetic stimulation. Specifically, the ΔF/F trace evoked by three consecutive pulses of optogenetic stimulation was fit with a weighted sum of three impulse responses sharing a characteristic rise time tau_R and decay time tau: fit values of tau_R and tau were the same for all three evoked responses, while response amplitudes were fit independently. Fit impulse responses in the model were set to be 30 s apart, following experimental stimulation conditions. The best-fit 80% of cells (MSE<2.06) were used to generate plots of population-average responses. "Percent of peak" in Figure 5H and Figure S6E were calculated from mean normalized ΔF/F values between 10-30 s after GtACR1 actuation. cVA responses for Figure 7D were calculated by subtracting mean GCaMP signal 10 s before cVA presentation from those obtained during cVA presentation (10 s). cVA responses from each cell delivered 30s after P1 stimulation were divided by cVA responses without concurrent P1 stimulation (cVA only), to calculate fold change (Figure 7E). cVA alone or P1+cVA stimulation were delivered in random order following initial selection for P1-responsive pCd neurons. Individual cell responses used in Figure 7C-E were the average of 2-3 trials per cell.

Behavioral data analysis. Analysis of lunging and unilateral wing extension was performed as described in ref (Hoopfer *et al.*, 2015). Briefly, fly posture was tracked from recorded videos using Caltech FlyTracker software, which is available for download at http://www.vision.caltech.edu/Tools/FlyTracker/, and bouts of behaviors were automatically annotated using the Janelia Automatic Animal Behavior Annotator (JAABA) (Kabra *et al.*, 2013). All annotations were manually validated to remove false positives. Behavioral assays with dead females (Figure 3D-F and J-K) were manually scored without using JAABA due to inaccuracy. Data shown in Figure 3A-C and G-I were also manually scored for consistency. Copulation latency for Figure 4A and B was manually scored, and the total number of males

that had engaged in copulation was summed across the 30-min period and plotted as a percentage of total flies for each time point. Courtship bouts shown in Figure S7 were manually annotated following the definition of courtship bouts described previously (Zhang *et al.*, 2018a). Statistical analyses were performed using Matlab and Prism6 (GraphPad Software). All data were analyzed with nonparametric tests. The cutoff for significance was set as an $\alpha<0.05$. Each experiment was repeated at least twice on independent group of flies. Outliers were defined as data points falling outside 1.5x the interquartile range of the data, and were excluded from plots for clarity, but not from statistical analyses.

Curve Fitting for Leaky bucket model. Rasters of courtship and lunging behavior in a 15-minute window were averaged across flies and binned in 10-second (for courtship) or 20-second (for lunging) time windows to produce a time-evolving population average behavior rate. Behavior rates for courtship and lunging were each fit with a three-parameter leaky integrator model with dynamics $\dot{r}(t) = -{r(t)}/{\tau} + I$, which has analytical solution $r(t) = (r_0 - \tau I)e^{-\frac{t}{\tau}} + \tau I$, where r is the behavior rate as a function of time t (in minutes), I is a constant sensory input, τ is the time constant of integration, and r_0 is the initial behavior rate at the start of recording.

Parameters I, τ, and r_0 were fit to minimize the mean squared error between model and data, for courtship and for lunging. Parameter values were jointly fit across the two behaviors (courtship and lunging) and across the four experimental conditions: pCd > Kir2.1 (manipulation), pCd > GFP, BPD > Kir2.1, and BPD > GFP (controls). To reduce the number of free parameters, the sensory input I was constrained to take the same value for all groups and conditions, while r_0 was fit separately for courtship and for aggression; only τ was fit independently for each group and each behavior.

3.8 Reference

Adams, M.D., Celniker, S.E., Holt, R.A.*, et al.* (2000). The genome sequence of Drosophila melanogaster. Science *287*, 2185-2195. PMC ID No. doi.

Anderson, D.J. (2016). Circuit modules linking internal states and social behaviour in flies and mice. Nature reviews Neuroscience *17*, 692-704. PMC ID No. doi 10.1038/nrn.2016.125.

Anderson, David J., and Adolphs, R. (2014). A Framework for Studying Emotions across Species. Cell *157*, 187-200. PMC ID No. doi 10.1016/j.cell.2014.03.003.

Archer, J. (2006). Testosterone and human aggression: an evaluation of the challenge hypothesis. Neuroscience & Biobehavioral Reviews *30*, 319-345. PMC ID No. doi.

Asahina, K., Watanabe, K., Duistermars, B.J.*, et al.* (2014). Tachykinin-Expressing Neurons Control Male-Specific Aggressive Arousal in Drosophila. Cell *156*, 221-235. PMC ID No. doi 10.1016/j.cell.2013.11.045.

Auer, T.O., and Benton, R. (2016). Sexual circuitry in Drosophila. Curr Opin Neurobiol *38*, 18-26. PMC ID No. doi 10.1016/j.conb.2016.01.004.

Bach, D.R., and Dayan, P. (2017). Algorithms for survival: a comparative perspective on emotions. In Nature reviews Neuroscience, pp. 311-319.

Baines, R.A., Uhler, J.P., Thompson, A.*, et al.* (2001). Altered electrical properties in Drosophila neurons developing without synaptic transmission. J Neurosci *21*, 1523-1531. PMC ID No. doi.

Bargmann, C.I. (2012). Beyond the connectome: How neuromodulators shape neural circuits. Bioessays *34*, 458-465. PMC ID No. doi.

Bath, D.E., Stowers, J.R., Hörmann, D.*, et al.* (2014). FlyMAD: rapid thermogenetic control of neuronal activity in freely walking Drosophila. In Nat Methods, pp. 756-762.

Cachero, S., Ostrovsky, A.D., Yu, J.Y.*, et al.* (2010). Sexual dimorphism in the fly brain. Curr Biol *20*, 1589-1601. PMC ID No. doi.

Chaudhuri, R., and Fiete, I. (2016). Computational principles of memory. Nature neuroscience *19*, 394-403. PMC ID No. doi 10.1038/nn.4237.

Chen, D., Sitaraman, D., Chen, N.*, et al.* (2017). Genetic and neuronal mechanisms governing the sex-specific interaction between sleep and sexual behaviors in Drosophila. Nat Commun *8*, 154. PMC ID No. 5533705. doi 10.1038/s41467-017-00087-5.

Chen, T.W., Wardill, T.J., Sun, Y.*, et al.* (2013). Ultrasensitive fluorescent proteins for imaging neuronal activity. Nature *499*, 295-300. PMC ID No. doi nature12354 [pii]

10.1038/nature12354.

Chen, Y., Essner, R.A., Kosar, S.*, et al.* (2019). Sustained NPY signaling enables AgRP neurons to drive feeding. eLife *8*. PMC ID No. PMC6513552. doi 10.7554/eLife.46348.

Chen, Y., Lin, Y.C., Zimmerman, C.A.*, et al.* (2016). Hunger neurons drive feeding through a sustained, positive reinforcement signal. eLife *5*. PMC ID No. PMC5016090. doi 10.7554/eLife.18640.

Chiang, A.S., Lin, C.Y., Chuang, C.C.*, et al.* (2011). Three-dimensional reconstruction of brain-wide wiring networks in Drosophila at single-cell resolution. Curr Biol *21*, 1-11. PMC ID No. doi 10.1016/j.cub.2010.11.056.

Clowney, E.J., Iguchi, S., Bussell, J.J.*, et al.* (2015). Multimodal Chemosensory Circuits Controlling Male Courtship in Drosophila. Neuron. PMC ID No. doi 10.1016/j.neuron.2015.07.025.

Crickmore, M.A., and Vosshall, L.B. (2013). Opposing dopaminergic and GABAergic neurons control the duration and persistence of copulation in Drosophila. Cell *155*, 881-893. PMC ID No. 4048588. doi 10.1016/j.cell.2013.09.055.

Datta, S.R., Vasconcelos, M.L., Ruta, V.*, et al.* (2008). The Drosophila pheromone cVA activates a sexually dimorphic neural circuit. Nature *452*, 473-477. PMC ID No. doi 10.1038/nature06808.

Diao, F., Ironfield, H., Luan, H.*, et al.* (2015). Plug-and-play genetic access to drosophila cell types using exchangeable exon cassettes. Cell reports *10*, 1410-1421. PMC ID No. 4373654. doi 10.1016/j.celrep.2015.01.059.

Dierick, H.A., and Greenspan, R.J. (2007). Serotonin and neuropeptide F have opposite modulatory effects on fly aggression. Nat Genet *39*, 678-682. PMC ID No. doi 10.1038/ng2029.

Ding, Y., Lillvis, J.L., Cande, J.*, et al.* (2019). Neural Evolution of Context-Dependent Fly Song. Curr Biol *29*, 1089-1099 e1087. PMC ID No. doi 10.1016/j.cub.2019.02.019.

Feinberg, E.H., Vanhoven, M.K., Bendesky, A.*, et al.* (2008). GFP Reconstitution Across Synaptic Partners (GRASP) defines cell contacts and synapses in living nervous systems. Neuron *57*, 353-363. PMC ID No. doi 10.1016/j.neuron.2007.11.030.

Gibson, William T., Gonzalez, Carlos R., Fernandez, C.*, et al.* (2015). Behavioral Responses to a Repetitive Visual Threat Stimulus Express a Persistent State of Defensive Arousal in Drosophila. Current Biology *25*, 1401-1415. PMC ID No. doi 10.1016/j.cub.2015.03.058.

Gobrogge, K.L., Liu, Y., Jia, X.*, et al.* (2007). Anterior hypothalamic neural activation and neurochemical associations with aggression in pair-bonded male prairie voles. In J Comp Neurol (Wiley Subscription Services, Inc., A Wiley Company), pp. 1109-1122.

Guo, Z.V., Inagaki, H.K., Daie, K.*, et al.* (2017). Maintenance of persistent activity in a frontal thalamocortical loop. Nature *545*, 181-186. PMC ID No. doi 10.1038/nature22324.

Homer (850 B.C.). The Iliad. Translated by R. Lattimore. (Chicago, IL, University of Chicago Press).

Hoopfer, E.D. (2016). Neural control of aggression in *Drosophila*. Curr Opin Neurobiol *38*, 109-118. PMC ID No. doi 10.1016/j.conb.2016.04.007.

Hoopfer, E.D., Jung, Y., Inagaki, H.K.*, et al.* (2015). P1 interneurons promote a persistent internal state that enhances inter-male aggression in Drosophila. eLife *4*. PMC ID No. 4749567. doi 10.7554/eLife.11346.

Inagaki, H.K., Fontolan, L., Romani, S.*, et al.* (2019). Discrete attractor dynamics underlies persistent activity in the frontal cortex. Nature *566*, 212-217. PMC ID No. doi 10.1038/s41586-019-0919-7.

Inagaki, H.K., Jung, Y., Hoopfer, E.D.*, et al.* (2014). Optogenetic control of Drosophila using a red-shifted channelrhodopsin reveals experience-dependent influences on courtship. Nat Methods, -. PMC ID No. doi.

Jefferis, G.S., Potter, C.J., Chan, A.M.*, et al.* (2007). Comprehensive maps of *Drosophila* higher olfactory centers: spatially segregated fruit and pheromone representation. Cell *128*, 1187-1203. PMC ID No. doi.

Jenett, A., Rubin, G.M., Ngo, T.-T.B., *et al.* (2012). A GAL4-driver line resource for Drosophila neurobiology. Cell reports *2*, 991-1001. PMC ID No. doi.

Kabra, M., Robie, A.A., Rivera-Alba, M., *et al.* (2013). JAABA: interactive machine learning for automatic annotation of animal behavior. In Nat Methods, pp. 64-67.

Kallman, B.R., Kim, H., and Scott, K. (2015). Excitation and inhibition onto central courtship neurons biases Drosophila mate choice. eLife *4*, 2027. PMC ID No. PMC4695383. doi 10.7554/eLife.11188.

Kimura, K.-I., Hachiya, T., Koganezawa, M., *et al.* (2008). Fruitless and doublesex coordinate to generate male-specific neurons that can initiate courtship. In Neuron, pp. 759-769.

Klapoetke, N.C., Murata, Y., Kim, S.S., *et al.* (2014). Independent optical excitation of distinct neural populations. In Nat Methods (Nature Publishing Group), pp. 338-346.

Kohatsu, S., Koganezawa, M., and Yamamoto, D. (2011). Female contact activates male-specific interneurons that trigger stereotypic courtship behavior in Drosophila. Neuron *69*, 498-508. PMC ID No. doi 10.1016/j.neuron.2010.12.017.

Kohatsu, S., and Yamamoto, D. (2015). Visually induced initiation of Drosophila innate courtship-like following pursuit is mediated by central excitatory state. Nature Communications *6*. PMC ID No. doi 10.1038/ncomms7457.

Kunwar, P.S., Zelikowsky, M., Remedios, R., *et al.* (2015). Ventromedial hypothalamic neurons control a defensive emotion state. eLife *4*. PMC ID No. PMC4379496. doi 10.7554/eLife.06633.

Lim, R.S. (2014). PhD Thesis. In Division of Biology (California Institute of Technology).

Lim, R.S., Eyjolfsdottir, E., Shin, E., *et al.* (2014). How food controls aggression in Drosophila. PloS one *9*, e105626. PMC ID No. 4146546. doi 10.1371/journal.pone.0105626.

Lorenz, K. (1966). On Aggression (New York, Harcourt, Brace & World).

Lorenz, K., and Leyhausen, P. (1973). Motivation of human and animal behavior; an ethological view, Vol xix (New York, Van Nostrand-Reinhold).

Manoli, D.S., Foss, M., Villella, A.*, et al.* (2005). Male-specific fruitless specifies the neural substrates of Drosophila courtship behaviour. Nature *436*, 395-400. PMC ID No. doi 10.1038/nature03859.

Mellert, D.J., Knapp, J.M., Manoli, D.S.*, et al.* (2010). Midline crossing by gustatory receptor neuron axons is regulated by *fruitless, doublesex* and the Roundabout receptors. Development *137*, 323-332. PMC ID No. 2799163. doi 10.1242/dev.045047.

Mohammad, F., Stewart, J.C., Ott, S.*, et al.* (2017). Optogenetic inhibition of behavior with anion channelrhodopsins. Nat Methods. PMC ID No. doi.

Nicolai, L.J., Ramaekers, A., Raemaekers, T.*, et al.* (2010). Genetically encoded dendritic marker sheds light on neuronal connectivity in Drosophila. Proc Natl Acad Sci U S A *107*, 20553-20558. PMC ID No. 2996714. doi 10.1073/pnas.1010198107.

Pan, Y., Robinett, C.C., and Baker, B.S. (2011). Turning males on: activation of male courtship behavior in Drosophila melanogaster. PloS one *6*, e21144. PMC ID No. 3120818. doi 10.1371/journal.pone.0021144.

Pfeiffer, B.D., Jenett, A., Hammonds, A.S.*, et al.* (2008). Tools for neuroanatomy and neurogenetics in Drosophila. In Proc Natl Acad Sci USA (National Acad Sciences), pp. 9715-9720.

Remedios, R., Kennedy, A., Zelikowsky, M.*, et al.* (2017). Social behaviour shapes hypothalamic neural ensemble representations of conspecific sex. Nature *550*, 388-392. PMC ID No. PMC5674977. doi 10.1038/nature23885.

Rickgauer, J.P., and Tank, D.W. (2009). Two-photon excitation of channelrhodopsin-2 at saturation. Proceedings of the National Academy of Sciences of the United States of America *106*, 15025-15030. PMC ID No. doi 10.1073/pnas.0907084106.

Rideout, E.J., Billeter, J.-C., and Goodwin, S.F. (2007). The sex-determination genes fruitless and doublesex specify a neural substrate required for courtship song. Current biology : CB *17*, 1473-1478. PMC ID No. doi 10.1016/j.cub.2007.07.047.

Schindelin, J., Arganda-Carreras, I., Frise, E.*, et al.* (2012). Fiji: an open-source platform for biological-image analysis. Nat Methods *9*, 676-682. PMC ID No. 3855844. doi 10.1038/nmeth.2019.

Schneider, C.A., Rasband, W.S., and Eliceiri, K.W. (2012). NIH Image to ImageJ: 25 years of image analysis. Nat Methods *9*, 671-675. PMC ID No. 5554542. doi.

Sobolewski, M.E., Brown, J.L., and Mitani, J.C. (2013). Female parity, male aggression, and the Challenge Hypothesis in wild chimpanzees. Primates *54*, 81-88. PMC ID No. doi.

Stockinger, P., Kvitsiani, D., Rotkopf, S.*, et al.* (2005). Neural circuitry that governs Drosophila male courtship behavior. Cell *121*, 795-807. PMC ID No. doi 10.1016/j.cell.2005.04.026.

Tauber, E., and Eberl, D.F. (2003). Acoustic communication in Drosophila. In Behav Processes, pp. 197-210.

Tinbergen, N. (1951). The study of instinct (Oxford Eng., Clarendon Press).

von Philipsborn, A.C., Liu, T., Yu, J.Y.*, et al.* (2011). Neuronal control of Drosophila courtship song. Neuron *69*, 509-522. PMC ID No. doi.

Wan, Y., Otsuna, H., Chien, C.B.*, et al.* (2009). An interactive visualization tool for multi-channel confocal microscopy data in neurobiology research. IEEE transactions on visualization and computer graphics *15*, 1489-1496. PMC ID No. 2874972. doi 10.1109/TVCG.2009.118.

Wang, L., and Anderson, D.J. (2010). Identification of an aggression-promoting pheromone and its receptor neurons in Drosophila. Nature *463*, 227-231. PMC ID No. doi.

Wang, L., Dankert, H., Perona, P.*, et al.* (2008). A common genetic target for environmental and heritable influences on aggressiveness in Drosophila. Proc Natl Acad Sci USA *105*, 5657-5663. PMC ID No. doi PMC2311352.

Wang, L., Han, X., Mehren, J.*, et al.* (2011). Hierarchical chemosensory regulation of male-male social interactions in Drosophila. Nature neuroscience *14*, 757-762. PMC ID No. 3102769. doi 10.1038/nn.2800.

Watanabe, K., Chiu, H., Pfeiffer, B.D.*, et al.* (2017). A Circuit Node that Integrates Convergent Input from Neuromodulatory and Social Behavior-Promoting Neurons to Control Aggression in Drosophila. Neuron *95*, 1112-1128 e1117. PMC ID No. 5588916. doi 10.1016/j.neuron.2017.08.017.

Wingfield, J.C., Hegner, R.E., Dufty, A.M., *et al.* (1990). The challenge hypothesis--theoretic implications for patterns of testosterone secretion, mating systems and breeding strategies. Am Nat *136*, 829-846. PMC ID No. doi.

Yamamoto, D., and Koganezawa, M. (2013). Genes and circuits of courtship behaviour in Drosophila males. Nature Rev Neurosci *14*, 681-692. PMC ID No. doi 10.1038/nrn3567.

Yu, J.Y., Kanai, M.I., Demir, E., *et al.* (2010). Cellular organization of the neural circuit that drives Drosophila courtship behavior. Current biology : CB *20*, 1602-1614. PMC ID No. doi 10.1016/j.cub.2010.08.025.

Zhang, S.X., Miner, L.E., Boutros, C.L., *et al.* (2018a). Motivation, Perception, and Chance Converge to Make a Binary Decision. Neuron *99*, 376-388 e376. PMC ID No. doi 10.1016/j.neuron.2018.06.014.

Zhang, S.X., Rogulja, D., and Crickmore, M.A. (2016). Dopaminergic Circuitry Underlying Mating Drive. Neuron *91*, 168-181. PMC ID No. doi 10.1016/j.neuron.2016.05.020.

Zhang, S.X., Rogulja, D., and Crickmore, M.A. (2019). Recurrent Circuitry Sustains Drosophila Courtship Drive While Priming Itself for Satiety. Curr Biol. PMC ID No. doi 10.1016/j.cub.2019.08.015.

Zhang, W., Guo, C., Chen, D., *et al.* (2018b). Hierarchical Control of Drosophila Sleep, Courtship, and Feeding Behaviors by Male-Specific P1 Neurons. Neuroscience bulletin. PMC ID No. doi 10.1007/s12264-018-0281-z.

Zhang, Y.Q., Rodesch, C.K., and Broadie, K. (2002). Living synaptic vesicle marker: synaptotagmin-GFP. Genesis *34*, 142-145. PMC ID No. doi 10.1002/gene.10144.

Zhou, C., Pan, Y., Robinett, C.C., *et al.* (2014). Central brain neurons expressing doublesex regulate female receptivity in Drosophila. Neuron *83*, 149-163. PMC ID No. doi 10.1016/j.neuron.2014.05.038.

Chapter 4

FUTURE DIRECTIONS

Although the data presented here provide insight into the complex networks that underlie behavioral temporal dynamics influencing social behaviors in fruit flies, it raises several new and interesting questions for future investigation: what are the roles of the other P1 follower cells in social behaviors, what is the mechanism of persistent neuronal activity? This chapter summarizes these unsolved questions and provides preliminary efforts to answer these.

4.1 Persistent P1 follower cells besides pCd neurons that are identified by functional connectomics screening.

During the initial screening using volumetric GCaMP imaging, we have identified 14 cell clusters (including P1 neurons themselves) that responded upon transient P1 stimulation (Figure 1). Among these clusters, 5 clusters (cluster #10, 11, 12, 13, and 14) showed persistent neuronal activity more than 5 times longer than P1 activity. We have used various criteria such as reproducibility and number of cells that are responded to determine cluster #11 and 12 (pCd) are likely to be the most important clusters that regulates P1 induced persistent social behaviors (Figure 4.1). However, it is still possible that other persistent clusters (cluster #10, 13, and 14) also plays important roles in persistent social states. For instance cluster #14 shows median tau value that is 1.5X greater than pCd clusters and may be a better candidate to regulate persistent feature of the P1 induced social state change. This cluster has not been followed up due to the practical difficulty derived from the fact that on average, only one cells per fly per hemibrain showed reliable response upon P1 stimulation (Figure 4.1) which make it difficult to photo-label using PA-GFP to identify cell morphology.

In addition, function of cluster #11 could not been investigated deeply due to the lack of specific genetic handle to label them even though it met all the criteria shown in Figure 1. The rough morphology of these neurons are identified using PA-GFP labeling method described in Chapter 3, and a GAL4 driver to target them are identified (Figure 4.2). However, these driver not only labeled cluster #11 but also many other cells especially in optic lobe region (Figure 4.2). Number of intersectional genetic methods such as GAL80 and FLP have been tried, but none of them successfully isolated cluster #11. Therefore, identification of multiple drivers that label cluster

#11 will be necessary to specifically isolate the target cells by split GAL4 strategy, which will enable one to test the role of that cluster in social behavior.

The functional connectomics screening presented here identified various P1 follower cells. Since expression of GCaMP molecules are restricted to Fruitless neurons, there could be Fruitless negative P1 downstream neurons that were not detected. Once such an example is the mushroom body neurons that were strongly responded upon P1 stimulation when GCaMP was expressed in entire brain. By studying the function of Fruitless positive cluster other than pCd as well as non-Fruitless positive neurons, we will be able to understand the circuitry of the social behaviors more comprehensive way.

4.2 Mechanism underlying persistent neuronal activity.

We have observed persistent neuronal activity from pCd neurons that outlast minutes after transient P1 activation. The decaying constant (83 s) of the GCaMP signal is comparable to the decaying constant obtained from behavioral experiment demonstrating the correlation between the persistent neuronal and persistent social behavior. However, the neuronal mechanism encoding persistent activity in pCd neurons are largely unknown.

Significant amount of effort has been devoted to understand the potential mechanisms that may underlie persistent activity. Most of the proposed mechanisms rely either on the intrinsic properties of individual neurons or on the connectivity within neural circuits to maintain the persistent activity (Major and Tank, 2004; Zylberberg and Strowbridge, 2017). Nevertheless, it remains unclear which mechanisms are at play in the many brain areas involved in persistent activity. Both single cell and network mechanisms are likely to co-operate in generating persistent activity in many brain areas.

In Chapter 3 (Figure 3.5), we have shown that pCd activity is necessary, but not sufficient to trigger persistent neuronal activity. Direct activation of pCd neurons (Figure 5A) did not induced persistent pCd activity, indicating that the persistent neuronal activity triggered by P1 stimulation is not due to the cell intrinsic property of the pCd neurons. Therefore, we hypothesized that other identified persistent P1 follower cells, cluster #10, 11, 13, and 14, might need to be co-activated with pCd to trigger persistent neuronal activity. Since we have previously identified a driver to label cluster #11 (Figure 4.2), we tested this hypothesis by comparing time constant of pCd with and without co-activation of cluster #11 (Figure 4.3A, B). Similar to pCd, activation of cluster

#11 does not induce persistent neuronal activity even though cluster #11 are persistent P1 follower cells, indicating they are not sufficient to trigger persistent activity (Figure 4.3A). However, when pCd and cluster #11 neurons are activation together, both populations showed long-lasting GCaMP responses (Figure 4.3B). Since anatomical study suggested that pCd and cluster #11 form synaptic connections (Figure 3C, D), we have performed functional imaging between pCd and cluster #11, which suggested mutual connection between the two populations. These data supports that neural circuit between these two (or more) populations are the underlying mechanism of the persistent neuronal activity.

Long-lasting neuromodulators are often emphasized for the sustained neuronal activity. We hypothesized that P1 neurons might release neuromodulators upon transient activation. To test this, we have stained P1 neurons with anti-bodies against known neuromodulators such as dopamine and several *Drosophila* neuropeptides (data not shown), but none of them gave positive result. Co-labeling of P1 neurons with known neuropeptide drivers (Asahina et al., 2014) also suggested that P1 neurons might not release neuropeptides. However, these results do not exclude the possibility that P1 neurons release long-lasting neuromodulators because there are only limited number of anti-bodies available for the neuromodulator. In order to verify whether P1 neurons potentially release neuromodulator, it will be necessary to perform mRNA sequencing.

Even if P1 neurons do not release any neuromodulators upon stimulation, there is a possibility that neuromodulators are released from P1 downstream neurons, which induces persistent brain activity. We have tested this hypothesis by functional imaging in a fly where GCaMP was expressed with drivers that are known to label neuromodulators such as TH-GAL4, Trh-GAL4, Dop-GAL4, and several neuropeptide GAL4 lines. Among those flies, cells labeled by Trh-GAL4 driver showed reliable GCaMP response. To test behavioral relevance of serotonin release in P1 induced persistent social behavior, we have knocked down serotonin receptor in Fruitless population, which caused reduced aggression after P1 stimulation (Figure 4). This result, together with imaging data suggests that serotonin may be an important component of the circuitry of persistent social behavior.

Persistent activity has been considered a form of circuit dynamics that can be used as a mechanism for accumulation of sensory or motor information. In chapter 3, we have shown that pCd neurons display integrator properties at the level of their physiology. pCd neurons exhibit

stepwise summation of P1 input (Figure 3.1E and Figure S3.3A), suggesting that pCd neurons work as an neural integrator. In Figure 3.5G2, acute inhibition of pCd neurons following P1 stimulation caused a decrease in pCd activity, which did not recover to control levels. This data is consistent with the idea that pCd neurons function as an integrator rather than attractor (Guo et al., 2017; Inagaki et al., 2019). The behavioral data shown in Figure 3.4F suggests that pCd neurons works as a leaky integrator, and the activity of the neurons represents the integrated conspecific sensory cues.

4.3 Other unsolved problems: conflicts between observations

Besides the two unsolved questions described above, there are several questions that are remain to be answered. First, in Chapter 3, we showed activation of pCd neurons do not induce persistent pCd activity (Figure 5A). However, activation of pCd neurons in presence of dead female triggers increased courtship behavior toward the dead female, and this effect last long after optogenetic pCd stimulation (Chapter 3, Figure 3.3F). This result indicates that in presence of female cue, activation of pCd neurons might be sufficient to trigger persistent neuronal activity. To test this hypothesis, we measured the decaying kinetics of pCd activation when tester male flies are touching female abdomen (Figure 4.6). Although female touching induced slower decay of pCd activity, it is not slow enough to explain the long-lasting effect observed in behavioral test. We suspect that this conflict might be derived from the fact that functional imaging has been performed in head-fixed, open cuticle preparation while behavioral experiment was done in freely behaving animal. To answer this question, it would be necessary to measure pCd neuronal activity in freely behaving animal which is currently technically infeasible.

Secondly, even though the decaying constant (~80 s) of pCd activity induced by P1 activation is comparable to the decaying constant obtained from P1 induced persistent courtship behavior, the effect of P1 activation in aggressive behavior last far longer (~ 10 min) than neuronal activity of the pCd neurons. This indicates that there might be two different underlying mechanisms that are responsible for the P1 induced persistent social behavior. In Chapter 3 (Figure S3.3), we demonstrated that repeated stimulation of the P1 neurons causes sensitization of the pCd neurons to the P1 stimulation that last even after pCd activity returned to the baseline activity, offering a useful point-of-entry to investigate mechanisms deriving persistent effect with two different time scale.

4.4 Limitations and future improvements.

Animals integrate sensory information and continuously modify their internal states according to given circumstance (Berridge, 2004; Kennedy et al., 2014), and physiological responses of the brain regions to the same stimuli can vary depending on the animals' states. This raises an important question that physiological measurement performed under head-fixed animals may not represent the brain activity during the behavioral performance. Ideally, we would like to record brain activity and behavior simultaneously as shown in mammalian studies where miniaturized microscopes are installed on animals' head and brain activity is measure by endoscopic imaging (Ghosh et al., 2011; Remedios et al., 2017). However, it is infeasible to apply this technique to fly study.

To measure GCaMP signals in freely behaving flies, galvanometer mirror-based tracking system has been developed in 2016 (Grover et al., 2016). This technique, Flyception, measures fluorescent signal from a fly brain through a surgically implanted transparent optical window while animal is freely walking. By using Flyception, we attempted to measure brain activity of a male fly during social behavior. However, use of Flyception technique was limited to the initial, exploratory phase of the social behaviors such as approaching since courtship and fighting behaviors are accompanied by high locomotor activity which make it difficult for the system to track the animals.

Measuring brain activity in a fly while animal is performing social behavior will require extensive technical improvement, and would not be practical at the current stage. Instead, we tried several ways to improve our head-fixed preparation to make it as natural condition as possible. In conventional head-fixed imaging preparation, flies cuticle is partially removed and artificially prepared saline solution is provided. Since ion concentration of the saline solution substantially affects physiological responses, we have tested microsurgery techniques (Sinha et al., 2013) where fly samples are prepared with laser surgery and the optical window is covered with transparent UV glue. In this case, fly brain is surrounded by hemolin, and no artificial solution is provided. We have compared physiological response of pCd neurons to the P1 stimulation between two different sample preparation, but found no significant differences. We also tried to provide sensory cues that are missing under head-fixed preparation, but present during the behavioral tests. As demonstrated in section 4.3 (Figure 5), providing female gustatory cue significantly increased pCd neurons' decaying constant. However, even with female abdomen

touching, stimulation of the pCd neurons did not induce persistent activity comparable to the P1 stimulation. It is possible that activation of pCd neurons in presence of all the social cues such as gustatory, olfactory, and visual cues induces persistent neuronal activity similar to the P1 activation.

4.5 Figures

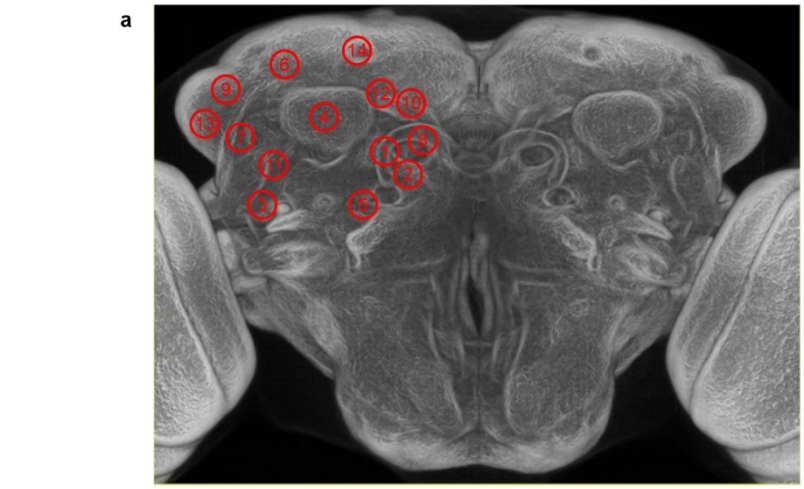

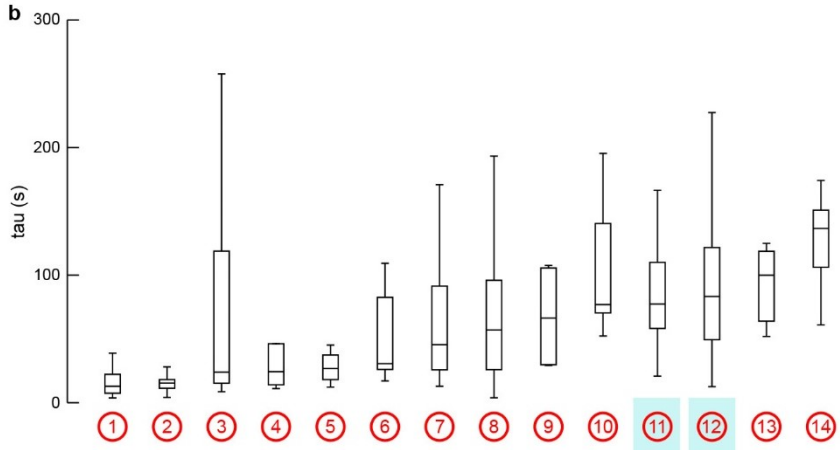

c

	1	2	3	4	5	6	7	8	9	10	11	12	13	14
Median tau (s)	12.9	15.4	24.0	24.3	26.7	30.6	45.5	57.0	66.4	76.9	77.4	83.3	100	137
# of cells detected from 12 flies	57	56	45	10	8	6	22	98	8	23	23	77	3	6
Fraction of flies showed detectable responses (%)	100	100	92	50	50	33	75	100	50	58	83	100	17	50
Average # of cell / fly / hemibrain	2.4	2.3	4.1	1.7	1.3	1.5	2.4	4.1	1.3	1.6	2.3	3.2	1.5	1

Figure 4.1. Identification of the P1 follower cells by volumetric imaging.

(A) Approximate cell body locations for the all P1 responding neurons identified by volumetric GCaMP imaging from 12 flies (B) Decay constants for identified P1 follower cells. Boxplots show the median (center line), 25th and 75th percentiles (box), and 1.5 times the interquartile range (whiskers). Outliers were defined as data points falling outside 1.5x the interquartile range of the data, and were excluded from plots for clarity. (C) Properties of P1 follower cells.

Red letters indicates the cells that meet criteria, and blue shaded areas show two cell clusters that meet all three criteria. We were unable to get specific genetic handle(s) for cell #11.

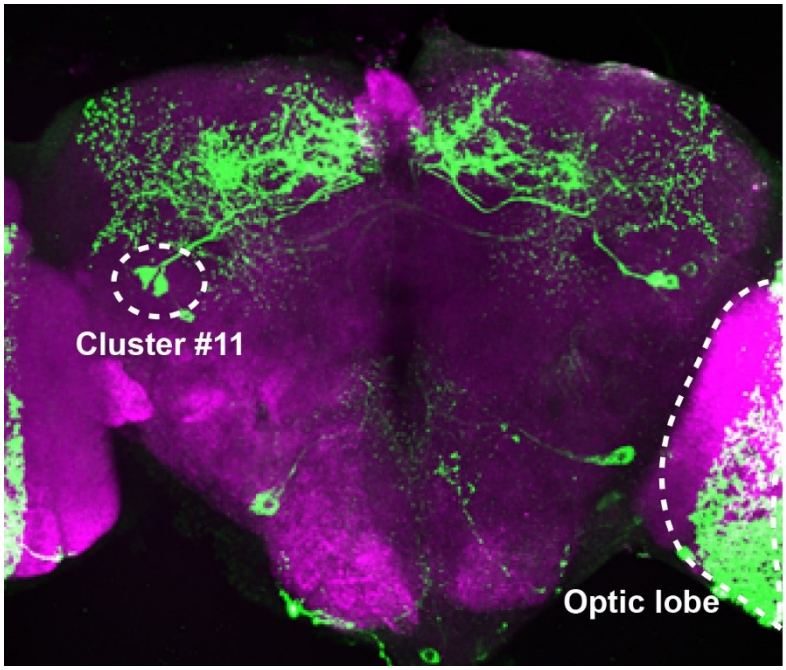

Figure 4.2. Expression pattern of the identified GAL4 drivers labeling cluster #11.

Although this driver labeled cluster #11 neurons, it labeled many other brain regions especially in optic lobe.

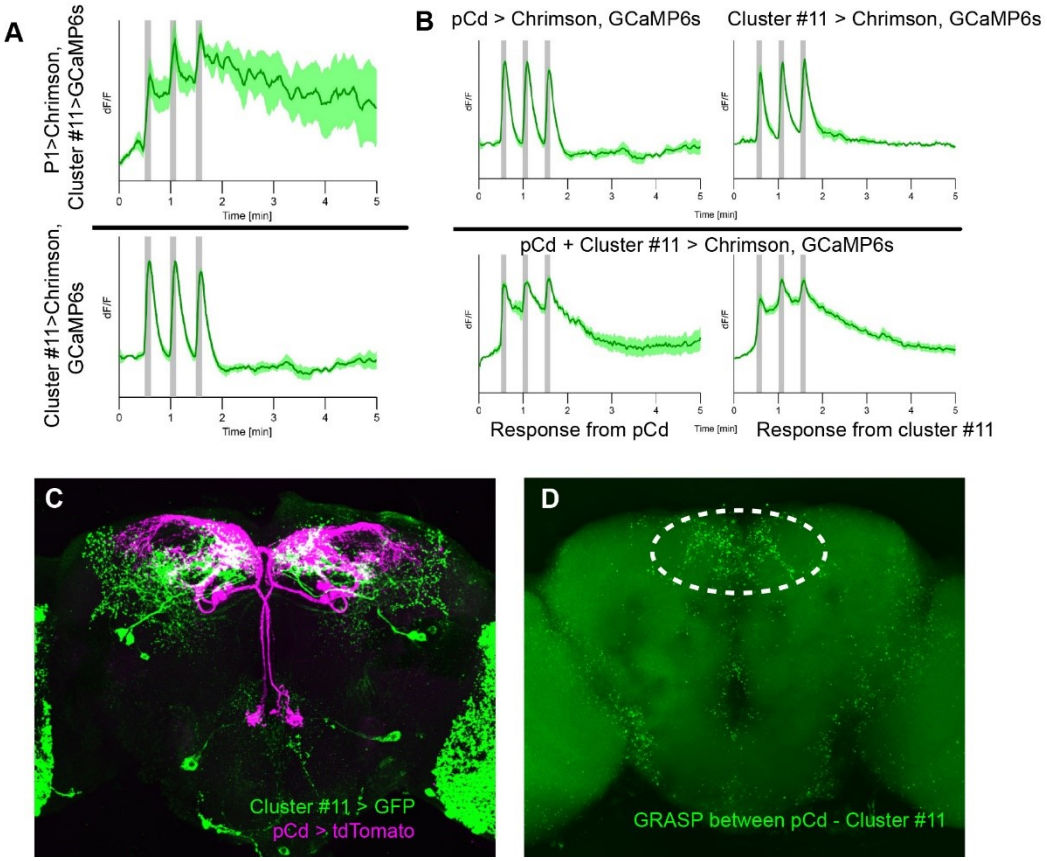

Figure 4.3. Co-activation of pCd and cluster #11 neurons and their connectivity.

(A) Direct activation of cluster #11 neurons does not induce persistent GCaMP signal (bottom) unlike P1 activation (top). n=5 trials, 3 flies. (B) Co-activation of pCd and cluster #11 neurons induces persistent responses in both pCd (bottom left) and cluster #11 (bottom right) neurons. (C) Projection patterns of pCd and cluster #11 neurons. Two clusters are projecting to the common area shown as white color. (D) GRASP signals between pCd and cluster #11 neurons are detected in the area where both clusters are projecting (indicated as white dashed circle).

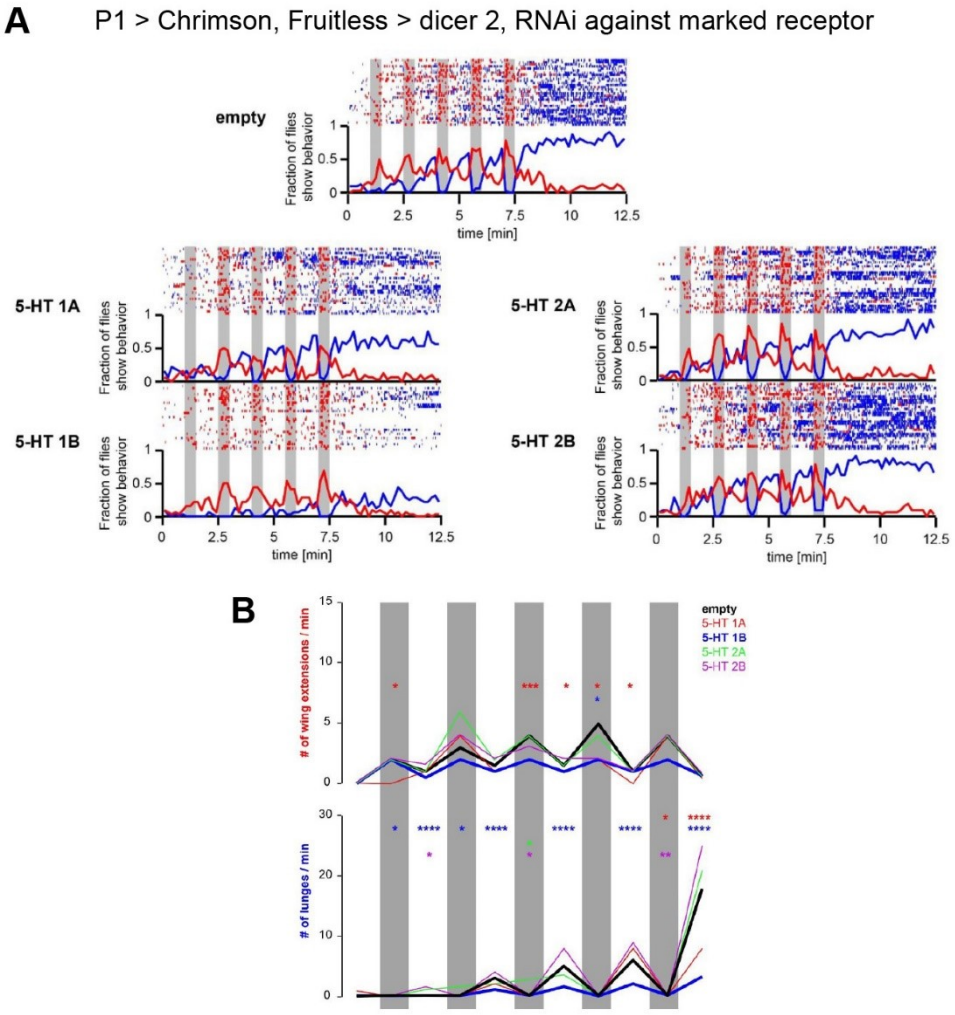

Figure 4.4 RNAi knock down of serotonin receptor reduces P1 induced persistent aggression.

(A) Raster plot showing courtship and aggression induced by P1 stimulation. Compared to control (empty, top), knocking down 5-HT 1B receptor in Fruitless population dramatically reduced persistent aggression. Grey bar indicates optogenetic stimulation of the P1 neurons. n = 64 each genotype. (B) Quantification and statistical analysis of (a). * $P < 0.05$, ** $P < 0.01$, *** $P < 0.001$, **** $P < 0.00001$.

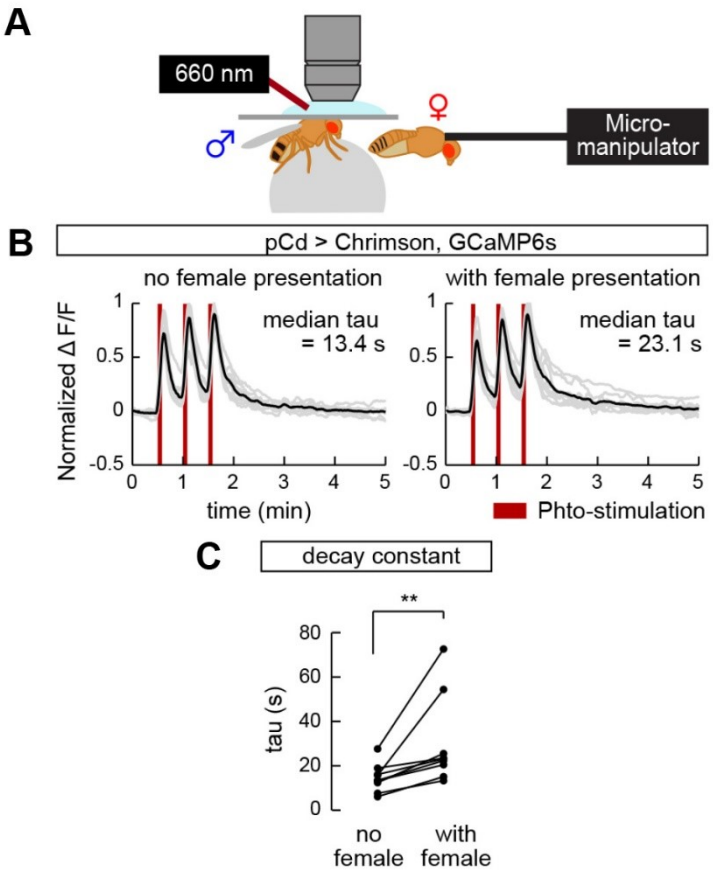

Figure 4.5. Presentation of female abdomen induced slight, but statistically significant increase in decay constant of cell autonomous response in pCd neurons.

(A) Schematic illustrating experimental design. (B) GCaMP responses (ΔF/F) to optogenetic activation of pCd neurons (dark red bar, 5 s, 10 Hz, 10 ms pulse-width) with (left) or without (right) female abdomen touching. Gray lines depict trial-averaged individual pCd cell responses (n=7 from 7 flies). (C) Individual pCd responses (ΔF/F) to optogenetic stimulation with or without female presentation. Statistical test used was a Wilcoxon signed-rank test. ** $P < 0.01$.

4.6 References

Asahina, K., Watanabe, K., Duistermars, B.J., Hoopfer, E., Gonzalez, C.R., Eyjolfsdottir, E.A., Perona, P., and Anderson, D.J. (2014). Tachykinin-expressing neurons control male-specific aggressive arousal in Drosophila. Cell *156*, 221-235.

Berridge, K.C. (2004). Motivation concepts in behavioral neuroscience. Physiol Behav *81*, 179-209.

Ghosh, K.K., Burns, L.D., Cocker, E.D., Nimmerjahn, A., Ziv, Y., Gamal, A.E., and Schnitzer, M.J. (2011). Miniaturized integration of a fluorescence microscope. Nat Methods *8*, 871-878.

Grover, D., Katsuki, T., and Greenspan, R.J. (2016). Flyception: imaging brain activity in freely walking fruit flies. Nat Methods *13*, 569-572.

Kennedy, A., Asahina, K., Hoopfer, E., Inagaki, H., Jung, Y., Lee, H., Remedios, R., and Anderson, D.J. (2014). Internal States and Behavioral Decision-Making: Toward an Integration of Emotion and Cognition. Cold Spring Harb Symp Quant Biol *79*, 199-210.

Major, G., and Tank, D. (2004). Persistent neural activity: prevalence and mechanisms. Curr Opin Neurobiol *14*, 675-684.

Remedios, R., Kennedy, A., Zelikowsky, M., Grewe, B.F., Schnitzer, M.J., and Anderson, D.J. (2017). Social behaviour shapes hypothalamic neural ensemble representations of conspecific sex. Nature *550*, 388-392.

Sinha, S., Liang, L., Ho, E.T., Urbanek, K.E., Luo, L., Baer, T.M., and Schnitzer, M.J. (2013). High-speed laser microsurgery of alert fruit flies for fluorescence imaging of neural activity. Proc Natl Acad Sci U S A *110*, 18374-18379.

Zylberberg, J., and Strowbridge, B.W. (2017). Mechanisms of Persistent Activity in Cortical Circuits: Possible Neural Substrates for Working Memory. Annu Rev Neurosci *40*, 603-627.